Contents of issue 2 vol. LVI

Engineering Transactions, T. **LVI**, nr 2, str. 93–184, Warszawa 2008

ENGINEERING TRANSACTIONS • *Engng. Trans.* • **56**, 2, 95–100, 2008
Polish Academy of Sciences • Institute of Fundamental Technological Research

PROFESSOR JAN ODERFELD

The Laudatio *speech delivered during the ceremony of awarding Prof. Jan Oderfdeld an honorary doctorate by Warsaw University of Technology and on the occasion of his 100th birthday*

I have a great honour of presenting a portrait of Professor Jan Oderfeld in all aspects of his scientific activity; i.e., as engineer, researcher, university teacher, promoter of scientific activity both in Poland and within international co-operation , doyen of the staff of Warsaw University of Technology (WUT), and a distinguished senior of Polish aviation.

Professor Jan Oderfeld is an extraordinary man. It is impossible to present in brief all his important achievements in a variety of fields he has been dealing with. One of his most distinctive characteristics consists in the fact that despite undertaking many different tasks at the same time and taking on many duties, he always executed and fulfilled them in excess, earning his places in all fields of his activity.

Professor Jan Oderfeld was born in Częstochowa on February 19th 1908. In 1924 he passed his school leaving exams in the Henryk Sienkiewicz Public Secondary School in Częstochowa. On August 31st, 1930 he obtained a Warsaw University of Technology diploma, after graduating at the Faculty of Mechanical Engineering. As early as in the course of studying he started coping with industrial problems of his interest; i.e., he got a job in the well-known machine-production plant "Pioneer" in Warsaw. After doing his military service he had built a team of engineers who undertook a very challenging task of constructing a turbine jet engine. In 1931, thanks to a private financial support they had managed to construct two prototypes of the engine that then underwent successfully their tests. In 1932, on the premises of Experimental Workshop of the Public Engineering Production Plant "Ursus" near Warsaw, the team constructed also a pulsatory jet engine intended for using in unmanned aerial vehicles. The pioneering work of young Polish engineers – Jan Oderfeld, Władysław Bernardzikiewicz and Józef Sachs was stopped in 1933 due to the lack of funds. A model of the jet engine designed that time can still be seen at the Museum of Technology in Warsaw. From 1932 to the beginning of World War II, engineer Jan Oderfeld was working for the Engine Production Plant "Skoda" – PZL in

Warsaw, at first as a production engineer and then, from 1936, as a design team head. He contributed actively to the design process and supervised testing of the aircraft piston engine "Foka" (Seal) that was mounted in the aircraft "Wilk" (Wolf) in 1938. Together with his team he had also constructed a gas turbine that could be assembled with the piston engine Cirrus. The turbine underwent its tests successfully in 1938. At the same time, i.e., from 1937 to 1939 he was engaged also in his individual engineering activity; e.g., he converted a carburettor aircraft engine into the injection one, which those days was really a novelty.

Those days, starting from 1937 he had launched his teaching activity and delivered a course in aircraft engines at the Air-Force Officer Cadet School in Warsaw. About seventy of his students fought in the Battle of Britain, many died.

Under German occupation within 1940–1945 engineer Jan Oderfeld worked in Skierniewice (a small town near Warsaw) running the cooperative machine-shop "Rolnik" (Farmer). Under his effective supervision, a small repair shop with few workers became a large production plant manufacturing agricultural machinery, nowadays known as the Mechanization Shop for Horti- and Agriculture, Limited Liability Company.

Immediately after the war had ended, starting with the academic year 1945/46, engineer Jan Oderfeld began to work for the Hipolit Wawelberg and Stanisław Rotwand High Engineering School, where in a position of temporary professor he lectured on engineering mechanics, aircraft engines and statistical quality inspection. At the same time, starting from 1945, he worked for the Polish Committee for Standardisation (PKN),where he made a significant contribution to restoring and completing of the standardisation achievements the interwar period had brought forth in Poland. He also initiated the statistical quality inspection in Poland achieving its successful implementation in both the industry and army. In the PKN at first he got the position of Standard Editing Department Head, becoming then the General Secretary and finally in 1948 he was appointed to the position of General Executive Officer, holding the post till 1951. The research he conducted in co-operation with Professor Hugo Steinhaus, a famous mathematician, was of crucial importance for standardisation and production inspection in the field of conformity assessment. Among many mathematical papers published that time by engineer Jan Oderfeld it is worthwhile to note those on the so-called principle of duality, that had created a basis for the Ph.D. Thesis on *Statistical set of products classified according to the alternative*, he defended successfully at the Wrocław University and Wrocław University of Technology (that time it was one academic centre) in 1951 (his supervisor was Professor Hugo Steinhaus). In co-operation with Professor Zdzisław Rytel he developed the Classification Scheme of Standards that in Poland has only recently been replaced with the International Classification of Standards (ICS). Within

the years 1951–1974 he pursued his activities in the field of applied mathematics heading the Group of Statistical Quality Inspection at the Mathematical Institute (now, the Industrial Application Department at the Institute of Mathematics of the Polish Academy of Sciences). The research conducted there covered a broad scope of mathematical apparatus applications; i.e., in machine-building, rubber and military industries, as well as in medicine, biology and pharmacology. Moreover, within the years 1951–1954 he gave lectures on statistical quality inspection at the Central School of Planning and Statistics (before World War II and at present known as the Warsaw School of Economics).

Professor Jan Oderfeld pursued his activity in many different fields developing co-operation with a variety of scientific and industrial centres. However, since 1949 he joined the staff of Warsaw University of Technology, his *Alma Mater*, where at first he took a temporary professor position, then in 1955 he was appointed an associate professor and in 1961 he became a full professor. Within the years 1949–1955 he headed the Chair of Aircraft Engines, while since 1955 till his retirement in 1978 he was heading the Chair of Theory of Machines and Mechanisms (at present: the Department of Machine and Robot Theory at the Faculty of Power and Aeronautical Engineering WUT). It was the first TMM chair in Poland, and it was founded by Professor Jan Oderfeld. In first several years of its activity the chair staff taught the subject at all faculties of the Warsaw University of Technology. Professor Jan Oderfeld had created a material base on which the chair pursued its activities, including laboratory, workshop and library. Soon after founding the Chair he developed the teaching course in the Theory of Machines and Mechanisms (TMM) and wrote several first handbooks on the subject in Poland. Within the years 1964–1966 he served as a Dean at the Faculty of Power and Aeronautical Engineering WUT. It was upon his recommendation that, later on, the teaching courses at all mechanical faculties of WUT were changed accordingly, including the following subjects: fundamentals of control engineering, dynamical metrology and fundamentals of experiment planning. He also forced through the idea of introducing numerical methods into both teaching and research.

Since his first paper published in 1933 Professor Jan Odelrfeld has prepared over 200 works in a broad scope of fields (over forty of them were published after his retirement), including 15 books and course books. One can never separate his magnificent scientific achievements from the expert knowledge he gained in practice. Due to the fact that his interests were always many-sided, it is very difficult to classify his works into particular fields. One can only attempt at dividing his activity into three intervals, that overlap each other to a large extent.

The first one, the origins of which date back before the war lasted over 30 years and covered the field of **aircraft engines**. As it was mentioned before, Professor Oderfeld was one of those who constructed the first Polish jet engines.

He dealt also with piston engines, mainly in the aspects of their cooling, timing gear and balance. After World War II he co-operated with the well-known Polish aircraft engine designer Wiktor Narkiewicz, dealing with the timing gear system design (including cams), optimal balance of crankshafts and combustion problems in the engines known in Poland as the WN – type ones. His contribution towards the success of those engines was significant (they were used in Polish aircraft; e.g., of the Bies (Demon) type).

The second interval of his activity that lasted over 30 years, was devoted to **applied mathematics**, mainly in the fields of standardisation and quality inspection. Among his significant achievements one should mention the results he obtained when solving the problems of concentrations in distribution, sign autocorrelogram, dimensional functions in standardisation and similarity of empirical curves. As a good example of his interdisciplinary interests may serve the research into biological system behaviour, conducted with the use of statistical mathematics apparatus.

A significant role Professor Jan Oderfeld played in struggling for standardisation of the system of units, and putting it into order should be emphasized as well. That issue was very important to him, he always claimed that from the engineering point of view, mathematics did not consist only in relations between dimensionless numbers. From the very beginning of his activity professor Jan Oderfeld has been far-sighted; for instance, against many prominent scientists he was in favour of the {kg, m,s} unit system. In the years 1946–1960 he had defended his viewpoint against the opponents within the international activity of ISO, which contributed significantly towards the world-wide implementation of SI system of units.

In the third interval lasting over 50 years the Professor has been dealing with the **theory of machines and mechanisms**, in its broad meaning, i.e., including metrology, control engineering, robotics and biomechanics. It has always been the main field of his activity. One should mention here the research he conducted into the engine balance and the timing gear cams he designed before the war. Later on, the Professor engaged, in a most creative way, into the development of theory of machines and mechanisms, especially in the aspects of classification, kinematics and precision of mechanisms, as well as dynamical similarity, fundamentals of experiments in mechanics of machines and optimisation in machine design. Being the world pioneer in engineering applications of optimisation he became a big name in the last of the aforementioned fields. His first approach to the problem was published as early as in 1954 within the context of economical machine design analysis. Later on, Professor Oderfeld established his scientific school in the field, based on the application of linear and non-linear programming to optimal design of machines and mechanisms. Many algorithms and methods the Professor had developed were implemented into the design practice of complex machines and

mechanisms; e.g., optimisation methods were employed in the design process of many well-known Polish jib cranes.

An original design of magnetic memory drum he patented together with Wiktor Narkiewicz should also be mentioned among his most significant achievements implemented on a large scale. For many years, those drums (produced by ELWRO Wrocław) were part of standard computer equipment in the countries of Eastern Europe, members of the former Council for Mutual Economic Assistance.

For several dozen of years, Professor Jan Oderfeld has pursued an intense activity within the frameworks of different national and international scientific and technical organisations; he was a member of the Committee of Machine Design of the Polish Academy of Sciences, worked for groups and committees of the Polish Federation of Engineering Associations, engaged into the activities of International Standard Organisation, being also a member of the Warsaw Scientific Society.

In 1969, when Professor Jan Oderfeld had served as the President of the Polish Committee for Theory of Machines and Mechanisms, he chaired the organising and scientific committee of the 2nd World Congress on the Theory of Machines and Mechanisms in Zakopane, Poland. During the Congress, representatives of 16 countries founded the International Federation for the Theory of Machines and Mechanisms (IFToMM) (at present: the International Federation for the Promotion of Mechanism and Machine Science). Professor Jan Oderfeld was one of the founding fathers of the organisation and served for ten years in its governing boards. Nowadays, the IFToMM association comprises several dozens of National Committees of TMM. The Professor was a tutor of many Polish scientists who have nowadays performed many prestigious duties within authorities, committees and working groups of the federation, proving the fact that the Polish School of TMM established by Professor Jan Oderfeld has become highly appreciated. Up to now, the Professor has maintained a close co-operation with both the Polish Committee of TMM (being its Honorary President) and IFToMM.

In 1953 Jan Oderfeld was among those who founded the Journal "Applicationes Mathematicae". Within the years 1954–1991 he was a member of the Editorial Board of scientific journal "Archives of Machine Design".

His accomplishments should be also recognised for his over thirty-year-activity within the framework of very popular in Poland Technical Knowledge Contests for secondary school pupils, he was one of the founders and organisers.

His remarkable achievements in the fields of science and teaching as well as his organizational activities, have brought him about many state decorations and medals, including a Commander's Cross of the Order of the Rebirth of Poland (1964), and a Commission of National Education Medal (1976). He was also

awarded many times by Polish and foreign authorities; e.g., Ministry of Higher Educations (including individual awards of the first degree in 1963 and 1978), Polish Society of Mathematics (1974) and other institutions. He was awarded a Gold Badge of Merit issued by the National Federation for Engineering Associations (NOT), was conferred with the rank of Honorary Member of Polish Society of Theoretical and Applied Mechanics, and received a "Pulaski Wings" award granted by the Aviation Chapter of Polish Association of Mechanical Engineers. During the 9th International Congress of IFToMM (Milan, 1995) he was conferred with the rank of Honorary Member of the Federation and Honorary Member of the Editorial Board of the journal "Mechanism and Machine Theory" published by the IFToMM. Recognizing his accomplishments in working for his Alma Mater, the Warsaw University of Technology awarded him a Medal of Merit.

The achievements of Professor Jan Oderfeld outlined above have proved that he can definitely be recognized as an eminent scientist of versatile mind, creative engineer, talented and effective initiator and supervisor of many organizations and various undertakings. For many followers of Professor Jan Oderfeld, including me, he is first of all a magnificent well-respected Teacher who has always been demanding and fair. For over fifty years of his teaching activity he educated a few classes of Air Force officers, many classes of engineers and ten doctors in technical sciences.

The following three rules constitute the motto he has always emphasized and recommended:

- **the theory cannot be separated from the engineering practice, they both must combine forming the engineering art;**
- **each experimental result obtained needs the error estimation;**
- **any detail may occur important for an engineer.**

Now, these rules we recommend to our students.

In view of the above, it is unquestionable that Professor Jan Oderfeld rendered a great service to both the academic community of Warsaw University of Technology as well as Polish and international academic communities. This fully justifies the decision taken by the WUT Senate and supported by the Senates of Universities of Technology in Łódź, Cracow and Gdańsk of awarding the Honorary Doctorate of WUT to Professor Jan Oderfeld.

Prof. Krzysztof Kędziora
Warsaw University of Technology

ENGINEERING TRANSACTIONS • *Engng. Trans.* • **56**, 2, 101–116, 2008
Polish Academy of Sciences • Institute of Fundamental Technological Research

RIGID BODY ASSEMBLY IMPACT MODELS FOR ADIABATIC CUTOFF EQUIPMENTS

M. Massenzio, S. Pashah, E. Jacquelin, A. Bennani

Université de Lyon, Lyon, F-69003, France
Université Lyon 1, UMRT9406, LBMC, IUT B
Département Génie Mécanique et Productique
Villeurbanne, F-69627, France

This paper is concerned with systems consisting of components colliding with each other. In particular, a high velocity adiabatic impact cutoff machine is investigated. For general understanding of the impact dynamics (affected by a large number of parameters), the mechanisms are modelled in a simplified and accurate manner. Two simple models are developed: the energy-balance model and the spring-mass model. The energy-balance model is based on the principle of total energy conservation. It provides only the punch minimum kinetic energy required for efficient cutting. Concerning the spring-mass model, the different components are represented by rigid masses and their deformations are modelled by springs (linear or non-linear in the case of contact stiffness). The resulting non-linear equations are solved using the Newmark numerical technique. The impact force, velocity, displacement and acceleration histories are calculated what makes possible a fine description of the cutoff cycle steps. The two models are helpful for both the design and tuning of the mechanisms involving impacts between their components.

Key words: impact, rigid body, adiabatic cutoff, spring-mass model, energy-balance model.

1. Introduction

A wide variety of engineering applications concern components colliding with each other. This is particularly the case in mechanisms including clearances or gaps. In most cases the principle of operation is based on repeated impacts: impact hammers, high velocity adiabatic impact cutoff, blanking or powder compaction machines, impact-forming machines, etc. On the other hand, impacts may be unwanted because they may prove to be harmful to the reliability of the equipment: rotors with bearing clearance, gears, wheel-rail interaction of high-speed trains, etc. The theoretical models presented in this paper are concerned with high-velocity adiabatic impact cutoff machines. Although similar to conventional presses, high-velocity adiabatic impact presses use high-speed punch motion to carry out the cutting operation. The tool velocity is generally between

10 m/s to almost 100 m/s, whereas in the case of conventional presses, the velocity is about 0.3 m/s and a static approach is satisfactory. When sufficient kinetic energy is imparted to the cutting tool, the material being cut cannot dissipate heat fast enough. The temperature increases adiabatically due to the extremely short time and energy concentration in the local area identified as the "adiabatic zone" [2–4, 7, 10, 11, 14]. The material softens instantly (adiabatic softening) and the moving die separates the material into two parts. The main benefits of adiabatic cutting are high quality end cuts, tight length or volume tolerances, square ends and high production rates. However, the key factor in the success of this technology depends both on creating sufficient energy to reliably reproduce the adiabatic softening phenomenon and on controlling the required energy. The former is a matter of technology, but the latter is associated with complex dynamic phenomena and is of interest for researchers [8]. The process exhibits a cutting tool thrusted by a ram. A clearance allows the tool to accelerate and reach the required velocity before hitting the material. The adiabatic softening completes the cut-off and a die base is needed to stop the tool. This process involves a large number of impacts between the various components of the machine.

Each machine component can be modelled as a nearly rigid body. The phenomena linked to two colliding bodies have been widely studied in the literature [13]. Impact initiates when two bodies move close to each other with relative velocity. The incidence occurs when a single contact point appears on the surface of each body. After incidence, the contact pressure in the small contact area prevents the interpenetration of the bodies. During the impact, the pressure in the contact area produces local deformations and indentations, and has a resultant action that acts on the colliding bodies in opposite directions. Initially, the force increases with increasing indentation and it reduces the relative velocity at which the bodies move close to each other. After a time, the work done by the contact force is sufficient to bring the relative velocity to zero. Subsequently, the elastic energy stored during compression drives the two bodies apart until finally they separate with a acertain relative velocity. As regards the impact between solid bodies, the contact force which acts during the collision, is the result of local deformations that are required for the surfaces of the two bodies to conform in the contact area. The local deformations can be elastic or plastic and vary according to the relative incident velocity and to the hardness of the colliding bodies. In addition to local deformations, there are also global deformations of the bodies. These global deformations mainly depend on the impact velocity, the mass ratio, the boundary conditions and the geometry of the bodies. The physical process during impact is strongly non-linear and discontinuous. A fine numerical analysis of the system is an alternative to tackle the problem (i.e. the finite – elements model). But, it is difficult to understand the phenomena

and to identify the leading parameters, which are required for the fine tuning of the machine. Some simplified models are available in the literature to study impact dynamics. Generally, the models are classified according to the dynamic response of the structure: impact on a half-space, quasi-static approach and complete models [13]. With the first two approaches, energy balance models can be used to predict the maximum contact force and the contact duration [1, 12]. However, the energy balance model is restricted to two free bodies with no external forces. It is not suitable to multi-body impact, and to the impact with an external force applied to the bodies.

In order to enable the design and fine tuning of the high velocity adiabatic impact cutoff machines, appropriate models need to be developed. The objective of this article is to study two models available to analyze the multi-impact dynamics: the energy balance model and the spring-mass model. Section 2 presents the analytical and numerical aspects of the spring-mass model developed for the purpose of the study. An example of a high velocity adiabatic impact cutoff machine is presented in Sec. 3. Sections 3.2 and 3.3 deal with the spring-mass and the energy-balance model results respectively. The two analyses are compared with each other and the relevances of each model are discussed.

2. Spring-mass model

2.1. Equations of motion

A general spring-mass model with n degrees of freedom is considered as shown in Fig. 1. The springs are non-linear and the behaviour law is written as:

$$P = k \cdot x^p \tag{2.1}$$

where P is the spring force, k is the contact stiffness parameter and p depends on the non-linear effect.

Considering a particular mass "i", the equation of motion is defined as the non-linear differential equation (Fig. 2):

$$\begin{aligned} &m_i \cdot \ddot{x}_i + \lambda_1 \cdot k_i \cdot |x_i - x_{i-1}|^{p_i} + c_i \cdot (\dot{x}_i - \dot{x}_{i-1}) \\ &\qquad +\lambda_2 \cdot k_{i+1} \cdot |x_i - x_{i+1}|^{p_{i+1}} + c_{i+1} \cdot (\dot{x}_i - \dot{x}_{i+1}) = F_i \\ &\text{where} \\ &\lambda_1 = 1 \quad \text{for } x_i > x_{i-1} \quad \text{else } -1 \\ &\lambda_2 = 1 \quad \text{for } x_i > x_{i+1} \quad \text{else } -1, \end{aligned} \tag{2.2}$$

which may be expressed as

$$[m] \cdot [\ddot{x}] + [c] \cdot [\dot{x}] + [P(x)] = [F] \tag{2.3}$$

for the complete system, where the mass matrix $[m]$ and the viscous damping matrix $[c]$ are given by:

$$[m] = \begin{bmatrix} m_1 & 0 & \dots & 0 \\ 0 & m_2 & & \vdots \\ \vdots & & \ddots & \\ 0 & \dots & & m_n \end{bmatrix},$$

(2.4)

$$[c] = \begin{bmatrix} c_1 + c_2 & -c_2 & 0 & \dots & 0 \\ -c_2 & c_2 + c_3 & -c_3 & & \vdots \\ 0 & -c_3 & \ddots & & \\ \vdots & & & & \\ 0 & \dots & 0 & -c_n & c_n + c_{n+1} \end{bmatrix}.$$

$[P(x)]$ is the non-linear forces vector and it is given by:

(2.5)

$$[P(x)] = \begin{bmatrix} k_1 \cdot x_1^{p_1} + k_1 \cdot (x_1 - x_2)^{p_2} \\ k_2 \cdot (x_2 - x_1)^{p_2} + k_3 \cdot (x_2 - x_3)^{p_3} \\ \vdots \\ k_n \cdot (x_n - x_{n-1})^{p_n} + k_{n+1} \cdot x_n^{p_{n+1}} \end{bmatrix}.$$

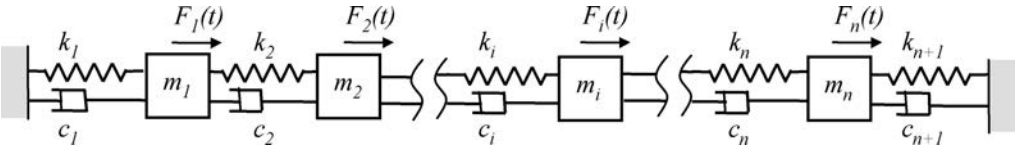

FIG. 1. Non-linear spring-mass system with n degrees of freedom.

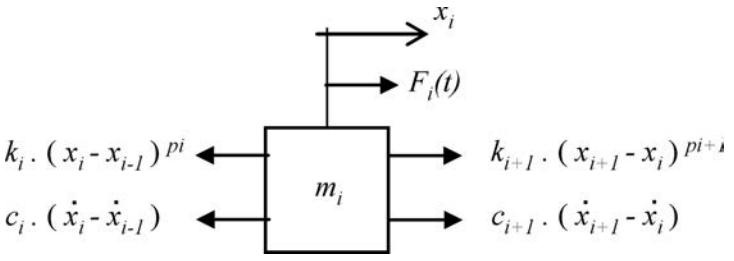

FIG. 2. Notation for the mass "*i*".

The velocity vector $[\dot{x}]$, acceleration vector $[\ddot{x}]$ and external forces vector $[F]$ are defined as:

$$[\dot{x}] = \begin{bmatrix} \dot{x}_1(t) \\ \dot{x}_2(t) \\ \vdots \\ \dot{x}_n(t) \end{bmatrix}, \qquad [\ddot{x}] = \begin{bmatrix} \ddot{x}_1(t) \\ \ddot{x}_2(t) \\ \vdots \\ \ddot{x}_n(t) \end{bmatrix}, \qquad [F] = \begin{bmatrix} F_1(t) \\ F_2(t) \\ \vdots \\ F_n(t) \end{bmatrix}. \tag{2.6}$$

2.2. Numerical integration

The Newmark numerical technique [9] is used to calculate the displacement vector $[x]$ from Eq. (2.3). First, the time duration of impact T is subdivided into q equal steps $\triangle t$, so that $\triangle t = T/q$. Considering that the displacement vector (x_i), the velocity vector $(\dot{x}_i)$ and the acceleration vector $(\ddot{x}_i)$ are known for time step $(t_i = i \cdot \triangle t)$, the method uses an approximation to calculate the value of the three vectors at the time step t_{i+1}. The non-linear equations of motion have to be linearized in order to suit the method. Assuming that the solution is known at time step t_i, the equation at time step t_{i+1} is given by:

$$[m] \cdot [\ddot{x}_{i+1}] + [c] \cdot [\dot{x}_{i+1}] + [P(x_{i+1})] = [F_{i+1}] \tag{2.7}$$

$[P(x_{i+1})]$ is expressed as:

$$[P(x_{i+1})] = [P(x_i)] + [K_i] \cdot [\triangle x_i] \tag{2.8}$$

where $[\triangle x_i] = [x_{i+1}] - [x_i]$ and $[K_i]$ is the stiffness tangent matrix at time step t_i. Equation (2.7) and Eq. (2.8) give:

$$[m] \cdot [\ddot{x}_{i+1}] + [c] \cdot [\dot{x}_{i+1}] + [K_i] \cdot [x_{i+1}] = [\overline{F}_{i+1}] \tag{2.9}$$

with

$$[\overline{F}_{i+1}] = [F_{i+1}] - [P(x_i)] + [K_i] \cdot [x_i]. \tag{2.10}$$

Since the right-hand side of Eq. (2.10) is completely known, this equation can be solved for x_{i+1}, using the Newmark method. The x_{i+1} found is only an approximate vector, due to the linearization process used in Eq. (2.10). To improve the accuracy of the solution and to avoid the development of numerical instabilities, an iterative process can be used within the current time step (e.g. Newton Raphson).

For the linearization approximation of Eq. (2.10), the tangent matrix stiffness is calculated. This is obtained by differentiating the vector of non-linear forces $[P(x)]$ with respect to the displacement vector $[x]$, i.e.:

$$[K] = \frac{\partial}{\partial [x]} [P(x)]. \tag{2.11}$$

From Eq. (2.5), one obtains:

$$
(2.12)\qquad [K] = \begin{bmatrix}
\begin{pmatrix} p_1\, k_1\, x_1^{p_1-1} \\ +\, p_2\, k_1\, (x_1 - x_2)^{p_2-1} \end{pmatrix} & \begin{pmatrix} -p_2\, k_1\, (x_1 - x_2)^{p_2-1} \end{pmatrix} & & \\
\begin{pmatrix} -p_2\, k_1\, (x_1 - x_2)^{p_2-1} \end{pmatrix} & \begin{pmatrix} p_2\, k_2\, (x_2 - x_1)^{p_2-1} \\ +\, p_3\, k_3\, (x_2 - x_3)^{p_3-1} \end{pmatrix} & & \\
\vdots & & & \\
0 & \cdots & \cdots & 0 \\
 & & & \vdots \\
 & & \ddots & \\
 & & & \begin{pmatrix} p_n\, k_n\, (x_n - x_{n-1})^{p_n-1} \\ +\, p_{n+1}\, k_{n+1}\, x_n^{p_n} \end{pmatrix}
\end{bmatrix}.
$$

3. Modelling of a simplified cutting machine

3.1. The model

Figure 3 (left) shows the simplified adiabatic cutting machine to be modelled (i.e. only the main parts of the actual machine are taken into account). The metal sheet lies on the cutting-off die which is assumed to be linked to the inertia reference frame, i.e. the suspension is not considered. The punch is moved by a hydraulic actuator (cylinder is not represented). Figure 4 a shows the cylinder force. The force is initially zero. It becomes constant for 0.1 s (37 000 N) and eventually returns to zero. A Haversine function is used to represent the smooth transitions between zero and 37 000 N. The transition duration is 2 ms. After the cutting phase, the punch is stopped by the die base. The spring-mass model associated is shown in Fig. 3 (right). The punch and the die base are represented by two rigid masses m_1 and m_2 respectively. The two masses are connected through a Hertzian spring that represents the contact load-deformation characteristics and the initial gap (K_{12}) [15], and the die base is attached to the reference frame through a linear spring (K_{22}). The metal sheet is represented by the relationship between the force and the displacement [5, 6] including the

material's properties, the thickness and the cutting perimeter of the sheet. This relationship and the initial gap are represented by the non-linear stiffness K_{11}, given in Fig. 4 b (with no gap). The initial gap of spring K_{11} is one of the tuning parameters of the machine. The distance between the punch and the metal sheet enables the punch to reach the required cutting velocity. The initial gap of spring K_{12} is the sum of the initial gap of spring K_{11}, of the metal sheet thickness and of a supplementary gap to assure that the metal sheet is completely cut before the punch impacts the die base. Numerical values of mass and stiffness are given in Table 1.

The numerical integration is performed as presented in Sec. 2.2, with a time step of 10^{-5} s and a time duration of 0.2 s. Four different initial gaps between the punch and the metal sheet are tested : no gap, 9 mm, 10 mm and 43 mm.

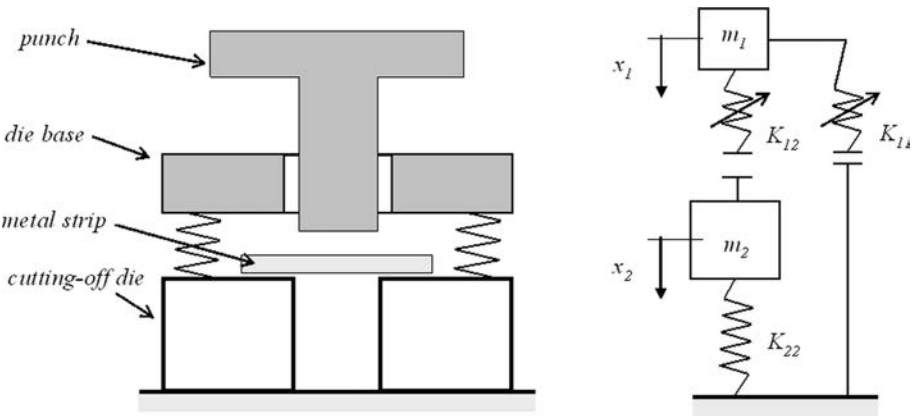

FIG. 3. The model (left: the simplified machine, right: the spring-mass model).

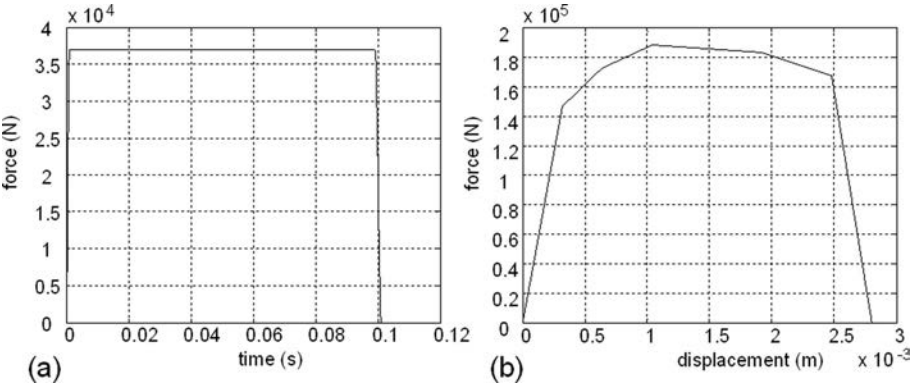

FIG. 4. Force applied to the punch (a); relationship between the force and the displacement (b).

Table 1. Numerical data of the two-degrees-of-freedom model.

Mass		Stiffness	
m_1	40 kg	K_{11}	initial gap – 4 values tested: 0, 9, 10 & 43 mm & cutting force-displacement relationship (Fig. 4 b)
m_2	100 kg	K_{12}	initial gap = initial gap of K_{11} + metal sheet thickness (2.8 mm) + supplementary gap (0.2 mm) & contact law : $P = 10^{13} \cdot x^{2,2}$ (x is the indentation)
		K_{22}	2.10^8 N/m

3.2. The spring-mass model

Figures 5, 6 and 7 show the punch and the die base displacement, velocity and acceleration history respectively, for the four initial gaps (0, 9, 10 & 43 mm). On a single plot, Fig. 8 shows the punch displacement relative to the metal sheet (synthesis of the above results). Figure 9 shows the force history between the punch and the metal sheet.

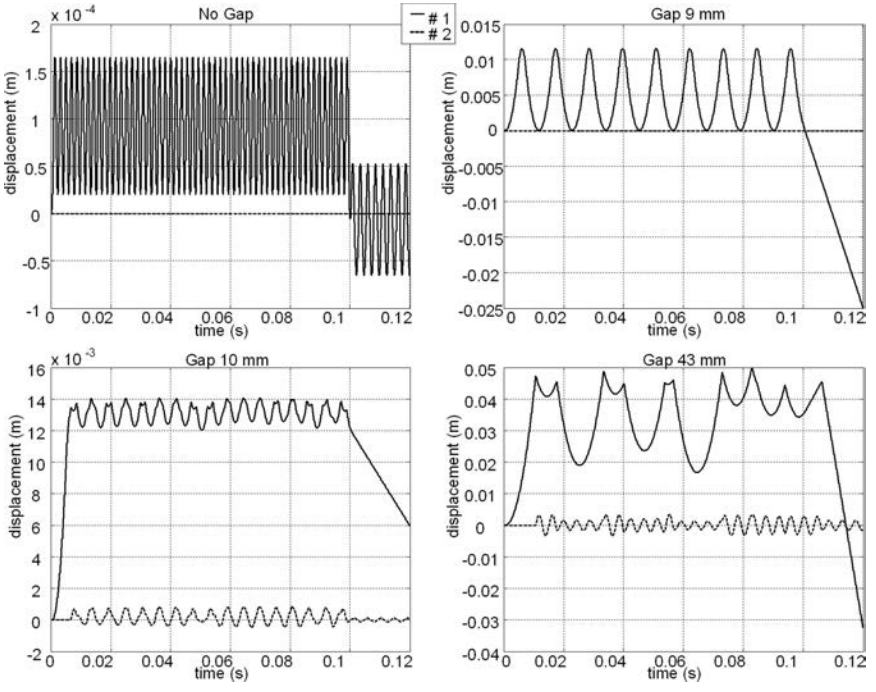

FIG. 5. The displacement history (no gap – gap 9 mm – gap 10 mm – gap 43 mm).

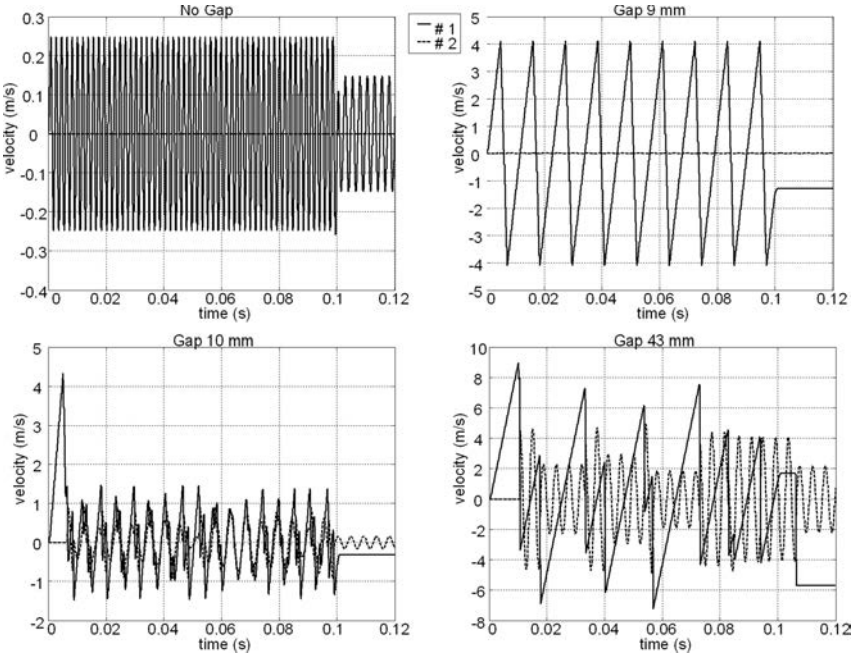

FIG. 6. The velocity history (no gap – gap 9 mm – gap 10 mm – gap 43 mm).

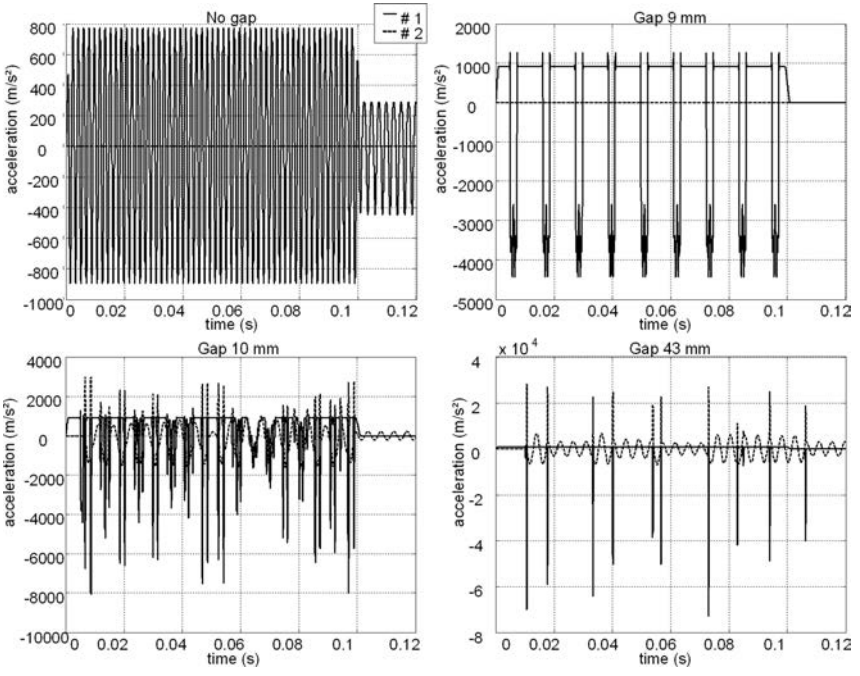

FIG. 7. The acceleration history (no gap – gap 9 mm – gap 10 mm – gap 43 mm).

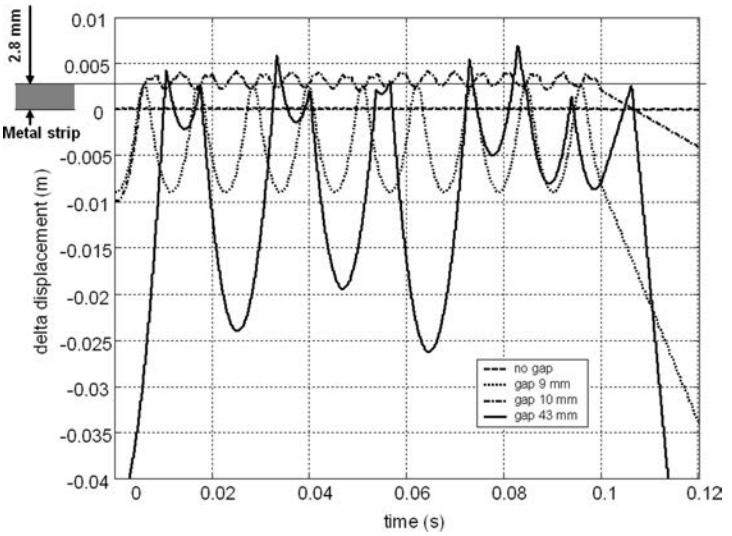

FIG. 8. The displacement relative to the metal sheet (no gap – gap 9 mm – gap 10 mm – gap 43 mm).

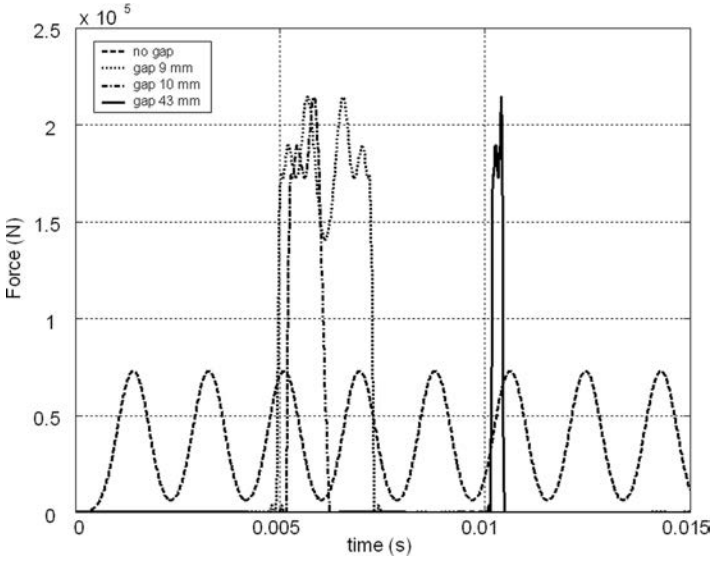

FIG. 9. The force history (no gap – gap 9 mm – gap 10 mm – gap 43 mm).

The results with no gap are typical of a system with one degree of freedom with Heaviside excitation (the punch is the mass and the metal sheet is the spring). The displacements are very small: between -0.204 mm and 0.164 mm within the range $0 - 0.1$ s. This means that the metal sheet is slightly indented.

After 0.1 s (*i.e.* no more ram force), the response oscillates between −0.065 mm and 0.052 mm, corresponding to the free vibrations of a one-degree-of-freedom system. With an indentation below 0.320 mm, the relationship between the force and the displacement is linear (Fig. 4 b). The corresponding stiffness is $K_{11} = 4.58.10^8$ N/m. The eigenfrequency of the one-degree-of-freedom system can be expressed as:

$$f = \frac{1}{2\pi}\sqrt{\frac{K_{11}}{m_1}} \tag{3.1}$$

leading to the value of 538 Hz. In Fig. 5, the 53.5 oscillations within the range $0-0.1$ s lead to the same eigenfrequency value. The velocity of the punch is also limited to very small values (less than 0.25 m/s), so as the acceleration (less than 900 m/s^2). Both results show that the dynamic effects are insignificant in the no-gap case. Furthermore, there is no loss of contact as shown by the harmonic behaviour of the acceleration. As the metal sheet is not cut, the die base remains at rest. Note that the model does not take into account the effect of repeated damage on the metal sheet, whereas the actual cutting process can lead to final cutting. Anyway, the adiabatic cutting process is efficient only if the first impact leads to complete cutting. If not, the quality of the surface condition is of no interest. The present model is not devised to take these effects into account.

With a gap of 9 mm, the metal sheet is not cut either. Figure 5 shows a maximum displacement of 11.5 mm. The indentation of the metal sheet is then 2.5 mm (lower than the thickness 2.8 mm, Fig. 8). In comparison with the case with no gap the mechanisms are different. The amplitude of the velocity and acceleration are higher: the maximum velocity is 4.09 m/s, and the maximum acceleration is 4426 m/s^2. Consequently, in Fig. 6 and 7 one can observe successive rebounds of the punch on the metal sheet.

The metal sheet is cut with an initial gap of 10 mm, as shown in Fig. 5. During the first impact, the displacement reached the value of 13.4 mm, corresponding to an "indentation" of 3.4 mm – larger than the thickness: 2.8 mm (Fig. 8). After the cutoff, the punch is stopped by the die base, and several punch impacts on the die base are observed until the external force returns to zero (0.1 s). Then, the punch has a uniform movement and the die base oscillates such as a one-degree-of-freedom system. Hence, the minimum velocity for the cutoff is 4.32 m/s. With a gap of 43 mm, the cutoff is similar to the latter case, with higher values for the displacement, velocity and acceleration.

Focusing only on the results for the initial gap of 43 mm, the cutting work can be divided into 4 steps as shown in Fig. 10.

- Step #1 is the acceleration of the punch. The leading parameters of this step are the cylinder force, the initial gap and the mass of the punch (m_1)

(Fig. 10 – 1). After 10 ms of free run, the punch impacts the metal sheet (Fig. 10 – 2 start).

- Step #2 is the cutting of the metal sheet, both influenced by the cylinder force (which is still active) and by the initial velocity (8.93 m/s). The duration of cutting is 0.33 ms (whereas it is about 3 ms with a conventional press). At the end of step #2 (Fig. 10 – 2 end), the punch velocity is still high: (7.9 m/s). During this step, the maximum acceleration of the punch is 4424 m/s^2, equal to the difference between the acceleration of the punch (37000/40 = 925 m/s^2) and the resistance force of the metal sheet (Fig. 4 b).
- Step #3 starts just after cutting as the punch impacts the die base (Fig. 10 – 3). Oscillations of the punch are due to successive rebounds on the die base under the action of the cylinder. These successive shocks induce free oscillations of the die base (behaving as a one-degree-of-freedom system). As the velocity of the punch is still high, the accelerations of the punch can reach very high values (73000 m/s^2); this result is of importance for the actual machine parts design). Step #3 lasts until the cylinder stops acting on the punch.
- In step #4, the free oscillations of the die base have to be treated by specific dampers. The uniform movement of the punch has to be clamped for the next cutting (Fig. 10 – 4). This step is of no interest for the present study and the results are not discussed in this paper.

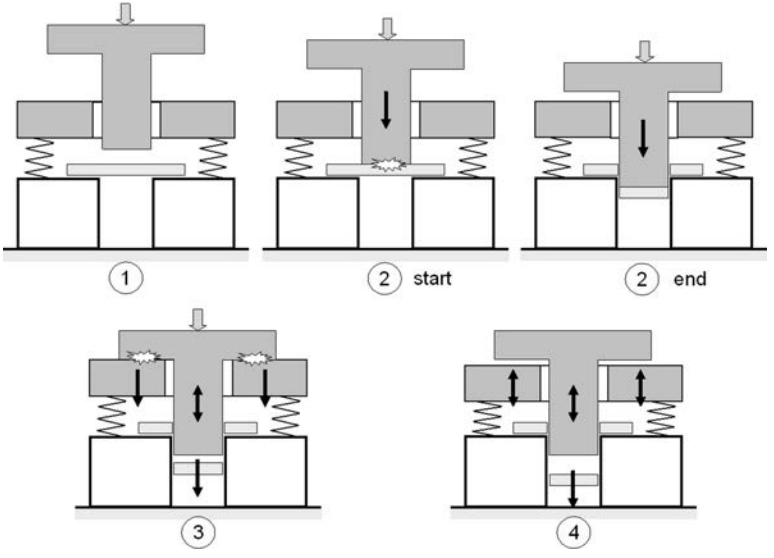

Fig. 10. The 4 steps of cutting.

It is clear from Fig. 8 that the minimum initial gap required for the cutting is 10 mm. In the no-gap case, step #1 is not possible and therefore there is no kinetic energy stored before contact for the cutting. The force of the punch on the metal sheet reaches the maximum value of 72 800 N (Fig. 9), which is higher than the force produced by the rams (37 000 N) due to dynamic effects, but less than the maximum force required for cutting (Fig. 4 b). The maximum forces for the three different gaps: 9 mm, 10 mm, 43 mm are approximately the same: 214 000 N. This is higher than the maximum force from the cutting relationship between the force and the displacement: 189 00 N (Fig. 4 b). Yet, with a 9 mm gap, the kinetic energy stored during step #1 is not sufficient and therefore step #2 is not fully completed.

Table 2. Results for the four gaps (spring-mass model).

Gap (mm)	Cutting?	before cutting (step #1)		during cutting (step #2)	
		Velocity (m/s)	Kinetic energy (J)	duration (ms)	Max acceleration (m/s^2)
0	no	0	0	–	896 (oscillations)
9	no	4.09	335	–	4426 (rebounds)
10	yes	4.32	373	1.07	8043
43	yes	8.93	1594	0.33	69800

Table 2 shows a synthesis of the main data required to analyze the cutting: velocity before impact and the corresponding kinetic energy, cutting duration and maximum acceleration of the punch. The data will be compared to the results from the energy-balance model as follows.

3.3. The energy-balance model

The force of the cylinder acting on the punch is 37 000 N. In the case of a static process (conventional press), the force required for cutting of the metal sheet is at least $1.89\ 10^5$ N (see relationship between the force and the displacement in Fig. 4 b). It is then the kinetic energy stored by the punch during the step #1 that controls the cutting.

The energy-balance model is based on the principle of conservation of total energy of the punch-metal sheet system. Assuming that the structure behaves quasi-statically, the kinetic energy of the impacting punch ($E_{\text{cin}} = \frac{1}{2}.m_1.v_1^2$ at the end of step #1) is equated to the energy required for the metal sheet cutting (E_{cut} – step #2):

$$E_{\text{cin}} = E_{\text{cut}}. \tag{3.2}$$

The constant force of the ram on the punch, essential during the step #1, is neglected during impact (step #2). Moreover, the energy losses from friction between parts, material damping and vibrations are neglected.

The required cutting energy (step #2) is the integral of the product of the force acting on the metal sheet (F_{cut}) and the deformation (x):

$$E_{\text{cut}} = \int_0^e F_{\text{cut}}.\mathrm{d}x, \tag{3.3}$$

where e is the thickness of the metal sheet, and F_{cut} is derived from the relationship between the force and the displacement (Fig. 4 b). For the present case, $E_{\text{cut}} = 436$ J.

During step #1, Newton's second law of motion applied to the punch led to:

$$F = m_1.\gamma_1, \tag{3.4}$$

where F is the ram's force that can be considered constant, and γ_1 is the punch acceleration. From Eq. (3.4) the punch acceleration is constant and equal to 925 m/s^2. As the initial velocity and displacement are zero, one can obtain the velocity and displacement functions:

$$v_1 = \gamma_1 \cdot t, \tag{3.5}$$

$$x_1 = \frac{1}{2} \cdot \gamma_1 \cdot t^2. \tag{3.6}$$

From Eq. (3.6), equating the displacement to the initial gap, one can solve the time of impact and consequently, the velocity and the kinetic energy before impact. The results (Table 3) agree with the spring-mass model (Table 2 – note that only the acceleration step #1 is concerned). Comparing the kinetic energy before impact and the result of Eq. (3.3): $E_{\text{cut}} = 436$ J, the energy-balance model does not predict complete cutoff with a 10 mm gap.

Table 3. Results for the four gaps (energy-balance model).

Gap (mm)	Acceleration (m/s^2)	Time of impact (ms)	Impact velocity (m/s)	Kinetic energy (J)
0	925	0	0	0
9	925	4.41	4.08	333
10	925	4.65	4.30	370
43	925	9.64	8.92	1591

Equating the minimum kinetic energy with the cutting energy from Eq. (3.3), the minimum impact velocity for cutting is:

$$v_1 = \sqrt{\frac{2.E_{\text{cut}}}{m_1}} \tag{3.7}$$

which gives a velocity of 4.67 m/s. With Eqs. (3.4), (3.5) and (3.6), the minimum gap (x_{gap}) is:

$$x_{\text{gap}} = \frac{E_{\text{cut}}}{F} \tag{3.8}$$

which gives a minimum gap of 11.8 mm. The minimum gap calculated by means of the energy-balance model agrees reasonably well with the results from the spring-mass model (minimum gap between 9 to 10 mm – Table 2).

4. Conclusions

This paper has presented two simple models, the energy-balance model and the spring-mass model, to describe the dynamics of mechanisms involving clearances or gap and featuring repeated impacts. Both models are applied to a high velocity adiabatic impact cutoff machine. The energy-balance model is based on the principle of total energy conservation: the impacting component kinetic energy is equated to the impacted component deformation energy. The spring-mass model uses the assumption that the components are rigid enough to be modelled by masses, and that the masses are connected by linear or non-linear springs. Both models include contact stiffness between the components by the use of non-linear springs.

The energy-balance model is able to predict the minimum kinetic energy required for the metal sheet cutoff. The model is simple for use, and the results provided are useful for tuning of one essential parameter of the machine: the value of the initial gap between the punch and the metal sheet. However, the model is limited to systems with only two components.

The development of the spring-mass model is more complex, and particularly a numerical integration of displacements is needed (Newmark numerical technique). Unlike the energy-balance model, it can be applied to systems with more than two components. The minimum kinetic energy calculated with the energy-balance model agrees reasonably well with the spring-mass model prediction. Moreover, the spring-mass model predicts the displacement, the velocity, the acceleration and the contact force history for each mass. Accurate analysis of the cutoff process shows that the kinetic energy of the punch before impact is the leading parameter, and that the force of the ram has a small influence during the cutoff. This fact can explain accurately why the energy-balance is efficient.

The two models presented in this paper can be applied to other vibratory machinery and equipment, featuring multi-degree-of-freedom oscillators with colliding components.

References

1. S. Abrate, *Modeling of impacts on composite structures*, Composite structures, **51**, 2, 129–138, 2001.
2. A.-S. Bonnet-Lebouvier, A. Molinari and P. Lipinski, *Analysis of the dynamic propagation of adiabatic shear bands*, International Journal of Solids and Structures, **39**, 16, 4249–4269, 2002.
3. T. J. Burns and M. A. Davies, *On repeated adiabatic shear band formation during high-speed machining*, International Journal of Plasticity, **18**, 1, 487–506, 2002.
4. X. W. Chen, Q. M. Li and S. C. Fan, *Initiation of adiabatic shear failure in a clamped circular plate struck by a blunt projectile*, International Journal of Impact Engineering, **31**, 7, 877–893, 2005.
5. A. Eberle, D. Klingbeil and J. Schicker, *The calculation of dynamic j_R-curves from the finite element analysis of a Charpy test using a rate-dependent damage model*, Nuclear Engineering and Design, **198**, 1–2, 75–87, 2000.
6. A. L. Gurson, *Continuum theory of ductile rupture by void nucleation and growth: Part I, yield criteria and flow rules for porous media*, Journal of Engineering Materials and Technology, **99**, 2–15, 1977.
7. J. R. Klepaczko, *Review on critical impact velocities in tension and shear*, International Journal of Impact Engineering, **32**, 1–4, 188–209, 2005.
8. G. W. Luo, *Dynamics of an impact-forming machine*, International Journal of Mechanical Sciences, **48**, 11, 1295–1313, 2006.
9. S. S. Rao, *Mechanical vibrations*, Second edition, Addison-Wesley Publishing Company, 1990.
10. K. M. Roessig and J. J. Mason, *Adiabatic shear localization in the dynamic punch test, part I: experimental investigation*, International Journal of Plasticity, **15**, 3, 241–262, 1999.
11. K. M. Roessig and J. J. Mason, *Adiabatic shear localization in the dynamic punch test, part II: numerical simulations*, International Journal of Plasticity, **15**, 3, 263–283, 1999.
12. K. N. Shivakumar, W. Elber and W. Illg, *Prediction of impact force and duration due to low velocity impact on circular composite laminates*, ASME, **52**, 674–680, 1985.
13. W. J. Stronge, *Impact Mechanics*, Cambridge University Press, Cambridge 2000.
14. X. Teng, T. Wierzbicki and H. Couque, *On the transition from adiabatic shear bending to fracture*, Mechanics of Materials, **39**, 2, 107–125, 2007.
15. S. Timoshenko and N. Goodier, *Theory of elasticity, 3rd edition*, McGraw-Hill, New-York 1970.

Received February 14, 2007; revised version October 2, 2007.

ENGINEERING TRANSACTIONS • *Engng. Trans.* • **56**, 2, 117–157, 2008
Polish Academy of Sciences • Institute of Fundamental Technological Research

CONSTITUTIVE MODELLING AND PARAMETER IDENTIFICATION FOR RUBBER-LIKE MATERIALS

Z. N o w a k

Polish Academy of Sciences,
Institute of Fundamental Technological Research
Department of Mechanics of Materials
Świętokrzyska 21, 00-049 Warszawa, Poland

The aim of the paper is to determine the phenomenological model to characterize the stress-strain relation and to simulate the behaviour of solid polyurethane (PUR) rubbers used in civil engineering, as well as to present the process of identification of model parameters for such materials. For the material studied the strain energy density function was established and a general constitutive relationship for the second-order tensor of Piola–Kirchhoff stress for elasticity is determined. Constitutive relationships for engineering stress in terms of the principal stretches are also specified. The paper presents the method of identification of parameters for constitutive models of hyperelasticity and hypoelasticity for the accessible experimental data. The applied identification procedure is based on the feature of two-phase structure of polyurethane material and is supported by the experimental data from uniaxial quasi-static tension and compression tests. In the analysis, the material behaviour was considered both for the case of incompressible deformation and also for the case of slightly compressible, nonlinearly elastic materials that are homogeneous and isotropic. The change of volume was admitted too, in range of large deformations in a tension and compression test. The attempt of description of stress-softening phenomenon was undertaken in rubber-like materials, for a given level of strain, under unloading (the Mullins effect) caused by the damage of microstructure of this material. Different descriptions of the stress-softening phenomenon were already proposed in the literature but they fail to give fully satisfactory conformity of experimental data with theoretical predictions. The phenomenological model by Elias–Zúñiga and Beatty, *A new phenomenological model for stress-softening in elastomers*, ZAMP, **53**, 794–814, 2002, for such materials was modified by different softening functions and a simplified version of this model was identified, based on the experimental data. In the proposed model, the damage of microstructure was described by a new exponential function, which depends on the current magnitude of intensity of strain and its earlier maximum value during the process of material loading. In this paper, a suitable analysis of existent models and their verification based on experimental data for polyurethane rubber is presented for uniaxial experiments. It is shown that the magnitude of stress-softening varies with strain and this phenomenon increases with the magnitude of the pre-strain and the type of loading: monotonic tension, compression or cyclic loading. The obtained results are presented graphically for uniaxial tension and compression.

Key words: rubber-like material, hyperelastic constitutive model, damage of polyurethane rubber.

1. Introduction

Polyurethane (PUR) materials, among other polymers and elastomers, exhibit high elasticity combined with high friction resistance what results in a wide array of applications, e.g. as engine mounts, bump stoppers or flexible seismic isolator pads. Polyurethanes are randomly segmented copolymers (Qi and Boyce [45], Król [46]), composed of hard and soft segments forming a two-phase microstructure. The hard domains are immersed in a rubbery soft segment matrix (Król [46]) and, depending on the hard segment content, the morphology of the hard domains changes from one of the isolated domains to one of the interconnected domains. Phase separation occurs in most PUR due to the intrinsic incompatibility between the hard segments and soft segments: the hard segments, composed of polar materials, can form carbonyl to amino-hydrogen bonds and thus, tend to cluster or aggregate into ordered hard domains, whereas the soft segments form the amorphous domains. The presence of hard domains in segmented polyurethanes is very important for their mechanical properties. In segmented polyurethanes, hard domains act as physical crosslinks, playing a role similar to chemical crosslinks in vulcanizates and imparting the material's elastomeric behaviour. Since hard domains also occupy significant volume and are stiffer than the soft domains, they also play the role of effective nano-scale fillers and render a material behaviour similar to that of a composite (Król [46]). At room temperature, soft domains are above their glass transition temperature and impart the material its rubber-like behaviour; hard domains are below their glassy or melting transition temperature and are supposed to govern permanent deformation, high modulus and tensile strength. The domain structure also imparts PUR's versatility in mechanical properties. A wide variety of property combinations can be achieved by varying the molecular weight of the hard and soft segments, their ratio and chemical type. At present, polyurethane materials form an important group of products because of their advantage in chemical resistance and excellent mechanical properties.

It is well known that rubber-like materials exhibit a strongly non-linear behaviour, characterized by large strain and a non-linear stress-strain behaviour under static conditions. Under cyclic loading conditions the stress-softening phenomena are observed. The stress-softening phenomenon, also called the Mullins effect, is characterized by an important loss of stiffness during the first cycles of fatigue experiments. More precisely, the Mullins effect is defined as a strain-induced stress-softening of the material, that takes place after the first monotonic loading path of loading cycles. Most of the hyperelastic models of elastomers assume that the Mullins effect takes place during the first cycle of loading and that it depends only on the maximum strain endured previously by the material. These prerequisites are quite acceptable in view of experimental observations.

As the physical foundations of the phenomenon are not well established, a majority of studies propose phenomenological constitutive equations. Many authors use the thermodynamical framework of Continuum Damage Mechanics (CDM), which was extended to the case of elastomers in order to simulate the Mullins effect.

The general three-dimensional case on the subject is due to SIMO [22] who derived a large-strain viscoelastic constitutive equation with damage for rubber-like materials. This model was improved by introducing microscopic concepts by GOVINDJEE and SIMO [23]. More recently, several authors developed phenomenological hyperelastic models with damage to describe the Mullins effect in engineering applications (DE SOUZA NETO *et al.* [11]; MIEHE [27]; MIEHE and KECK [47]; DE SIMONE *et al.* [39]). Another approach used to develop constitutive equations for the Mullins effect is based on the two-phase model of MULLINS and TOBIN [24]. These concepts postulate that the polymer network evolves under deformation; they assume that parts of the network are broken and others are deformed during loading. In this approach, the stress should be corrected by a scalar deformation function that depends on the given measure of deformation, expressed as a scalar function of the principal invariants of the left Cauchy–Green tensor.

Similarly, BEATTY and KRISHNASWAMY [16] derived a constitutive equation that generalized the previous papers by JOHNSON and BEATTY [15] on particular deformation states. In this work, the two-phase theory of MULLINS and TOBIN [24] is considered, and the transformation of hard regions into soft regions is entirely controlled by a stress-softening function, that depends on the maximum strain previously endured by the material. This function corrects the strain-energy function under loading; a different form of it was recently proposed by ELIAS–ZÚÑIGA and BEATTY [17]. The paper presented by OGDEN and ROXBURGH [19] applied an approach which differs from the aforementioned theories because the stress-softening function (that depends on the maximum strain energy endured by the material) is activated only on unloading paths. This theory greatly simplifies the identification of material parameters, but it does not respect the physical phenomenon of network changes during loading. The constitutive equations based on network evolution are more specific for polymers than CDM, but the corresponding thermodynamical framework is not well-defined. Nevertheless, it appears that the constitutive equations obtained by the two approaches, i.e. CDM and the network evolution, are similar. More complex models based on viscoelasto-plastic theories have been also proposed as, for example, in the papers by LION [40], SEPTANIKA and ERNST [41] and ANDRIEUX and SAANOUNI [42].

There is no general agreement on the explanation of the microscopic and mesoscopic origins of the Mullins effect. MULLINS [26] suggested that stress soft-

ening in two-phase elastomers is due to the breakdown of interactions between the filler particles and the rubber matrix. The mesoscopic properties of real materials, however, are not uniform, and the polymerization process generates non-uniformity in the distances between the filler particles. The interactions between the phases suggests that after the primary loading, the material structure must be more complex than in the virgin state in which the chains are short. This condition is a necessary condition for prediction of the stress softening. It is not, however, a special feature of the MULLINS [26] or ELIAS–ZÚÑIGA and BEATTY [17] models, and it must also hold for any model with limited chain extensibility. For example, the model used by MARCKMANN *et al.* [43] based on the eight-chain Arruda–Boyce model exhibits the same effect. The model presented by HORGAN *et al.* [12] suggests that during the primary loading, degradation of the material occurs. It is possible that as degradation continues, a rearrangement of the network, involving displacement of network junctions, may also take place.

The main objective of this paper is to identify the phenomenological model of the polyurethane elastomer materials used in the civil engineering and railway industry. Here, the emphasis is laid on models that can be implemented in finite-element software and used for engineering applications. The mechanical behaviour of a representative PUR material is studied in a series of uniaxial tension and compression tests, investigating cyclic loading effects on the large-strain deformation behaviour. A constitutive model for the observed stress-strain behaviour is then developed and compared directly to experimental data. Both the monotonic uniaxial tension loading and uniaxial compression and subsequent unloading curves are examined. The experimental data presented recently by KWIECIEŃ and ZAJĄC [20] and KWIECIEŃ *at al.* [21], exhibit a non-monotonic variation of stress softening with the extent of deformation. The analysis of experimental results has also shown that the property of stress softening in polyurethane elastomer strongly depends on the magnitude of pre-strain. Uniaxial tension and compression examples are presented in order to highlight the influence of the loading path on the material behaviour. The identification of material parameters for uniaxial monotonic loading leads to a good qualitative agreement for both the uniaxial tensile and compression conditions. As most of the phenomenological models developed for the Mullins effect are based on the microstructural damage of the JONHSON and BEATTY [15] theory, it is of great importance to rationalize its use and to exhibit its advantages and limitations in this context.

This paper is restricted to hyperelasticity with isotropic damage. Cyclic compression experimental data are used to construct the evolution equation of the stress-softening variable and to exhibit some limitations of this approach. The emphasis is laid on the restrictions of the damage theory as applied to the Mullins effect with respect to physical phenomena, and on the choice of the damage soft-

ening function and criterion. The corresponding analysis for different forms of softening functions appearing in constitutive models are considered and the results for the axial tests are presented. The new forms of the softening function assumed in our model of the Mullins effect aim to explain the difficulties in fitting the data by models which were formulated by OGDEN and ROXBURGH [19], ELIAS–ZÚÑIGA and BEATTY [17], QI and BOYCE [45] and others.

We begin in Sec. 2 with a brief description of physical aspects of the internal damage of rubber-like materials with micro-phase separation. In Sec. 3, the constitutive framework is presented. The emphasis is laid on the uniaxial tension and compression. Section 4 is devoted to the experimental results for polyurethane elastomers. The parameters identification process, as the integral part of constitutive modelling, are presented and discussed in Sec. 5 and the conventionally represented uniaxial experimental data are reanalysed in a manner consistent with the theory.

The numerical part of the identification work for uniaxial cycle loading with Mullins effect is presented in figures in Sec. 6. We concentrate on the Mullins effect and we are not concerned with hysteresis, residual strain, thermal and viscoelastic effects. The proposed model is purely phenomenological and does not take into account the physical structure of the material; hence it can be applied to any material exhibiting the Mullins effect. We assume that the virgin material is isotropic with respect to an undeformed and unstressed state. In Sec. 6.1 we define the terms damage function, which depends on the principal stretches, and damage point, which depends on the principal directions and the history of the right stretch tensor. Finally, the concluding remarks are given in Sec. 7.

2. Physical aspects of internal damage of rubber

2.1. Micro-phase separation in polyurethane elastomers

The specific structural feature of high-molecular weight polyurethane elastomers, is their segmented structure. The PUR chain is composed of hard segments and soft segments arranged alternately. The structure of the segmented PUR was already schematically presented and such schemes are presented in [28–30, 42]. The structure of a PUR macro-molecule results from the spatial arrangement of polymer chains in the condensed phase, i.e. after the polymerisation process and possibly after cross-linking. Considerable structural diversification of PUR chains gives rise to strong interactions, both within individual macro-molecules and between different macro-molecules. The hard segments can interact with each other. That phase is hardly miscible with the soft phase which has been formed with the use of much less polar, soft segments. If the hard phase and soft phase within a PUR become completely immiscible, two separate

phase transition points can be frequently observed as two clearly different glassy temperatures for soft segments and for hard segments. That is specific just for segmented PUR elastomers.

In some cases, additional crystalline phases can form within each of those phases. The interactions through hydrogen bonds can also create separate hard domains within the soft phase or separate soft domains within the hard phase. That certainly produces a multi-phase system in which usually the continuous soft phase makes the matrix. The matrix is penetrated through by some part of the hard phase or by the whole of it. Alternatively, the hard phase can be dispersed in the matrix. Separation of micro-phases is not precise, however, and some hard segments are dispersed within the domains of soft segments and the intermediate phase is thus formed. The degree of phase separation in PURs is controlled by numerous factors: chemical structure of PUR chains, polarity of their structural fragments, sizes of hard segments and soft segments, molecular weights and molecular weight distribution in PURs, the method employed to shape the final PUR product (bulk, foil, fibre) and process parameters adopted for that method (temperature, melt cooling rate, solvent evaporation rate, possible presence or absence of mechanical stresses). From the theoretical viewpoint, phase separation can be controlled by the thermodynamic factors which result from differences in the structures of hard segments and soft segments, and by kinetic factors which for example promote separation of some segments due to their higher mobility, and thus with lower viscosity of the reaction mixture which is just polymerizing. The micro-phase separation is generally more prominent in polyurethanes due to stronger interactions between ester groups and urethane groups than between ether groups and urethane groups.

2.2. Intermolecular interactions. Elastomer phase structure

The fundamental static properties for PUR elastomers materials are defined by Young's modulus E, shear modulus G and by unit elongation and Poisson's ratio $\nu = 0.3 - 0.5$. The static properties also involve hardness resistance. The mechanical properties of the parent material will be decided by the structures of PUR chains and by the phase structures of PURs. That problem has been extensively described in literature since mechanical properties affect directly the range of applicability of PUR elastomers and PUR coatings. Polyurethane materials behaviour under quasi-static loads is determined by the elastomer phase structure, and that in turn is controlled by the organisation of its segments. In polyurethane materials, the mechanical properties make the resultant of structural factors and physical chemical interactions such as like size and flexibility of hard and soft segments, ability to form hydrogen bonds, van der Waals force, entanglement of chains, orientation of segments, cross-linking bonds, micro-phase separation

and content of crystalline phase. The most important contribution comes from the chemical structure and from the size and structure of hard and soft segment resulting from this.

The sizes of hard segments increase when the number of those segment increases. Initially, they form a system of separate islands which do not contact each other and are dispersed within the matrix of soft segments. Above a certain limit number, some of them start to touch each other, what forms the system of hard domains. Further increase in the number of hard segments favours their association and the roles of phases become opposite. Both the cohesion energy and hydrogen bonds in hard domains are higher than in soft domains. Hence, the role of hard domains is sometimes compared to that of a filler material which is used to reinforce the elastomer structure and to improve its mechanical properties: in particular, its strength and hardness. On the other hand, higher elasticity is favourable for intermolecular interactions. In contrast to mechanical strength, which is controlled first of all by the structure of hard segments, elasticity is affected mainly by soft segments. The capacity for crystallisation of phases, which is conditioned by the structural regularity, contents of individual segments and efficient phase separation, is favourable for higher tensile strength, tearing strength, hardness and higher stresses at the predefined elongation levels. The mechanical properties of PURs can be also considerably affected by the method adopted for the final treatment of the product, like soaking or racking. That increases the phase separation and orderly arrangement of elastomer within its crystalline structures, i.e. elastomer strength is advantageously improved in that way (see Pompe *et al.* [48]).

2.3. The role of a damage parameter

Although rubbery-like materials may be regarded as purely elastic, damaging does take place due to straining. The internal degradation in this case is mainly characterized by rupture of the molecular bonds, concentrated in regions containing impurities and defects. In general, the damage response of such materials is predominantly brittle. In rubber-like materials, even at very small overall straining, damage can occur in the form of progressive breakage of shorter polymer chains. In Sec. 6.2 we have shown that it is convenient to introduce a damage parameter to describe the evolution of alteration of the network. This can be done in a purely empirical way, and this is the approach used by Beatty and co-workers in several publications (Beatty and Krishnaswamy [16]; Elias–Zúñiga and Beatty [17] and references contained therein) and also by Marckmann *et al.* [43]. First of all, it is possible to use the theory of pseudo-elasticity as proposed by Ogden and Roxburgh [19]. In this theory it is assumed that the material response of the body can be described in terms of a pseudo-energy function,

defined per unit volume, of the form $W(f(I),\ \alpha)$, where α is a damage parameter and $f(I)$ is a function of invariants I_1, I_2 and I_3 of the deformation tensor. (The role of α here is somewhat different from that of the damage parameter α introduced in Sec. 6.2). In this case it is no longer appropriate to regard W as a stored energy because, through α, irreversible effects are accounted for.

It is often convenient to regard shear modulus for the ith-cycle loads μ_i as functions of a damage parameter, here denoted by α, such that $\alpha \in [0, 1]$, where 0 is associated with the original material and 1 with the fully damaged material (this is a normalization of the scale). The fully damaged material corresponds to an asymptotic state in which no further damage is caused by stress-strain cycling with increasing number i.

3. Constitutive models for rubber elasticity

The elastic properties of rubber-like materials are usually represented in terms of a strain-energy function, denoted by W and defined per unit reference volume (see, for example, Beatty and Krishnaswamy [16]; Ogden [6–8]). The state of strain in the material is characterized by a tensor measure of deformation, such as the left Cauchy–Green deformation tensor $\mathbf{B}$. Several forms for the strain energy function of rubber-like materials have been proposed since 1940 in the literature. These can be grouped into these dealing with incompressible materials and those extended to deal with compressibility. They can further be split, depending on the material group being modelled, whether for example the material under consideration is rubber, polymer or foam. The most widely cited strain energy expressions are the Mooney–Rivlin, Ogden [cf. 6–7] and Blatz and Ko (see e.g. Krishnaswamy and Beatty [31]) models. However, for different strain energy functions, mainly two different kinds of models can be identified.

The first kind is based on experimental observations and phenomenological considerations. The corresponding models are both mathematically simple and quite efficient (Ogden [6, 7]). The second group of models were developed by considering the physics of the elastomer network. First, conformations of a single polymer chain are determined; then, the behaviour of the whole network is derived using statistical developments. For small and moderate strains, the neo-Hookean (Treloar [52]) and the phantom (James and Guth [53]) models can be mentioned. For large strains, the stretching limit of chains is taken into account and non-Gaussian statistics are employed (Treloar and Riding [54]; Arruda and Boyce [55]; Wu and van der Giessen [56]). The use of these models reduces the number of relevant material parameters because of their physical foundations, but their mathematical derivations are more complicated than those of phenomenological constitutive equations. For a complete review of the constitutive models for rubber elasticity, the reader can be referred

to Ogden *et al.* [34], Lambert–Diani and Rey [1] or Boyce and Arruda [57]. It has to be mentioned that the present approach can be easily applied to every form of the strain energy function. In the present study, the emphasis is laid on identification of the model with stress-softening phenomenon for the available macroscopic uniaxial loading experimental data only, so that a simple phenomenological strain energy function is chosen.

3.1. The strain energy function for rubber

The hyperelastic materials are described under assumption of existence of the potential of energy of strain $W(\lambda)$, by which the stored strain energy on unit initial volume fraction as a function of strains is defined in the material. In literature, different forms of strain energy potentials are proposed, depending on the form of constitutive model, e.g. Mooney–Rivlin or Ogden. The strain energy function W can be expressed as a function of invariants of a deformation tensor I_1, I_2 and I_3. If the left Cauchy–Green deformation tensor $\mathbf{B}$ is employed as the deformation tensor, the deformation invariants can be rewritten in terms of the principal stretches λ_i $(i = 1, 2, 3)$,

$$
\begin{aligned}
I_1 &= \mathrm{tr}\mathbf{B} \;\; = \lambda_1^2 + \lambda_2^2 + \lambda_3^2, \\
I_2 &= \frac{1}{2}\{(\mathrm{tr}\mathbf{B})^2 - \mathrm{tr}(\mathbf{BB})\} = (\lambda_1\lambda_2)^2 + (\lambda_2\lambda_3)^2 + (\,\lambda_3\lambda_1)^2\,, \\
I_3 &= \det(\mathbf{B}) = J^2 = (\lambda_1\lambda_2\lambda_3)^2\,.
\end{aligned}
\tag{3.1}
$$

When the material is incompressible, the third invariant $I_3 = 1$, and W is represented as a function of I_1 and I_2 only, $W = W(I_1, I_2)$. In the case of isotropic elastic incompressible virgin materials, $W = W_0$ and the general expansion of W_0 is considered in the form:

$$
W_0 = C_{ij}(I_1 - 3)(I_2 - 3) \tag{3.2}
$$

in which C_{ij} $(i, j = 1, \ldots, n)$ are the material parameters. Several phenomenological models were derived by truncating the series of Eq. (3.2). In order to satisfactorily reproduce the large strain response of the material, the Mooney–Rivlin model is adopted (cf. Elias–Zúñiga and Beatty [17]). The corresponding strain energy function is given by

$$
W_0 = \sum_{i=1}^{3} C_{i0}(I_1 - 3), \tag{3.3}
$$

where C_{10}, C_{20} and C_{30} are the three material parameters. As this model depends only on the first principal invariant, it is not well-adapted to moderate

strain because it does not improve the Gaussian theory. Nevertheless, its mathematical simplicity and ability to reproduce the whole behaviour of elastomers are sufficient qualities for the present study.

Some of the simplest incompressible models proposed in the literature involve a strain-energy function of the form $W_0 = f(I_1)$, and are called generalized neo-Hookean models. In the molecular theory of elasticity, these models involve the introduction of a (non-Gaussian) distribution function, denoted φ, for the end-to-end distance of the polymeric chain. By contrast, a Gaussian distribution function for φ is associated with the special case corresponding to the classical neo-Hookean model

$$W_0^H = \mu(I_1 - 3) \tag{3.4}$$

for incompressible materials, where μ ($\mu > 0$) is the shear modulus in the reference configuration.

In the framework of the phenomenological theory, similar models have been developed by considering the idea of limiting chain extensibility, i.e. by considering strain-energy functions that have a singularity when the first invariant I_1 reaches a certain finite value. The simplest model with limiting chain extensibility is due to GENT [58], who proposed the strain-energy function

$$W_0^G(I_1) = -\frac{1}{2}\mu J \ln\left(1 - \frac{I_1 - 3}{J}\right), \tag{3.5}$$

where μ is again the shear modulus in the reference configuration and $J > 0$ is the constant limiting the value of $(I_1 - 3)$ that accounts for limiting polymeric chain extensibility. In the limit as the chain-extensibility parameter tends to infinity ($J \to \infty$), Eq. (3.5) reduces to Eq. (3.4), cf. HORGAN *et al.* [12]. From a phenomenological point of view, limiting chain extensibility may be introduced in many ways, and a detailed review of some of the possibilities may be found in HORGAN *et al.* [12] or HORGAN and SACCOMANDI [44].

All the strain-energy functions considered in constitutive modelling will be assumed to satisfy the following conditions: 1. The strain energy is zero in the reference configuration; 2. The stress is zero in the reference configuration; 3. The strain-energy function is positive definite. The specific form of strain-energy densities used to model our rubber-like material behaviour in Sec. 5 and 6 are given in the following subsections.

3.1.1. The Mooney–Rivlin model. The potential in the Mooney–Rivlin model is usually presented for incompressible hyperelastic materials in the following form (see e.g.: [6, 8]):

$$W_0^M = C_{10}(\overline{I}_1 - 3) + C_{01}(\overline{I}_2 - 3), \tag{3.6}$$

where W is the strain energy in unit initial volume fraction, C_{10} and C_{01} are two parameters and $\bar{I}_1$ and $\bar{I}_2$ are the first and second invariants of strain deviator defined in terms of the deviatoric principal stretches $\bar{\lambda}_i$ which have the forms (cf. [2, 3, 8, 9])

$$\bar{I}_1 = \bar{\lambda}_1^2 + \bar{\lambda}_2^2 + \bar{\lambda}_3^2 \quad \text{and} \quad \bar{I}_2 = \bar{\lambda}_1^{(-2)} + \bar{\lambda}_2^{(-2)} + \bar{\lambda}_3^{(-2)}, \tag{3.7}$$

where $\bar{\lambda}_i = \lambda_i J^{(-\frac{1}{3})}$ and λ_i are principal stretches of the total strain tensor.

Initial shear modulus μ_0 in the Mooney–Rivlin model is defined by

$$\mu_0 = 2(C_{10} + C_{01}).$$

3.1.2. The standard Ogden model. Among the hyperelastic models, in case of polyurethane materials, the OGDEN model (cf. [6, 7]) gives good results; this will be the basis of the model elaborated and which takes into account the material damage. In the case of incompressibility, the strain energy function is presented in the form ([6, 7, 8]):

$$W_0^{\mathrm{Og}} = \sum_{i=1}^{N} \frac{2\mu_i}{\alpha_i^2} \left(\bar{\lambda}_1^{\alpha_i} + \bar{\lambda}_2^{\alpha_i} + \bar{\lambda}_3^{\alpha_i} - 3 \right), \tag{3.8}$$

where μ_i and α_i are material parameters and N is the number of material parameters (in practice $N \leq 6$), usually $N = 1$. Initial shear modulus μ_0 in Ogden model is defined by

$$\mu_0 = \sum_{i=1}^{N} \mu_i. \tag{3.9}$$

From the general form of strain energy potential of the Ogden model we can obtain also the peculiar material discussed above, e.g.: Mooney–Rivlin, by special selection of μ_i and α_i.

In the above constitutive description, the coefficient of change of length λ_i $(i = 1, 2, 3)$ can be defined as

$$\lambda_i = l_i/L = (L + \Delta l_i)/L, \tag{3.10}$$

where $\Delta l_i = l_i - L$ is the change of length in direction i.

3.2. The standard hypoelastic model

In literature, for description of rubbery-like materials behaviour was also used, different from the previous one, an objective hypoelastic rate model which can be presented by the following formula:

$$\overset{\circ}{\mathbf{T}} = 2\mu\mathbf{D} + \lambda^* \operatorname{tr}(\mathbf{D})\mathbf{I}, \tag{3.11}$$

where $\overset{\circ}{\mathbf{T}}$ is an objective measure of rate of the Cauchy stress $\mathbf{T}$, $\mathbf{D}$ is the rate of stretching (deformation) tensor and it is the symmetric part of the velocity gradient tensor, $\mathbf{I}$ is the unit tensor and μ and λ^* are elastic material constants. For a hypoelastic constitutive equation, in case of uniaxial tension (compression) along direction-*11*, when $\lambda_2 = (\lambda_1)^{-\nu}$ (for incompressible elastic materials) and if we use logarithmic strain measure, the following formula is obtained:

$$\mathrm{T}_{11} = E \ln(\lambda_1),$$

where E is elastic modulus and ν is Poisson's ratio.

Nominal stress in hypoelasticity is given by

$$\frac{P}{A_0} = E\ (\lambda_1)^{-2\nu} \ln(\lambda_1), \tag{3.12}$$

where A_0 is the initial area of sample cross-section.

Experimental data presented by Kwiecien and Zając [20] and Kwiecien *et al.* [21] for polyurethane material, allow to assume in the identification analysis, as potential candidates, the hyperelastic constitutive models proposed by Mooney–Rivlin and Ogden [6–8]. It is useful to compare these constitutive models with logarithmic model of hypoelasticity. For these descriptions it is possible to define the basic parameters of models, as well as the essential from the point of application of analysed material models, the basic quantities as: initial shear modulus μ_0, elastic modulus E and Poisson's coefficient ν. For example: initial shear modulus μ_0 is given by: $\mu_0 = 2(C_{10} + C_{01})$ (see e.g. papers [1–10]).

3.3. Introduction of damage

Under repeated tensile or compression strain, many rubber-like materials such as polyurethane (PUR), exhibit a reduction in stress after the initial extension, the so-called Mullins effect or stress-softening, and the mechanism(s) responsible for this is considered to be very important. Damage functions are important tools for analysing the stress-softening materials. In previous isotropic models [4, 5, 14], softening effects are governed by their "damage" functions and their corresponding damage points (sometimes referred to as softening points [5] or maximum-loading parameters [15]). In Sec. 6 we will define a damage function ξ (which may depend on the material properties) such that $0 \leq \xi(x) \leq 1$, $x \in R$ and ξ increases (strictly) monotonically as x moves away from the point $x = 1$, $\xi(1) = 0$.

Before using the proposed model, the two elastic parameters C_{10} and C_{01} and the parameters describing the evolution laws for damage have to be identified. It was performed through uniaxial tension and compression tests results (monotonic for elastic parameters and non-monotonic for damage parameters),

especially by exploiting the shear modulus properties (see Sec. 3.2). Different stages of the procedure are summarized in Sec. 5 and 6. Let us assume that as a first approximation, the term with I_2 has been neglected since the tension test case enables to split the contribution of the two first invariants and moreover, simulation by the Ogden model with only the first invariant and experimental results are in good agreement, also here $\mu_2 = 0$. The behaviour of the elastomers is commonly represented by hyperelastic models, characterized by the strain energy function W, which is often considered to be dependent on the invariants I_1, I_2, I_3 of the Cauchy–Green deformation tensor $\mathbf{C}$ (or another strain tensor). Among the usual hyperelasticity laws (Mooney–Rivlin, Ogden, etc.), the best one for the studied material is the model of Ogden, as shown in Fig. 1. The agreement between experiments and the model is quite good in a monotonic uniaxial tension and compression tests, but for cycle compression tests some phenomena are not taken into account, essentially a decrease of the shear modulus during the cycles and a decrease of the stiffening for high strains, as Figs. 2 and 3 show. The experimental results in a cycle compression test case (realised with some loads and unloadings) are shown in the axes of the engineering stress σ and principal stretch λ. Actually, the occurrence of micro-defects leads to a degradation of the mechanical material properties. Nevertheless it is worthy to note that for a damaged material, the type of load is crucial. In case of tension, the occurrence of micro-defects induces a decrease in the material properties; on the contrary, in case of compression, when the micro-defects are closed, the initial properties are recovered. The model exposed in the Set. 6 takes into account these experimental observations.

4. Experimental uniaxial tension and compression tests

The material used in this study was a commercial polyurethane material. After compression moulding, the polymer was solidified at a slow cooling rate to ensure that the structure and morphology of the compressed plates will be homogeneous across the thickness and along the length. This material is a two-component elastomer based on main feature of polyurethanes: hard segments A (viscosity 4.40 Pas) and soft segments B (viscosity 0.26 Pas) were compound in and it was combined in proportions 100:10, and the received material had average mass density $\rho = 0.90$ kg/dm^3 and hardness under Shore A 55±5. In the next Sections, in the uniaxial tension identification process, the experimental data of the following tests were accepted: 2R-1, 5R-1 and 7R-1 (paddle sample). In case of uniaxial compression, the following data were used: 9C-1, 7C-1, 6CC-1, 5CT-1, 4C-1, 1C-1, 3CC, 8CZ and 8CG (cylindrical sample with diameter $\phi \approx 46$ mm). All investigations were conducted only with quasi-static strain rates. Results of these tests are contained in the report by Kwiecień and Zając [20] and

published also by KWIECIEŃ *et al.* [21], and are presented in a part in this paper (in Secs. 4.1 and 4.2).

4.1. Tensile test

The stress-strain behaviour of the PUR was determined by means of a INSTRON testing system. The method has been described in detail in the literature. Consequently, only its essential features will be recalled here. Both the quasi-static and dynamic tests were performed at room temperature 295 K. The tensile samples were made from PUR plates. Dog-bone shaped flat specimens were used for the uniaxial tension tests. The length and width of the homogeneous section of the uniaxial tension specimens were 45.0 mm and 17.0 mm, respectively. The specimen thickness was 3.0 mm.

In Fig. 1, the force versus $1/\lambda$ curve is plotted for several tests, and in Fig. 2 the nominal stress versus λ is plotted.

4.2. Compression test

Investigations of compression were performed on disc specimens, cut off from polyurethane plates. The diameter of the specimens was $\phi = 46$ mm and the thickness for the quasi-static compression tests was approximately $H = 50$ mm.

The sample was compressed between two circular dies. The quasi-static compression tests were carried out in a hydraulic testing machine with the rates of deformation equal to 10^{-3} s^{-1}. The surface of each specimen was covered by a thin layer of anti-friction coating before testing. The friction between the sample and the die faces was not accounted for in the true stress-strain calculations because the friction coefficient was likely to be very low (<0.1) between the PUR sample and the steel dies. Consequently, the engineering stress was simply calculated as the load per actual cross-section of the compressed zone: $\sigma = P/(\pi\phi^2/4)$. Three tests were performed for each group of specimens to assure sufficient reliability of the results.

4.3. Typical stress-strain behaviour

The stress-strain relations obtained during uniaxial quasistatic tension of the polyurethane studied are presented in Figs. 3, 4, 5. The curve's number in these pictures indicates the test number. The stress and the strain quantities are referred to the current (instantaneous) value of the specimen cross-section and the thickness values. An example of the stress-strain curves obtained during axial tension of three specimens of PUR subjected to loading with the same strain rate 3×10^{-4} s^{-1} is shown in Fig. 3. The axial stress vs. axial strain curves shown in Figs. 3–5 were obtained under uniaxial loading at 20°C. The

reproducibility of each curve was checked by three tests performed under the same conditions. This graph is therefore typical for the behaviour of PUR at room temperature. In this part, a simulation of a cycle compression experiment is performed, as described in Fig. 9. Several interesting features deserve attention. First, all experiments showed that the material's behaviour was the same as above (elastic), but nearly incompressible with $\nu \leq 0.499$. As below in Sec. 6, Figs. 7, 8 and 10 show the experimental data for polyurethane in uniaxial cycle compression test as a function of strain intensity measure $\sqrt{M-m}$, or as a function of axial change of length λ for the loading and unloading tests.

5. Identification of models for monotonic loadings

5.1. Outline of the optimization method

The experimental data used in this paper are the data of Kwiecień and Zając [20] and Kwiecień *et al.* [21] for the uniaxial tension and compression and the numerical values have been obtained from the virgin experimental tables. These data have been used to identify the parameters of the specific strain-energy functions by means of the least squares (LS) technique.

Let $\hat{\boldsymbol{\lambda}} = [\lambda_1^1, \lambda_1^2, \ldots, \lambda_1^m]^T$ be the vector of values of a measure of stretch, appropriate to the considered deformation and let $\boldsymbol{\sigma} = [\sigma_1, \sigma_2, \ldots, \sigma_m]^T$ be the corresponding values of stress, which may be either nominal stress or Cauchy stress, depending on the deformation. Hence $(\hat{\boldsymbol{\lambda}}, \boldsymbol{\sigma})$ are the given pairs of data values. The considered material model is represented by the strain-energy function U, from which the stress is calculated and written $F(\hat{\boldsymbol{\lambda}}, \boldsymbol{\beta}) : \mathbb{R} \times \mathbb{R}^n \to \mathbb{R}$, where $\hat{\boldsymbol{\lambda}}$ takes the values λ_1^i , $i = 1, \ldots, m$, and $\boldsymbol{\beta} = [\beta_1, \beta_2, \ldots, \beta_n]^T$ is a set of n material parameters to be identified.

Let us define the objective function as the squared 2-norm

$$\sum_{i=1}^{m} \left(F\left(\lambda_1^i, \boldsymbol{\beta}\right) - \boldsymbol{\sigma}_i^{\exp}\right)^2. \tag{5.1}$$

Hence, the minimization problem is given by

$$\min_{\boldsymbol{\beta}} \sum_{i=1}^{m} \left(F\left(\lambda_1^i, \boldsymbol{\beta}\right) - \boldsymbol{\sigma}_i^{\exp}\right)^2. \tag{5.2}$$

If $F(\hat{\boldsymbol{\lambda}}, \boldsymbol{\beta})$ is a non-linear function with respect to $\boldsymbol{\beta}$, then a non-linear least squares problem arises.

It is assumed that our material is almost incompressible like majority of the materials with similar elastic properties as rubber.

In the uniaxial deformation tests along the direction-*11* we have

$$\lambda_1 = \lambda, \quad \lambda_2 = \lambda_3 = \frac{1}{\sqrt{\lambda}}, \quad \lambda = 1 + \varepsilon_1. \tag{5.3}$$

The invariants of strain in uniaxial tests have the form

$$\overline{I}_1 = I_1 = \lambda^2 + 2\lambda^{-1}, \quad \overline{I}_2 = I_2 = \lambda^{-2} + 2\lambda. \tag{5.4}$$

With a known potential of strain energy it is possible to determine the dependence of the nominal stress as a function of strain. For the model of the Mooney–Rivlin, we have

$$\frac{P}{A_0} = 2\left(1 - \frac{1}{\lambda^3}\right)(\lambda C_{10} + C_{01}) = 2\left\{\left(\lambda - \frac{1}{\lambda^2}\right)C_{10} + \left(1 - \frac{1}{\lambda^3}\right)C_{01}\right\}, \tag{5.5}$$

which can be defined in the form

$$\frac{P}{2A_0\left(\lambda - \dfrac{1}{\lambda^2}\right)} = C_{10} + \frac{C_{01}}{\lambda}, \tag{5.6}$$

where P is the external axial force in the test, A_0 is initial area of cross-section and λ is the coefficient of change of length (stretch). The right-hand side of the above equation is linear with respect to variable $1/\lambda$, what enables preliminary qualification of constants C_{10}, C_{01}. The left-hand side represents equivalent stress. Figure 1 shows this reduced stress change as a function of the reciprocal of the axial stretch for tests 2R-1, 5R-1 and 7R-1. For these tests it has been established that $C_{10} = 0.6832$, $C_{01} = 0.01209$.

In a general formulation for the Mooney–Rivlin model, we can identify parameters C_{10} and C_{01} from the relation

$$\frac{P}{A_0} = 2\left(1 - \frac{1}{\lambda^3}\right)(\lambda C_{10} + C_{01}). \tag{5.7}$$

The Ogden model introduced generally earlier, in uniaxial tests has now the form:

$$\sigma_{11} = \frac{2\mu}{\alpha}\left[\lambda^{\alpha-1} - \lambda^{-1-\left(\frac{\alpha}{2}\right)}\right] \tag{5.8}$$

and we have to identify two material parameters μ i α.

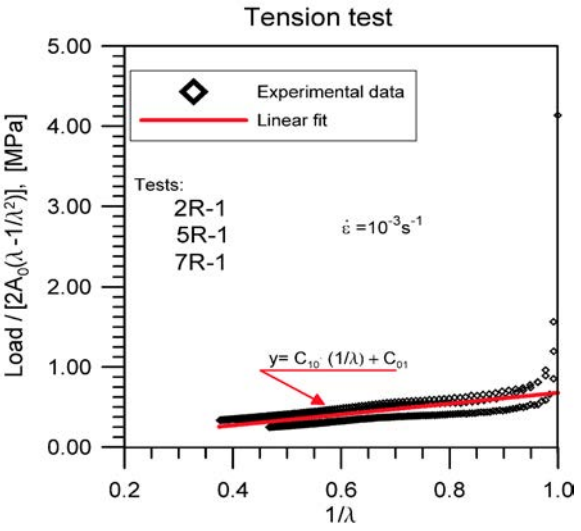

FIG. 1. Dependence of the change of reduced stress $\dfrac{P}{2A_0\quad \lambda - \dfrac{1}{\lambda^2}}$ as a function of the reciprocal of the relative axial stretch $\dfrac{1}{\lambda}$ in uniaxial tension. Experimental data from KWIECIEŃ *et al.* [20, 21].

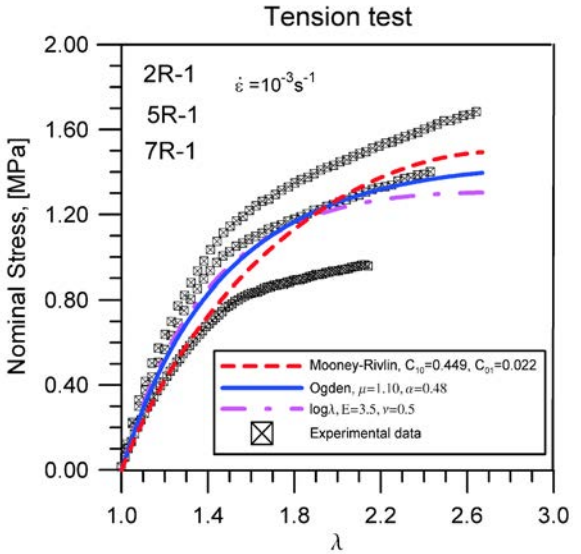

FIG. 2. The nominal stress as a function of the axial stretch λ for polyurethane rubber in a uniaxial tension test, with strain rate 3×10^{-4} s^{-1} for different constitutive models relations Eqs. (3.6), (3.8), (3.12) (broken and solid lines). Experimental data (quadrate marks) from KWIECIEŃ *et al.* [20, 21].

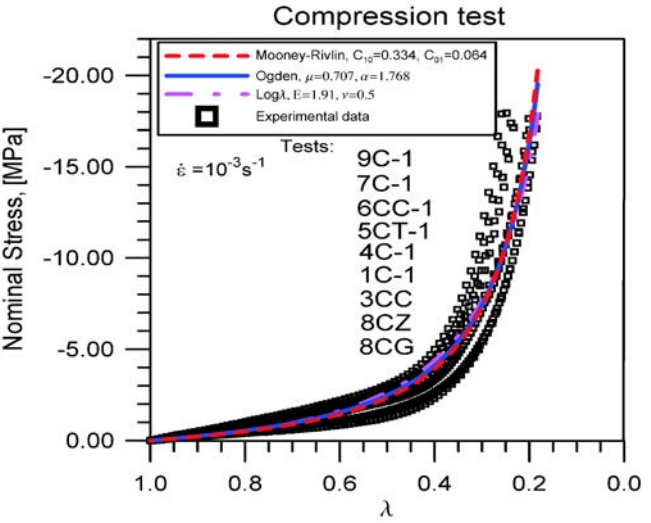

FIG. 3. The nominal stress as a function of the axial stretch λ for polyurethane rubber, in uniaxial compression test with strain rate 3×10^{-3} s^{-1} for different constitutive models relations Eqs. (3.6), (3.8), (3.12) (broken and solid lines). Experimental data (quadrate marks) from KWIECIEŃ *et al.* [20, 21].

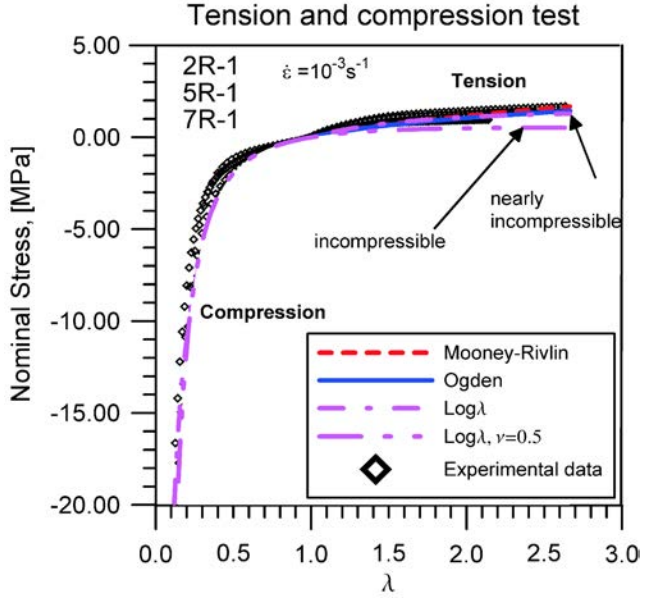

FIG. 4. The nominal stress in uniaxial tension and compression tests as a function of the axial stretch λ, for different constitutive models, Eqs. (3.6), (3.8), (3.12) (broken and solid lines). Experimental data (diamond marks) from KWIECIEŃ *et al.* [20, 21].

In logarithmic description, in uniaxial tests the following relation is given:

$$\frac{P}{A_0} = E\ (\lambda)^{-2\nu}\ \ln(\lambda) \tag{5.9}$$

and we have to identify E and ν.

The results of identification process were obtained for tension and compression tests separately and they are presented in Fig. 2 (for tension) and in Fig. 3 (for compression). The results of simulation plotted in Fig. 2 and in Fig. 3 are compared with experimental results. Quadrate marks are used for experimental data, whereas full lines are used for simulation. Identified parameters differed so much that next test of the same process of identification was undertaken for the same file of data for both tests, to identify for this material the set of parameters independent of the type of test. Results of such identification are introduced in Fig. 4. This curve shows the ability of the rubber elasticity models to estimate the material properties.

6. Hyperelastic material with damage

6.1. Remarks on the use of damage mechanics to describe the Mullins effect

The phenomenon of internal damage in common engineering solid materials depends upon the specific type of the material considered. In addition, for the same material, damage evolution may take place, initiated by very different physical mechanisms, which mainly depend on the type, rate of loading, temperature, as well as on environmental factors such as exposure to corrosive substances. As mentioned in the Introduction, the Mullins effect in rubber elastic materials is often modelled by means of the CDM. Originally, continuum damage mechanics was based on the definition of effective stress (cf. Lemaitre and Chaboche [59]). This theory assumes that, under loading, the material surface on which internal forces are applied is decreasing because of the emergence of micro-defects and micro-voids. Taking into account these physical considerations, in the case of the Mullins effect in solid rubber, following consequences are introduced for the damage evolution:

1. It was proved experimentally that the Mullins effect recovers with time and that this recovery is highly accelerated by annealing (Mullins [26]). So, the damage in rubber materials may decrease if the whole life of the material is considered.
2. The damage evolution does not differ under different deformation modes: some authors observed the occurrence of stress-softening under tension and compressive conditions.

3. It is mainly recognized that rupture in rubber parts is not directly related to stress-softening. Therefore, high values of the damage parameter should not be considered as a criterion for rupture or occurrence of cracks.

More precisely, the Mullins effect is not a damage but a stress-softening phenomenon. It is due to the rearrangement of the polymer network under deformation when some links between chains (entanglements), or between chains and reinforcement particles (for example carbon black) are broken (Bueche [51]). Therefore, it should be stressed that CDM can be used to model the Mullins effect in elastic rubber materials with some restrictions and care.

6.2. Description of microstructure damage

Let us consider an isotropic, homogeneous and incompressible rubber-like material. This material is considered to be hyperelastic and subject to isotropic damage in order to describe the Mullins effect. Consequently, it is defined by the existence of a strain energy function, that depends on the deformation gradient $\mathbf{F}$ and on a scalar damage variable α. This variable characterizes the elastic stress-softening of the material. Taking into account the objectivity requirement, the isotropy and the incompressibility, the strain energy function can be written as

$$W = W(I_1; I_2; \alpha),$$

where I_1 and I_2 are the two first principal invariants of the left Cauchy–Green tensor $\mathbf{B} = \mathbf{F}^T\mathbf{F}$ defined in Sec. 3. The third invariant $I_3 = \det(\mathbf{B})$ is equal to 1 due to the incompressibility assumption.

Consider now that the effective Cauchy stress T^*, which acts on the damaged material, is related to the virgin Cauchy stress T_0 by Lemaitre and Chaboche [59] $T^* = T_0(1-\alpha)$. In case of three-dimensional continuum, the damage model for Mullins effect was proposed by De Souza Neto *et al.* [11]. In this model, the current value of the engineering stress $\boldsymbol{\sigma}$ in the stress-softened material is given by

$$\boldsymbol{\sigma} = \xi(\alpha)\,\boldsymbol{\sigma}_0,$$

where the damage function $\xi(\alpha)$ is a differentiable, nondecreasing function of a damage variable $\alpha \in [0,1]$. The engineering stress in the virgin material is determined by (cf. De Souza Neto *et al.* [11])

$$\boldsymbol{\sigma}_0 = \frac{\partial \psi_0(\mathbf{F})}{\partial \mathbf{F}}, \tag{6.1}$$

where $\psi_0(\mathbf{F})$ is the strain energy function for an isotropic, incompressible hyperelastic solid at the current deformation gradient $\mathbf{F}$. The relation Eq. (6.1) is valid only during monotonic loading. The strain energy function in Eq. (6.1) can

be considered as a‘ product of the surface reducing parameter $(1-\alpha)$ and the strain energy function of the virgin undamaged material, denoted W_0:

$$W(I_1;I_2;\alpha) = (1-\alpha)W_0(I_1;I_2). \tag{6.2}$$

The damage variable α, or the relative strain measure, is defined by $\alpha = \dfrac{\psi_0}{D}$, where $D \equiv \max\limits_{0\le s\le t} \psi_0(s)$ is the maximum previous value of the strain energy in a deformation history up to the current time t, and s is a running time variable. The evolution of α variable with the deformation must be specified by an additional constitutive law during the loading, unloading and reloading deformation cycles.

Similarly, like Ogden and Roxburgh [19], Beatty and Krishnaswamy [16] introduce a generalized Johnson and Beatty [15] elastic material model of stress-softening. In this model, the Cauchy stress $\mathbf{T}$ during loading of the material is a product of the Cauchy stress $\mathbf{T}_0$ in an isotropic parent material model and an isotropic scalar-valued damage function $\xi(m)$, that depends on the current value of the magnitude of intensity strain m. At a material point $\mathbf{X}$, the magnitude of strain intensity denoted by m, is defined by $m = \sqrt{\mathbf{B}\mathbf{B}} = \sqrt{\mathrm{tr}\,\mathbf{B}^2}$, where $\mathbf{B}$ is the left Cauchy–Green deformation tensor. $\mathbf{B} \equiv \mathbf{F}\cdot\mathbf{F}^T$ and $\mathbf{F}$ is the deformation gradient which, in case of incompressibility, requires $\det(\mathbf{F}) = 1$ for all $\mathbf{F}$, so that

$$\mathbf{T} = \xi(m)\mathbf{T}_0. \tag{6.3}$$

During loading when m is fixed at its current maximum value, $m_{\max} = \max\limits_{0\le s\le t} m(s)$ and the material is unloaded, the Cauchy stress $\mathbf{T}^*$ in the stress-softening elastic material is given by

$$\mathbf{T}^* = \xi(m_{\max})\mathbf{T}_0 = \xi(m_{\max})\,\frac{\mathbf{T}}{\xi(m)} = \frac{\xi(m_{\max})}{\xi(m)}\;\mathbf{T} = \xi(m_{\max},m)\;\mathbf{T}. \tag{6.4}$$

The same relations hold when the Cauchy stress is replaced by the engineering stress. The common feature of virgin material response in the described models is that this response, described by the parent material stress $\mathbf{T}_0$, is determined by a standard strain energy function for a perfectly elastic, incompressible and isotropic material, which may be hyperelastic.

The loading, unloading and neutral loading from the obtained maximum value $m_{\max} = M$, require $\dot m > 0$, $\dot m < 0$ and $\dot m = 0$, respectively. Intensity m of tensor $\mathbf{B}$ as a function of invariants $I_k(I_1 = \mathrm{tr}\mathbf{B},\ I_2 = \dfrac{1}{2}[I_1^2 - \mathrm{tr}(\mathbf{B}^2)]$, $I_3 = \mathrm{de}(\mathbf{B}))$ is given by

$$m = \sqrt{I_1^2 - 2I_2}. \tag{6.5}$$

For all deformations of an incompressible material, we have $I_3 \equiv 1$ and $m \geq \sqrt{3}$, where equality is valid when and only when $\mathbf{B} = \mathbf{1}$. By use of the spectral decomposition of tensor $\mathbf{B}$

$$\mathbf{B} = \lambda_1^2\ \mathbf{e}_1 \otimes \mathbf{e}_1 + \lambda_2^2\ \mathbf{e}_2 \otimes \mathbf{e}_2 + \lambda_3^2\ \mathbf{e}_3 \otimes \mathbf{e}_3,$$

where λ_i are the principal stretches and $\mathbf{e}_i$ are the associated orthonormal principal directions, the intensity of strain m becomes

$$m = \sqrt{\lambda_1^4 + \lambda_2^4 + \lambda_3^4}. \tag{6.6}$$

We consider, like Elias–Zúñiga and Beatty [17], that the material is an isotropic elastic and incompressible material and is described by a time-independent constitutive equation of the form

$$\mathbf{T}_0 = 2\frac{\partial W}{\partial I_1} \cdot \mathbf{B} - 2\frac{\partial W}{\partial I_2} \cdot \mathbf{B}^{-1} - p\ \mathbf{1}, \tag{6.7}$$

in which $\mathbf{T}_0$ is the Cauchy stress, p is hydrostatic pressure and W is the strain energy function per unit reference volume.

Let us assume that our previous strain attained maximum value $m_{max} = M$ during monotonic loading; in such case the stress-softened material response for subsequent unloading and reloading is defined by

$$\mathbf{T}^* = \xi(m(\lambda); M)\mathbf{T}_0. \tag{6.8}$$

The isotropic scalar-valued damage function $\xi(m(\lambda); M)$, called the softening function at the damage level $m_{\max} = M$, is a positive monotone increasing function of the strain intensity in the interval $m \in \{m(\lambda = 1); M\}$ and satisfies the conditions

$$0 \leq \xi(m; M) \leq 1, \quad \xi(M; M) = 1. \tag{6.9}$$

Damage function ξ is determined by a constitutive equation that describes the evolution of microstructural damage that begins immediately after deformation from the natural, undeformed state of the virgin material. Its value $\xi(\sqrt{3}; M)$ characterizes the extent of damage at M, initiated at $m = \sqrt{3}$.

The relations (6.8) for $\mathbf{T}^*$ and (6.9) for the function ξ show that the virgin material and stress-softened material response values coincide only in the unstressed state $\mathbf{T}^* = \mathbf{T}_0 = \mathbf{0}$ and at each softening point $m = M$; otherwise, the stress-softened material response is everywhere smaller than the virgin material response. The material behaviour described by (6.8) for $m \leq M$ is ideally elastic for both loading and unloading, until the value of m exceeds its maximum

previous value M. Thereafter, the material recalls its virgin material response described by (6.7).

For our rubber elastic material, the ratios of the physical stress components $\mathbf{T}^*$ in the stress-softened material to the corresponding physical components $\mathbf{T}_0$ in the virgin material, for the given deformation, are determined by the softening function alone.

That is, in accordance with Eq. (6.8) and Eq. (6.9)

$$\frac{\mathbf{T}^* ij}{\mathbf{T}_0 ij} = \xi(m; M) \leq 1, \quad \text{for} \quad i, j = 1, 2, 3 \quad \text{(no summation)}. \tag{6.10}$$

In Eq. (6.10) the equality holds when and only when $m = m_{\max} = M$.

6.3. The form of damage function $\xi(\sqrt{3}; m)$

For the two-phase material model proposed by Mullins–Tobin in 1957 and analysed also by Beatty and Krishnaswamy [16], each material *point* consists of hard phase and soft phase. The total amount of hard phase in solid rubber is much less than the amount of soft phase present in the amorphous microstructure. Elias–Zúñiga and Beatty [17] and Beatty and Krishnaswamy [16] suppose that stress-softening begins immediately after initiation of loading of the original material when $\lambda = 1$ ($m = \sqrt{3}$). As deformation progresses, the volume fraction $\alpha(\sqrt{3}, m)$ of the initial portion of hard phase is transformed to an equivalent portion of soft phase (the rubbery phase), so that the volume fraction α of soft phase increases monotonically with extension (compression). Following Elias–Zúñiga and Beatty [17] we assume that the initiation of stress-softening is possible to appear only after deformation has reached a threshold value λ_a, say $\alpha(\sqrt{3}, m(\lambda_a)) = 0$ for all $\lambda \leq \lambda_a$ and for all $m \leq \sqrt{3}$ we have $\alpha(\sqrt{3}; \sqrt{3}) = 0$. Then the degree of softening of a original material subjected to a maximum previous strain $m_{\max} = M$ is determined by the volume fraction $\alpha(\sqrt{3}, M)$ of hard phase that is transformed by deformation to the new soft phase. During deformation of material $m > \sqrt{3}$, our stress-softening measure $\alpha(\sqrt{3}, m)$ is related to our softening function $\xi(\sqrt{3}, m)$ with the properties described by Eq. (6.8) as follows:

$$\alpha(\sqrt{3}; m) = 1 - \xi(\sqrt{3}; m). \tag{6.11}$$

Relation (6.11) provides a physical basis for the damage function in this theory of stress-softening of rubber-like materials. To determine the softening function from experimental data, the simple relation Eq. (6.10) can be applied to various hypothetical damage functions having the property $0 \leq \xi \leq 1$. In the literature, different forms of damage functions have been introduced for analytical

study, see JOHNSON and BEATTY [15], OGDEN and ROXBURGH [19], DE SOUZA NETO *et al.* [11] or BEATTY and KRISHNASWAMY [16]. JOHNSON and BEATTY [15] suggest for ξ an exponential type function $\xi(\sqrt{3};m) \equiv e^{-b(m-\sqrt{3})}$, which is studied in several papers, e.g. by BEATTY and KRISHNASWAMY [16], but no direct comparison with experiments is provided. ELIAS–ZÚÑIGA and BEATTY [17] propose an exponential-type equation of law for ξ defined by

$$\xi(m;M) \equiv e^{-b\sqrt{M-m}} \tag{6.12}$$

where b is a positive material constant, named the softening parameter.

The softening function ξ proposed by ELIAS–ZÚÑIGA and BEATTY [17] yields a stress-softening measure α by which the growth of damage may be determined

$$\alpha(\sqrt{3};m) = 1 - \xi(\sqrt{3};m) = 1 - e^{-b\sqrt{m-\sqrt{3}}}. \tag{6.13}$$

Application of Eq. (6.13) in Eq. (6.10) determines the stress-softening material model with exponential softening $\xi = e^{-b\sqrt{M-m}}$, for which the stress after unloading follows in accordance with

$$\mathbf{T}^* = \mathbf{T}_0\, e^{-b\sqrt{M-m}}. \tag{6.14}$$

The relation (6.14) describes the family of models determined by different values of M which we obtain by describing the elastic, isotropic and incompressible material in the form presented by Eq. (6.7)

During monotonic loading, the strain in material is the actual strain and it is the maximum of strain and $\mathbf{T}^* = \mathbf{T}_0$. If the material is not reloaded again, the strain intensity m decreases from $m = m_{\max}$ and reaction of the material is ideally elastic according to Eq. (6.14) for all $m \leq m_{\max} = M$.

Relation (6.14) or (6.10) after use of logarithm, can be written in the form

$$\ln\left(\frac{\mathbf{T}_0}{\mathbf{T}^*}\right) = -\ln\left[\xi(\sqrt{3};m)\right]. \tag{6.15}$$

The applied theory of rubber-like materials deformation is relatively simple and it is based on purely phenomenological consideration, and identification of the material parameters does not require the measurement of any microscopic quantities. Indeed, behaviour of the material at damaged states is characterized by curves determined from the loading/unloding experiments.

For uniaxial deformation tests of tension and compression, when stretch in axial direction is denoted by $\lambda_1 = \lambda$ with condition of incompressibility $\lambda_1\lambda_2\lambda_3 = 1$, we can determine $\lambda_2 = \lambda_3 = 1/\sqrt{\lambda}$.

For the Mooney–Rivlin model, nominal stress $\boldsymbol{\sigma} = \dfrac{\mathbf{T}_0}{\lambda}$ for monotonic loading is described by Eq. (6.8) and it is obtained for axial loading in the form:

$$\sigma_{11} = 2\left\{\left(\lambda - \frac{1}{\lambda^2}\right) C_{10} + \left(1 - \frac{1}{\lambda^3}\right) C_{01}\right\}, \tag{6.16a}$$

for monotonic loading and

$$\sigma_{11}^{*} = 2\left\{\left(\lambda - \frac{1}{\lambda^2}\right) C_{10} + \left(1 - \frac{1}{\lambda^3}\right) C_{01}\right\} \xi(m; M), \tag{6.16b}$$

for stress-softening loading, where current value of $m = m(\lambda)$ and maximum value of m, $M = m(\lambda_{\max}) = m(\Lambda)$ before unloading is calculated in accordance with:

$$m = \sqrt{\lambda^4 + \frac{2}{\lambda^2}}, \quad M = \sqrt{\Lambda^4 + \frac{2}{\Lambda^2}}, \tag{6.17}$$

where $\Lambda = \lambda_{\max}$ and $M(\lambda_{\max})$ for our experimental compression test $M = 6.21$.

6.4. The identification procedure of parameters of damage function $\xi(m; M)$

Experimental data of stress-softening elastic material response in a strain-controlled test may be used to determine the specific form and all parameters of the softening functions. We shall use only the isotropic scalar function, and this form will only require a small number of equations to be solved when a curve-fitting method is used to obtain its parameters values.

As it is seen in Fig. 5, both models of Mooney–Rivlin show a reasonably good agreement with the experimental data – not only for the primary loading path but also for the reloading paths for the chosen three deformation cycles. In Fig. 5 solutions for both models with identified values of material parameters for three deformation cycles are also shown. It appears that none of these two models gives satisfactory prediction for the three deformation cycles. Naturally, when more deformation cycles are included in the analysis, values of the softening parameters can be better adjusted with the hope of obtaining better fitting of the data. However, no satisfactory prediction can be obtained in this way. The softening functions in the form of Eq. (6.12) proposed by Elias–Zúñiga and Beatty [17] or Eq. (6.13), also fail to give fully satisfactory coincidence of the experimental and theoretical results. The magnitude of softening function $\xi = 1 - \alpha$, shows a strongly non-monotonic behaviour in the characteristic S-shaped form. Variations in shapes of the curves for different deformation cycles show that different values of the softening parameters are needed to fit the experimental data for a particular choice of the softening function. Otherwise more

softening parameters may be needed for definition of this function. In Fig. 7 the softening functions Eq. (6.12) and Eq. (6.13) which were used in fitting the KWIECIEŃ and ZAJĄC [20] or KWIECIEŃ *et al.* [21] data, are also plotted. Differences in shapes of the softening function curves and data curves are striking and this explains the difficulties in fitting experimental data by theoretical models.

In our identification analysis we have applied the following form of function $\xi(m; M)$:

$$\xi(\sqrt{3}; m) \equiv e^{-b(M-m)d}, \tag{6.18}$$

where b, M and d are material parameters.

This form of $\xi(m; M)$ requires only two parameters to fit the data via a nonlinear least-squares method based on the natural logarithm. For the least-squares method we minimize the expression

$$F = \sum_i \big\{\ln\big(\xi(m_i; M)\mathbf{T}_0(m_i)\big) - \ln\big(\mathbf{T}_{\exp}(m_i)\big)\big\}^2. \tag{6.19}$$

The above minimizing statement is equivalent to minimizing

$$F = \sum_i \left\{\ln\big(\xi(m_i; M)\big) - \ln\left(\frac{\mathbf{T}_{\exp}(m_i)}{\mathbf{T}_0(m_i)}\right)\right\}^2, \tag{6.20}$$

which is suitable for the least-square method to obtain the parameters values. We have identified the values of b and d in Sec. 6.7.

6.5. The other forms of damage function $\xi(m; M)$

For better fit we use a new form of ξ function as a combination of two functions, one being (like before) some kind of exponential function $W^*(\lambda)$ and a function $g^*(\lambda)$. Now the function of damage ξ takes the form

$$\xi^*(\lambda) \equiv g^*(\lambda)W^*(\lambda) = g^*(\lambda)K\, e^{-b(\lambda)^d} = \big(1 - g(\lambda)\big)K\, e^{-b(\lambda)^d}. \tag{6.21}$$

The function $g(\lambda)$ in Eq. (6.18) is assumed to be of a logistic form, i.e.,

$$g(\lambda) \equiv \frac{g_0}{1 + \exp(F - E\ \lambda)} \tag{6.22}$$

where K, g_0, F and E are material parameters. The form of $W^*(\lambda)$ is known as the Weibull function.

6.6. The identification of parameters of damage function $\xi(m; M)$ in uniaxial tension test

In order to determine the material parameters, that appear in the virgin strain energy function W_0 and the evolution equation of the damage variable $\alpha(\lambda)$, uniaxial tensile and cyclic uniaxial compression tests were performed. The uniaxial tensile experiments were conducted on dog-bone flat specimens; the compression test – on specimens which are disc. All experiments were performed under enforced displacement conditions. An example of experimental data is depicted in Fig. 5 for uniaxial tensile tests. In this figure, the experimental stresses are function of principal stretch λ_1. In experimental tension tests the material was subjected to stretching until achievement of maximum stretching and rupture of sample, and in these tests was not executed the cycle of unloading and reloading. However, let us trace the description of behaviour of such a material also in a situation when the material experienced unloading after achievement of maximum strain just before rupture of the sample. In the case of uniaxial tension it is shown that the Mullins effect can occur almost exclusively during the first loading cycle, and all secondary cycles, i.e. the second, third cycles, are close. Thus, only theoretical stress-softening example which can take place between the first and the third cycles is considered. It is to be noted that reloading paths do rejoin the primary loading curve at the maximum strain. In fact, as the samples are unloaded to zero displacement, they remain in a deformed configuration due to the time-dependent behaviour of the material (creep phenomenon). Consequently, the next reloading stretch level should be higher than the first loading stretch level to rejoin the first path (JOHNSON and BEATTY [15]). As in most of the studies concerning the Mullins effect, the stress-softening behaviour should be separated from other inelastic phenomena, such as hysteresis and relaxation. Concerning the hysteresis phenomenon, unloading paths of cycles are not considered and it is assumed that the equilibrium paths are the loading paths. Nevertheless, the stress-softening model can be developed for loading paths. Once the virgin strain energy function has been chosen, the form of the damage evolution equation (Eqs. (6.12) and (6.18)) has to be established. As detailed in the theoretical part of the paper (Sec. 6.2), the present approach focuses on the use of a measure of deformation expressed as a function of the two first invariants of tensor $\mathbf{B}$ (Eq. (3.1)). As the first approach, we assume a very simple measure of the deformation state that depends only on I_1:

$$m = \sqrt{\lambda_1^4 + \lambda_2^4 + \lambda_3^4}. \tag{6.23}$$

The damage function $\xi(m; M)$ will be determined using the experimental results. The general method used here is described in Sec. 6.3 without reference to the kind of experiments, but results for uniaxial tensile data are presented.

Consider the experimental results as shown in Fig. 5; the stress-strain relationship reduces to a sequence of loading curves at different maximum strains. For the Mooney–Rivlin model, nominal stress in test of monotonic loading and unloading and cycled reloading and unloading, can be calculated from a formulas given above for the known form of softening function $\xi(m; M)$.
For the form of function ξ given by Eq. (6.12)

$$\xi(m; M) = e^{-b\sqrt{M-m}}$$

we define the nominal stress as a function of m.

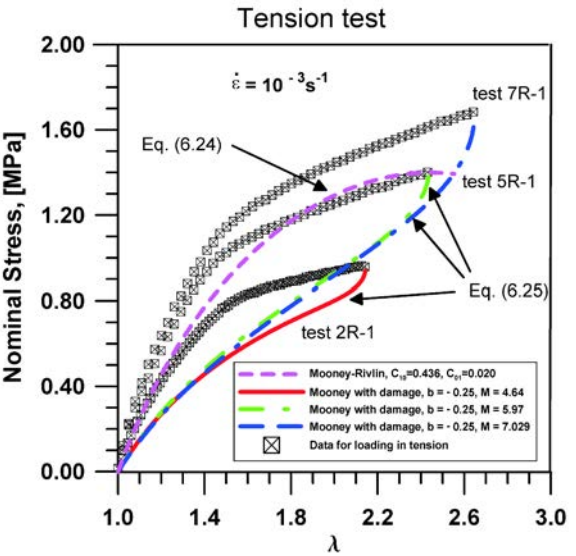

FIG. 5. Nominal stress in uniaxial tension test as a function of axial change of length λ for loading test (experimental data) and relation Eq. (6.24), and three expected paths of unloading from the states with maximum intensities of strain M, defined just before rupture $\lambda = \lambda_{\max}$, for different samples described by Eq. (6.25) with the same damage parameter b.

In this figure, the nominal stress $\boldsymbol{\sigma}$ is given as a function of the first invariant I_1. Two types of stress-strain curves can be identified: the primary curve represented by a dashed line and secondary curves represented by solid lines. Depending on the type of curve, the stress-strain relationships are different:

- for the primary curve, the current stress σ_{11} is given by

$$\sigma_{11} = 2\left\{\left(\lambda - \frac{1}{\lambda^2}\right) C_{10} + \left(1 - \frac{1}{\lambda^3}\right) C_{01}\right\}, \tag{6.24}$$

for monotonic loading, and

- for the i-*th* secondary curve

$$\sigma_{11}^{*} = 2\left\{\left(\lambda - \frac{1}{\lambda^2}\right) C_{10} + \left(1 - \frac{1}{\lambda^3}\right) C_{01}\right\} e^{-b\sqrt{M-m}}, \tag{6.25}$$

for unloading and reloading.

Parameters C_{10} and C_{01} were identified for monotonic loading and accepting $\lambda = \lambda_{\max}$ for each sample and with Eq. (6.17) for m and M. For one cycle of loading it was possible to identify for this model of material with damage of microstructure, one parameter of damage b.

The results of process of identification have been presented in Fig. 5.

6.7. The identification of parameters in compression test

In compression tests the material was subjected to cyclic loading and unloading. Displacement of the upper surface of a cylindrical sample as a function of time is presented in Fig. 6.

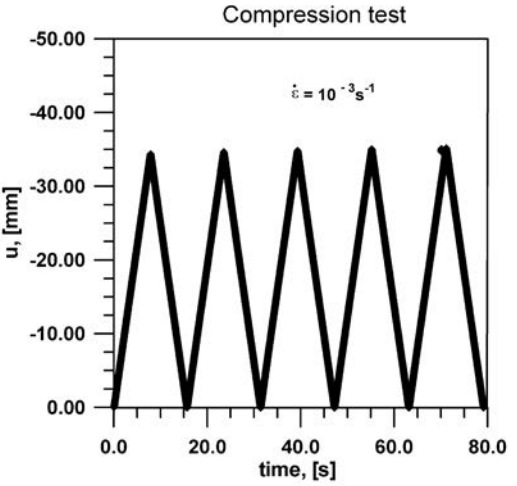

FIG. 6. Change of displacement of the top surface central point of a sample as a function of time in uniaxial quasi-static compression test. Experimental data for samples 6CC-1, cf. [20].

Similarly to the case of tension, let us use the Mooney–Rivlin model for determination of the nominal stress in monotonic loading and cycle unloading and again loading, with the same damage function $\xi(m; M) = e^{-b\sqrt{M-m}}$.

We define nominal stress by the formula similar to that of the tension tests:

$$\sigma_{11} = 2\left\{\left(\lambda - \frac{1}{\lambda^2}\right) C_{10} + \left(1 - \frac{1}{\lambda^3}\right) C_{01}\right\}, \tag{6.26}$$

for monotonic loading, and

$$\sigma_{11}^{*} = 2\left\{\left(\lambda - \frac{1}{\lambda^2}\right) C_{10} + \left(1 - \frac{1}{\lambda^3}\right) C_{01}\right\} e^{-b\sqrt{M_c - m}}, \tag{6.27}$$

for unloading and reloading.

In compression tests parameter C_{10} and C_{01} were also identified like before for monotonic loading and assuming $\lambda = \lambda_{\max}$ and Eq. (6.17) for m and $M_c = M(\lambda_{\max})$. For our experimental compression test $M_c = 6.21$.

Parameter b in the Mooney–Rivlin model can be immediately determined using the relation (6.15) and the results of process of identification for the first and last cycle are presented in Fig. 7.

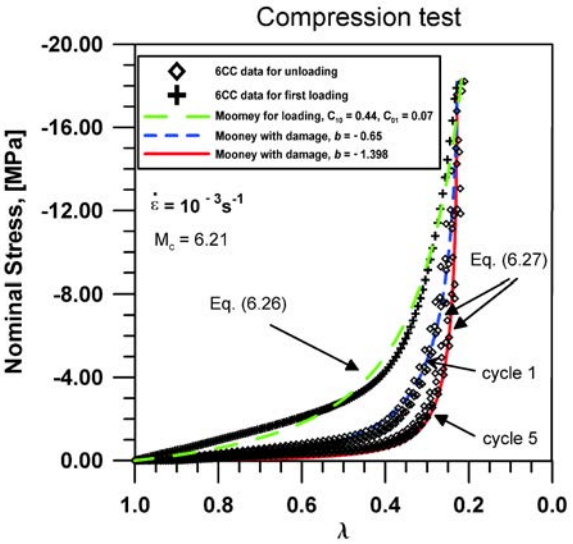

FIG. 7. Nominal stress in uniaxial cycle compression tests as a function of axial change of length λ for loading test (experimental data) and relation Eq. (6.26), and two extreme paths of unloading from the states with maximum intensities of strain M defined for identified models with damaged microstructure described by Eq. (6.27).

Next, we have applied the relation Eq. (6.15) with function $\xi(m; M) = e^{-b\sqrt{M-m}}$ for the first and last cycle and the results of the identification process were presented in Fig. 8.

Now, we applied other forms of the ξ function than that given in Eq. (6.18), to check the possibility of a better fit of models with damage to the experimental data. It is shown that the forms of $\xi(m; M)$ with power $d = 1/2$ and one b parameter can not fit the data for all values of stretches and the values of b are obtained via a non-linear least-squares method based on the natural logarithm. Result for the first and last cycle are presented in Fig. 9.

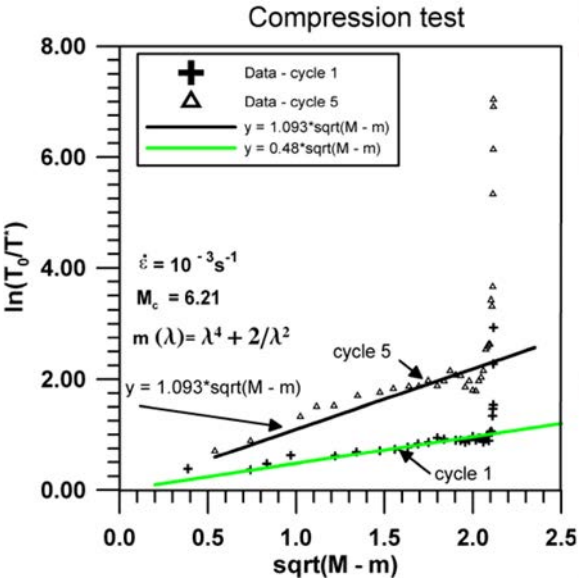

FIG. 8. The value of $\ln \dfrac{T_{0\,11}}{T^*_{11}} = \ln \dfrac{\sigma_{11}}{\sigma^*_{11}}$ in uniaxial compression test as a function of $\sqrt{M-m}$ for unloading test (experimental data) and two extreme values of identified damage parameter b (for first cycle $b = 0.48$ and for last cycle $b = 1.093$) with $M = 1.2$ for one sample.

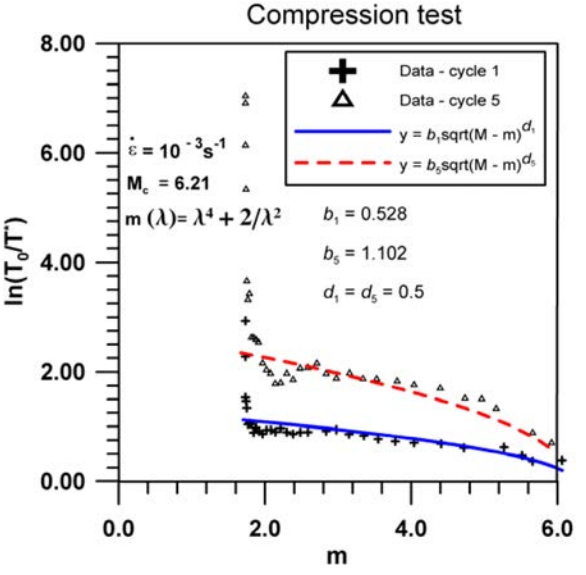

FIG. 9. The value of $\ln \dfrac{T_{0\,11}}{T^*_{11}} = \ln \dfrac{\sigma_{11}}{\sigma^*_{11}}$ in a uniaxial compression test as a function of strain intensity m for unloading test (experimental data), with two identified forms of function $\xi = e^{-b(m-\sqrt{3})^d}$ for extreme cycles of unloading.

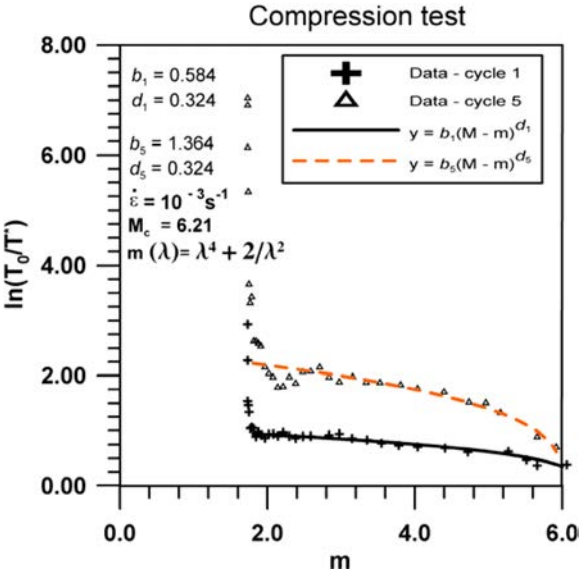

FIG. 10. The value of $\ln \dfrac{T_{0\,11}}{T^*_{11}} = \ln \dfrac{\sigma_{11}}{\sigma^*_{11}}$ in uniaxial compression test as a function of strain intensity m for unloading test (experimental data), with two identified forms of function $\xi = e^{-b(M-m)^d}$ for extreme cycles of unloading.

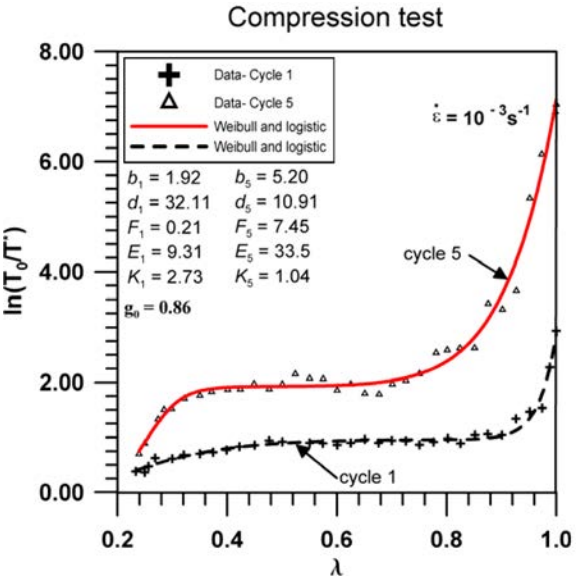

FIG. 11. The value of nominal stress in uniaxial cycle compression tests as a function of axial change of length λ for loading test (experimental data) and two extreme paths of unloading from the states with maximum intensities of strain M defined for identified models with damaged microstructure described by Eqs. (6.21) and (6.22), $\xi^*(\lambda) = K(1 - g(\lambda))e^{-b(\lambda)^d}$.

The identification was performed also for function ξ in the form (6.18)

$$\xi(\sqrt{3}; m) = e^{-b(m-\sqrt{3})^d}.$$

We assume now that the power d in this function can be different than $d = 1/2$. The identification results indicate that the best fitting is obtained with $d = 0.324$. Results of our model adjustment to experimental data for such function ξ are presented in Fig. 10.

The results of identification process for a new function $\xi^*(\lambda)$ given in Eq. (6.21) and Eq. (6.22) for the first and last cycle are presented in Fig. 11.

It is evident that this form of $\xi^*(\lambda)$ with four parameters fitting the data can be also obtained via a non-linear least-squares method, based on the natural logarithm and the results of our model adjustment to experimental data [20, 21] for rubber-like material.

6.8. Comparison of model prediction with experiment

The results of simulation for a tension test are presented in Fig. 1. This figure shows the comparison of the response in terms of force versus inverse stretch $(1/\lambda)$ for the classical model of Mooney–Rivlin. Figures 2–4 show the nominal stress as a function of the axial stretch λ.

In the Mooney–Rivlin model for uniaxial tension with stress-softening, four material parameters have to be determined: two for the virgin strain energy, i.e. C_{10} and C_{01}, and two for the evolution equation of the damage, i.e. b and M. Due to the use of a measure of deformation instead of the strain energy function as the damage criterion, the monotonic primary curve could be fitted first by using the data reported in Fig. 5; and then the determination of W_0 reduces to the classical problem of fitting a hyperelastic model, using the primary loading curve. Nevertheless, taking into consideration the limitations discussed above, it is more efficient to perform a global identification using the stress-strain data for both the uniaxial tensile and uniaxial compression tests. For the identification process, the difference between the model and experimental results is calculated simultaneously on all curves. Computations are performed using the known square difference algorithm. The values of material parameters obtained are presented in Fig. 5 and the identification results are compared with experiments.

For uniaxial compression – deformation state, the results are compared with experimental data in Figs. 7–11, respectively. Theoretical results are globally in good agreement with experiments; so, the model describes successfully the transition between different loading curves in cyclic experiments and exhibits the influence of the maximum strain on the softened behaviour. Finally, considering Eq. (6.18) and the values of material parameters given in Fig. 5, the present

approach is applicable until 300% of the deformation in uniaxial tension. In this way, simulation of large strain problems can be considered. This curve shows the ability of the rubber elasticity models to estimate the degradation of the material properties. The stiffening effect for all ranges of strain is here very well estimated. It is important to note that the chosen material function $g(\lambda)$ is a logistic function (see [10, 13]), which is a case of S-shape function and which enables to fit the damage model.

If we compare our theory with the experimental data of MULLINS and TOBIN [24], MULLINS [26] on simple tension and compression as the first step of modelling, we shall only use the isotropic scalar function ξ proposed in Sec. 6, remembering that this form will require only a small number of parameters to be identified, when a curve-fitting method is used, to obtain its parameter values, OGDEN and RUXBURGH [19]. According to [19], the component of the energy function for the original material takes the form $W(\lambda_1;\, \lambda_2;\, \alpha) = (1-\alpha)W_0(\lambda_1;\, \lambda_2)$.

7. Conclusions and final remarks

In this paper, the different models proposed in literature for the description of the Mullins effect in rubber-like solids, e.g. the Mooney–Rivlin and the Ogden model, are studied, which are phenomenological in nature, and a microscopically based interpretation of some of the constitutive parameters may be given (see HORGAN and SACCOMANDI [44]). In this way, it was possible to modify a model for the Mullins effect. The mathematical simplicity of the phenomenological models of rubber-like materials allows to determine all their features analytically and to provide new insights into the physical mechanisms underlying the Mullins effect. The solid rubber structures are able to undergo very large deformation up to 300% or 600%, which involves damage of the elastomer. The proposed model, which is based on the continuum damage mechanic, also applied a phenomenological approach, and is simple with few parameters to identify and it is efficient to take into account the degradation of material properties. Moreover, it enables to take into account the asymmetry of the response of the damaged material in tension and compression, which is a worthy aspect to be taken into account in modelling of rubber-like materials. Concerning the simulation, even if the finite element e.g. ABAQUS code enables to perform tension or shear experiment simulation up to higher strains, all the difficulties are not overcome. Of course, one more difficulty is always due to the finite element distortion which could appear when deformation becomes large, even if the sensibility is diminished through the use of a material formulation.

This paper shows that constitutive Eqs. (6.16a) and (6.16b) for axial deformation in tension and compression tests describe the behaviour of the stud-

ied material well, near monotonic as well as cyclic loading. The form of these equations was determined using the model of Mooney–Rivlin for monotonic loading, and the model for cyclic loading proposed by MULLINS and TOBIN [24] and modified by ELIAS–ZÚÑIGA and BEATTY [17], which takes into account the decrease of strength capacity of rubber-like materials under unloading and reloading. The studied material belonging to elastomers material is a two-phase material which consists of hard and soft segments (rubber). Macroscopic behaviour of such materials is the result of conversion of a hard phase into soft phase during deformation and the observed macroscopic growth of the microstructural strains is the result of percentage changes of content of every phase for the given level of macroscopic strain. In the presented models of elastomers, simplified mechanism of deformation is applied, which is mathematically simplified in comparison with the model of non-Gaussian type proposed in papers e.g.: BUECHE [51], GOVINDJEE and SIMO [23]. The well-known in literature, analytical models of Ogden and Mooney–Rivlin hyperelasticity of rubber-like materials are not suitable to describe the behaviour of such materials under reversible loadings. It should be stressed that the applied constitutive description of the interpretation of the experimental results, does not require for each material phase the specification of the constitutive relation. In description of the rubber-like material behaviour under the applied loading it is sufficient to know the constitutive relation for the soft phase. It is also essential, that elastic deformations of hard phase in majority of its volume do not undergo any changes in the process of deformation. The description of mechanisms of influence between the hard and soft phases and conversion of a hard phase into a soft one require, however, additional studies. In paper by GOVINDJEE and SIMO [23] was proposed a certain general explanation of the interaction between phases in the general state of strains, however the analysis of mechanisms of exchange of these phases is missing. It is also justified to consider the additional effects, which have influence on the decrease of strength capacity of rubber-like materials, e.g. such as induced anisotropy (cf. MULLINS [25]). In order to do this, we should consider the effect of arrangement of hard phase as well as suitable growth of the length of free chains network bonds.

Our calculations have shown the efficiency of the models used to simulate the complex phenomena such as the Mullins effect in rubber-like materials. A good compatibility was obtained between the numerical results and the experimentally observed behaviour of polyurethane materials with damages in the finite strains conditions. To determine the proposed phenomenological model of material based on experimental data, we need to identify five constants: C_{10}, C_{01}, M, d and parameter b of softening rate in Eq. (6.5). Different models, e.g. the microstructural model of BEATTY and KRISHNASWAMY [16] or phenomenolog-

ical model of OGDEN and ROXBURGH [19], require considerable calculations to obtain good compatibility with experiment and they require identification of the considerably larger number of material parameters. The models with networks of non-Gaussian distribution of the chains, e.g. the 8-chain Arruda–Boyce model, require identification of only several physical parameters, but these models are not studied in the present paper.

The proposed phenomenological theory of stress-softening behaviour of deformed rubber-like materials described by the constitutive Eq. (6.14) with identified parameters, for the studied material, is suitable for modelling the uniaxial tension and compression tests. For the studied rubber-like material, we can determine constitutive model, as a result of determination of the general form of strain energy density function W, by simple parameters identification. To do this we determine $\dfrac{\partial W}{\partial I_1} = f(I_1)$ and the identification of parameters is performed by the experiment for uniaxial tension test for $\lambda \geq 1$. Keeping the well-known parameters of function $f(I_1)$, we determine $\dfrac{\partial W}{\partial I_2} = h\ (I_2)$ and the identification of parameters can be performed by experiment for the whole range of strains for $\lambda > 0$. The form of strain energy density function W is a result of general form of the Rivlin strain energy density function for hyperelastic material and can be obtained also from different universally applied approximations with application of constants C_{01} and C_{10}. Therefore definite parameters C_{01} and C_{10} for this material can be possibly used in accessible commercial packets of finite elements. In our analysis it was established that the studied rubber-like material, described by the constitutive Eq. (6.14), is characterized in the range of uniaxial tension and compression by the following parameters: $C_{10} = 0.335$ and $C_{01} = 0.00045$ and the estimated initial shear modulus equals $\mu_0 = 2(C_{10} + C_{01}) = 0.67$ [MPa] for the Mooney–Rivlin model with assumption of incompressibility; $\mu = 0.65$ and $\alpha = 1.755$ and estimated initial shear modulus $\mu_0 = \mu = 0.65$ [MPa] for the Ogden model with assumption of incompressibility; Young's modulus $E = 1.41$ [MPa] and Poisson's coefficient $\nu = 0.50$ and the estimated initial shear modulus $\mu_0 = 0.47$ [MPa] for logarithmic model. The assumption of small compressibility improves the agreement of estimations with experiment when Young's modulus $E = 2.44$ [MPa] and Poisson's coefficient $\nu = 0.32$, and the estimated initial shear modulus equals $\mu_0 = 0.942$ [MPa].

Our analysis is limited to the uniaxial experimental tests for this material and the stress behaviour was not studied in more complex deformation states, e.g.: biaxial tension or simple shear. So, we should identify the introduced functions and parameters based on the experimental data for complex states of loading. Such more general verification is required if we would like to apply the modified model for a wide class of hyperelastic materials.

Contrary to observations based on the analysis of experimental data presented in this paper, the softening functions $\hat{\xi} = 1 - \hat{\alpha}(m; M)$ in pseudo-elastic models of the Mullins effect, are always assumed to be monotonously increasing functions of m for all values of the pre-strain M. This is the main reason for the observed qualitative differences in shapes of the softening curves due to theoretical models and the experimental data curves (see Fig. 2 and Fig. 5). This explains also the difficulties in fitting the experimental data by theoretical models. It should be noted further that the modified version of Eq. (6.18) of the virgin softening function Eq. (6.12) can not essentially improve the predictions of pseudo-elastic models of the Mullins effect, because the softening function $\xi(m; M)$ in Eq. (6.18) is also a monotonously increasing function of the axial change of length λ. The predictions of pseudo-elastic models of the Mullins effect with application of the new softening functions Eq. (6.21) and Eq. (6.22) presented in Fig. 11 are very successful.

It is also very important to mention that stress softening is an inherently anisotropic phenomenon, and for description of this we need to understand the method of incorporating the induced anisotropy. However, it has been also pointed out that the anisotropic model cannot be properly developed at the present stage, because suitable experimental data are not available or published. The extension of the results presented here to other states of deformation such as simple or pure shear, is a straightforward matter and the development of a general 3D model presents no conceptual difficulties. So far it has been shown that rubber-like materials constitutive theory is effective due to using the form of energy function given by Eq. (6.2).

Acknowledgements

The author is grateful to the State Committee for Scientific Research (KBN, Poland) for its financial support through the grant No. 4 T07E 052 27.

References

1. J. Lambert-Diani, C. Rey, *New phenomenological behaviour laws for rubbers and thermoplastic elastomers*, Eur. J. Mech. A/Solids, **18**, 1027–1043, 1999.

2. K. Farahani, H. Bahai, *Hyper-elastic constitutive equations of conjugate stresses and strain tensors for the Seth-Hill strain measures*, I. J. Eng. Science, **42**, 29–41, 2004.

3. L. Anand, *A constitutive model for compressible elastomeric solids*, Computational Mechanics, **18**, 339–355, 1996.

4. MSC. Marc Volume A: *Theory and User Information*, Chapter 7 Material Library, Elastomer, 7-50-7-60.

5. Z. Guo, L. J. Sluys, *Application of a new constitutive model for the description of rubber-like materials under monotonic loading*, Int. J. of Solids and Structures, **43**, 2799–2819, 2006.

6. R. W. Ogden, *Large deformation isotropic elasticity – on the correlation of theory and experiment for incompressible rubberlike solids*, Proc. R. Soc. Lond., A **326**, 565–584, 1972.

7. R. W. Ogden, *Large deformation isotropic elasticity – on the correlation of theory and experiment for compressible rubberlike solids*, Proc. R. Soc. Lond., A **328**, 567–583, 1972.

8. R. W. Ogden, *Elastic deformations of rubberlike solids*, H.G. Hopkins and M.J. Sewell [Eds.], The Rodney Hill 60th Anniversary Volume (Pergamon, Oxford, UK 328, 499–537, 1982.

9. J. Simo, R. L. Taylor, *Quasi-incompressible finite elasticity in principal stretches. Continuum basis and numerical algorithms*, Comp. Meth. in Appl. Mech. and Eng., **85**, 273–310, 1991.

10. E. M. Arruda and M. C. Boyce, *A three-dimensional constitutive model for the large stretch behaviour of rubber elastic materials*, J. Mech. Phys. Solids, **41**, 389–412, 1993.

11. E. A. De Souza Neto, D. Perić and D. R. J. Owen, *A phenomenological three-dimensional rate-independent continuum damage model for highly filled polymers: formulation and computational aspects*, J. Mech. Physics of Solids, **42**, 1533–1550, 1994.

12. C. O. Horgan, R. W. Ogden and G. Saccomandi, *A theory of stress softening of elastomers based on finite chain extensibility*, Proc. R. Soc. Lond., A **460**, 1737–1754, 2004.

13. D. De Tommasi, G. Puglisi and G. Saccomandi, *A micromechanics-based model for the Mullins effect*, J. Rheol., **50**, 495–512, 2006.

14. M. M. Attard and G. W. Hunt, *Hyperelastic constitutive modeling under finite strain*, I. J. Solids and Structures, **41**, 5327–5350, 2004.

15. M. A. Johnson and M. F. Beatty, *The Mullins effect in equibiaxial extension and its influence on the inflation of a balloon*, I. J. Eng. Science, **33**, 223–245, 1995.

16. M. F. Beatty and S. Krishnaswamy, *A theory of stress-softening in incompressible isotropic materials*, J. Mech. Physics of Solids, **48**, 1931–1965, 2000.

17. A. Elias-Zúñiga and M. F. Beatty, *A new phenomenological model for stress-softening in elastomers*, ZAMP, **53**, 794–814, 2002.

18. A. Elias-Zúñiga, *A phenomenological energy-based model to characterize stress-softening effect in elastomers*, Polymer, **46**, 3496–3506, 2005.

19. R. W. Ogden and D. G. Roxburgh, *A pseudo-elastic model for the Mullins effect in filled rubber*, Proc. R. Soc. London, A **455**, 2861–2678, 1999.

20. A. Kwiecień, B. Zając, *Wyniki testów rozciągania, ściskania i ścinania materiału ICOSIT*, Raport KBN (in Polish), Kraków 2006.

21. A. Kwiecień, J. Kubica, P. Stecz, B. Zając, *Flexible joint method (FJM) – A new approach to protection and repair of cracked masonry*, First European Conference on Earthquake Engineering and Seismology (a joint event of the 13th ECEE & 30th General Assembly of the ESC), Geneva, Switzerland, 3–8 September 2006, Paper Number: 282.

22. J. C. Simo, *On a fully three-dimensional finite-strain viscoelastic damage model: formulation and computational aspects*, Comput. Methods Appl. Mech. Eng., 60, 153–173, 1987.

23. S. Govindjee, J. C. Simo, *A micro-mechanically based continuum damage model for carbon black-filled rubbers incorporating Mullins' effect*, Journal of the Mechanics and Physics of Solids, 39 (1), 87–112, 1991.

24. L. Mullins, N. R. Tobin, *Theoretical model for the elastic behaviour of filler-reinforced vulcanized rubbers*, [in:] Proceedings of the Third Rubber Technology Conference, London 1954 (Published in 1956), 397–412, 1956.

25. L. Mullins, *Effect of stretching on the properties of rubber*, Journal of Rubber Research, 16 (12), 275–289, 1947.

26. L. Mullins, *Softening of rubber by deformation*, Rubber Chemistry and Technology, 42 (1), 339–362, 1969.

27. C. Miehe, *Discontinuous and continuous damage evolution in Ogden-type large-strain elastic materials*, Eur. J. Mech. A/Solids, 14, 697–720, 1995.

28. C. Miehe, S. Göktepe, F. Lulei, *A micro-macro approach to rubber-like materials – Part I: the non-affine micro-sphere model of rubber elasticity*, Journal of the Mechanics and Physics of Solids, 52, 2617–2660, 2004.

29. C. Miehe, S. Göktepe, *A micro-macro approach to rubber-like materials. Part II: The micro-sphere model of finite rubber viscoelasticity*, Journal of the Mechanics and Physics of Solids, 52, 2231–2258, 2005.

30. S. Göktepe, C. Miehe, *A micro-macro approach to rubber-like materials. Part III: The micro-sphere model of anisotropic Mullins-type damage*, Journal of the Mechanics and Physics of Solids, 53, 2259–2283, 2005.

31. S. Krishnaswamy, M. F. Beatty, *The Mullins effect in compressible solids*, Int. J. of Eng. Science, **38**, 1397–1414, 2000.

32. B. Meissner, L. Matejka, *A structure-based constitutive equation for filler-reinforced rubber-like networks and for the description of the Mullins effect*, Polymer, 47, 7997–8012, 2006.

33. G. Heinrich, M. Kaliske, *Theoretical and numerical formulation of a molecular based constitutive tube-model of rubber elasticity*, Comput. Theor. Polym. Sci., 7 (3/4), 227–241, 1997.

34. R. W. Ogden, G. Saccomandi, I. Sgura, *Fitting hyperelastic models to experimental data*, Computational Mechanics, 34 (6), 484–502, 2004.

35. R. Kazakeviciute-Makovska, *Experimentally determined properties of softening functions in pseudo-elastic models of the Mullins effect*, International Journal of Solids and Structures, 44, 4145–4157, 2007.

36. C. O. Horgan, J. G. Murphy, *Plane strain bending of cylindrical sectors of admissible compressible hyperelastic materials*, Journal of Elasticity, 81(2), 129–151, 2005.

37. Z. P. Huang, J. Wang, *A theory of hyperelasticity of multi-phase media with surface/interface energy effect*, Acta Mechanica, 182 (3–4), 195–210. 2006.

38. C. O. Horgan, J. G. Murphy, *Invariance of the equilibrium equations of finite elasticity for compressible materials*, Journal of Elasticity, 77 (3), 187–200, 2004.

39. A. DeSimone, J. J. Marigo and L. Teresi, *A damage-mechanics approach to stress softening and its application to rubber*, Eur. J. Mech. A, 20, 873–892, 2001.

40. A. Lion, *A constitutive model for carbon-black-filled rubber: experimental investigations and mathematical representation*, Continuum Mech. Thermodyn., 8, 153–169, 1996.

41. E. G. Septanika, L. J. Ernst, *Application of the network alteration theory for modeling the time-dependent constitutive behaviour of rubbers*, *Part I.*, Mech. Mater., 30, 253–263, 1998.

42. F. Andrieux and K. Saanouni, *On a damaged hyperelastic medium: Mullins effect with irreversible strain*, Int. J. Damage Mech., 8, 82–103, 1999.

43. G. Marckmann, E. Verron, L. Gornet, G. Chagnon, P. Charrier and P. Fort, *A theory of network alteration for the Mullins effect*, J. Mech. Phys. Solids, 50, 2011–2028, 2002.

44. C. O. Horgan, G. Saccomandi, *A molecular-statistical basis for the Gent constitutive model of rubber elasticity*, J. Elasticity, 68, 167-176, 2002.

45. H. J. Qi and M. C. Boyce, *Stress-strain behaviour of thermoplastic polyurethanes*, Mechanics of Materials, 37, 817–839, 2005.

46. P. Król, *Synthesis methods, chemical structures and phase structures of linear polyurethanes. Properties and applications of linear polyurethanes in polyurethane elastomers, copolymers and ionomers*, Progress in Materials Science, 52, 915–1015, 2007.

47. C. Miehe, J. Keck, *Superimposed finite elastic-viscoelastic-plastoelastic stress response with damage in filled rubbery polymers. Experiments, modelling and algorithmic implementation*, J. Mech. Phys. Solids, 48, 323–365, 2000.

48. G. Pompe, A. Pohlers, P. Pötschke, J. Piontec, *Influence of processing conditions on the multiphase structure of segmented polyurethane*, Polymer, 39, 5147, 1998. (280)

49. W. Kuran, M. Sobczak, T. Listos, C. Debek, Z. Florjanczyk, *New route to oligocarbonate diols suitable for the synthesis of polyurethane elastomers*, Polymer, **41** (24), 8531–8541, 2000. (42)

50. M. Herrera, G. Matuschek, A. Kettrup, *Thermal degradation of thermoplastic polyurethane elastomers (TPU) based on MDI*, Polymer Degradation and Stability, **78** (2), 2002.

51. F. Bueche, *Molecular basis for the Mullins effect*, Journal of Applied Polymer Science, 4 (10), 107–114, 1960.

52. L. R. G. Treloar, *Stress–strain data for vulcanised rubber under various types of deformation*, Trans. Faraday Soc., **40**, 59–70, 1944.

53. H. M. James and E. Guth, *Theory of the increase in rigidity of rubber during cure*, J. Chem. Phys., **15**, 669–683, 1947.

54. L. R. G. Treloar and G. Riding, *A Non-Gaussian theory for rubber in biaxial strain. I. Mechanical properties*, Proc. Roy. Soc. London A, **369**, 261–280, 1979.

55. H. M. Arruda and M. C. Boyce, *A three-dimensional constitutive model for the large stretch behavior of rubber elastic materials*, J. Mech. Phys. Solids, **41**, 389–412, 1993.

56. P. D. Wu and E. van der Giessen, *On improved network models for rubber elasticity and their applications to orientation hardening in glassy polymers*, J. Mech. Phys. Solids, **41**, 427–456, 1993.

57. M. C. Boyce and E. M. Arruda, *Constitutive models of rubber elasticity: a review*, Rubber Chem. Technol., **73**, 505–523, 2000.

58. A. N. Gent, A new constitutive relation for rubber, Rubber Chem. Technol., **69**, 59–61, 1996.

59. J. Lemaitre, J. L. Chaboche, Mechanics of Solid Materials, Springer-Verlag, Berlin, 1987.

Received March 22, 2007; revised version December 19, 2007.

ENGINEERING TRANSACTIONS • *Engng. Trans.* • **56**, 2, 159–180, 2008
Polish Academy of Sciences • Institute of Fundamental Technological Research

BENDING OF FRAGMENTED ARCHITRAVES RESTORED WITH BOLTED TITANIUM BARS: A NUMERICAL ANALYSIS

S. K. Kourkoulis, E. Ganniari–Papageorgiou

National Technical University of Athens, School of Applied Sciences
Department of Mechanics, Laboratory of Testing and Materials
5, Heroes of Polytechnion Avenue, Zografou Campus, 157-73 Athens, Greece

The mechanical behaviour of restored structural members of ancient monuments is studied in the present paper with the aid of the Finite Element Method. The study is motivated by the needs of the conservation project in progress on the Parthenon Temple of the Acropolis of Athens; the results however could be valuable for various stone monuments under conservation. Centrally fractured prismatic marble architraves (epistyles) of rectangular cross-section restored with either threaded or smooth titanium bars are modelled. The architraves are resting on marble blocks simulating the capitals (abacuses) of the columns of the temple. They are subjected to bending under uniformly distributed loading along their span, following the results of earlier studies, concerning the influence of the loading mode on the overall behaviour of restored structural members. The method used for determination of the reinforcement required is the one introduced recently by the scientists working for the restoration of the Acropolis monuments. All the loads that could be applied on the member after it is replaced in its initial position in the monument were taken into account, including the own weight of the member, the weights of the members that will rest on it after the restoration, as well as possible dynamic (earthquake) loads. Emphasis is laid on the influence of the threads of the bolted bars in comparison to the results for the unbolted ones, in an effort to quantify the maximum anchoring length required in order to minimize the intervention on the authentic stones. The distribution of the stress and strain fields all over the architrave-abacus-reinforcing bar system is investigated and conclusions are drawn concerning the extreme stresses and the points where they are developed.

1. Introduction

Restoring and conserving an ancient monument is a complicated, multidisciplinary scientific task. Many problems are to be considered and solved before final decisions are made. These problems vary from elementary ones (for example the strength and deformability of the materials used) to rather complex ones (such as preservation of the structural system, determination of the minimum possible intervention, reversibility of the interventions and of course, their durability). Archaeologists, architects, materials scientists, civil and chemical engineers collaborate in order to meet the final target, i.e. the extension of the life of the

monument. The decisions made are usually a compromise between various, and often contradictory, points of view.

A typical example of a complicated restoration program is that of the Parthenon Temple of the Acropolis of Athens. Parthenon, the masterpiece of Fidias and Kallikratis, was built in the 5th century BC as a temple of goddess Athena. It is the most famous surviving building of ancient Greece and it has been praised as the finest achievement of Greek architecture. The Parthenon is an enduring symbol of Ancient Greece and of Athenian democracy and it is regarded as one of the world's greatest cultural monuments.

The temple has been damaged by fire during the invasion of the Herulians, but the exact date of the fire and subsequent repairs are debated (suggestions range from 150 B.C. to 267 A.D.). Later Parthenon was converted to a Christian church of the Virgin Mary (around 600 A.D.). At the time of the Latin Empire it became, for about 250 years, a Roman Catholic Church. In 1456, Athens fell to the Ottomans and the Parthenon was converted into a mosque. Besides the successive conversions, European visitors in the 17th century testified that the building was largely intact. In 1687, the Parthenon suffered its greatest blow when the Venetians attacked Athens, and the Ottomans fortified the Acropolis and used the building as a gunpowder magazine. A Venetian mortar exploded in the magazine and the building was partly destroyed. The internal structures were demolished, the roof collapsed, and some of the pillars, particularly those on the southern side, were decapitated. After this, much of the building fell into disuse and a smaller mosque was erected.

The condition of the monument was aggravated by older restoration projects (between 1840 and 1930) and many structural problems appeared (intrusion of moisture, appearance of funguses, corrosion and inflation of the iron joints and fracture of marble structural members). The Athens' 1981 earthquake made the situation worse and from this moment on, an ambitious scientific restoration project was approved by the Hellenic State, which is in progress until today. Series of problems have been confronted in the frame of this project concerning especially protection of the authentic material and minimization of the interventions on the original structural elements of the Temple. Various innovative solutions were proposed and applied and nowadays these solutions are considered as guidelines for the scientists working on similar projects.

In the frame of the above project, a pioneer method was developed for the restoration of fractured structural elements in an effort to confront the problem of the structural stability of the monument [1]. The method is based on the use of titanium bars in combination with suitable cement mortar and permitted to reduce the interventions on the authentic material in comparison to older approaches. It takes into account all the loads that could be applied on the member after it is replaced in its initial position in the monument, namely the weight

of the member and these of any other members that will rest on it after the restoration is completed as well as possible dynamic loads [2, 3]. For the theoretical development of the method it is assumed that the stresses do not exceed the linearity limit, the strains developed in the marble body and in the reinforcing bar are compatible with each other, the marble behaves as a transversely isotropic material, the bending loads act normally to the bedding planes and the cross-sections remain plane and normal to the longitudinal, neutral axis of the beam.

Recently the method was assessed experimentally and numerically [4, 5]. It was concluded that the reproduction of actual bending conditions in the laboratory does not give reliable results since the simulation of bending under uniform load by a laboratory multi-point bending test does not lead to accurate conclusions unless the number of loading points is increased dramatically, something unrealizable for practical reasons. Thus the engineer who designs basing on an experimentally evaluated and calibrated model, should increase the safety factor accordingly, in order to take into account the fact that the stress field of the test may be weaker compared to the actually developed one. It was, also, indicated that some of the assumptions adopted are not always satisfied. Indeed, the axial strains do not vary linearly along the height of the architrave but rather they follow a sigmoid distribution. In addition, the neutral axis is translated towards the bottom side of the architrave, rendering the calculations carried out considering the centroidal longitudinal axis as the neutral one, a rather rough approximation of the real conditions.

It became therefore clear that the method for the calculation of the reinforcement required should be studied further before definite conclusions concerning its applicability are drawn. Towards this direction, the problem of joining together fractured structural elements is studied here using a more sophisticated numerical model, in an effort to enlighten the influence of some critical points related to the shape of the reinforcing bars.

2. The material: Dionysos marble

The material used by the ancient Greeks for erection of the monuments of the Parthenon Temple of the Acropolis of Athens was the Pentelic marble which is an extremely durable white marble quarried from Mount Pentelicus in Attica. However, the ancient quarries are nowadays exhausted and the needs of the restoration and conservation programs are covered almost exclusively by Dionysos marble, since it was found to be the most compatible candidate substitute of the authentic Pentelic marble [6, 7].

From the physical point of view, Dionysos marble is composed by 98% of calcite, 0.5% of muscovite, 0.3% of sericite, 0.2% of quartz and 0.1% of chlorite.

Its specific density is 2730 kg/m^3, its apparent density is 2717 kg/m^3 and its absorption coefficient by weight is around 0.11% [8]. The coefficient of thermal expansion is 9×10^6/°C between 15°C and 100°C. Its very low porosity varies between 0.3% in the virgin state to 0.7% after the action of various natural weathering and corrosive agents (superficial porosity). Its grain size varies around 0.43×10^{-3} m and the crystals have a polygonic shape of almost uniform size. The dimensions of the largest crystals vary between 900 μm × 650 μm and 950 μm × 874 μm. It is of white colour with a few thin parallel ash-green veins, following the schistosity of marble and containing locally silver areas due to the existence of chlorite and muscovite [9].

Concerning its mechanical behaviour, the Dionysos marble is an anisotropic material, characterized by three different anisotropy directions (parallel to the layers, along the width of the web and along the thickness of the web) and thus it appears to be orthotropic. The values of its mechanical properties reported in literature vary within very broad limits. It is mentioned characteristically that the values of its tensile strength vary between 2.4 MPa and 19.5 MPa, while the respective experimental values of Young's modulus range between 23 GPa and 90 GPa [6, 7, 10]. However, a long series of direct tension and uniaxial compression tests with cylindrical specimens [11] indicated that the material can be considered as transversely isotropic, since the mechanical properties along the first two of the above anisotropy directions are very similar to each other and therefore, the Dionysos marble can be described with the aid of five elastic constants: two elastic moduli, in the plane of transverse isotropy and normal to it, two Poisson's ratios characterizing the lateral strain response in the plane of transverse isotropy to a tensile stress acting parallel and normal to it, and the shear modulus in the planes normal to the plane of isotropy. It was also concluded that Dionysos marble appears to be slightly non-linear, both in the tension and in the compression regime, and slightly bimodular, i.e. the elastic modulus in tension is slightly different from the respective one in compression [12]. The values of the elastic moduli, Poisson's ratios and the values of tensile strength, σ_t, are recapitulated in Table 1, while in Fig. 1 the stress-strain curve is shown for the whole tension-compression regime.

Table 1. Mechanical properties of Dionysos marble in direct tension (loading rate equal to 10^{-6} m/min).

	E [GPa]	ν	σ_f [MPa]
Strong Direction	84.5	0.26	10.8
Intermediate Direction	79.5	0.26	9.5
Weak Direction	50.0	0.11	5.3

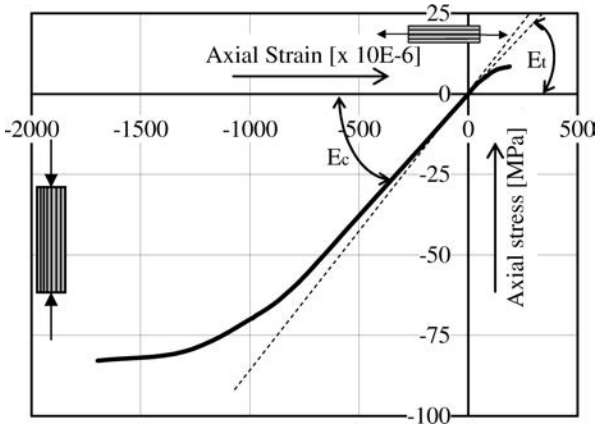

FIG. 1. The stress-strain curve of Dionysos marble along the strong anisotropy direction.

From the above tests it was also concluded that the size effect is very pronounced for Dionysos marble. For example, the Ultimate Compressive Strength of cylindrical specimens of height-to-diameter ratio equal to 2 is strongly dependent on the size of the specimens used for the laboratory tests and, as it is seen in Fig. 2, the dependence appears to be not monotone: a clear maximum exists for specimens of diameter equal to about 125 mm. The size effect appears to be independent of the lubrication conditions between the end platens and the bases of the specimens, although the absolute strength values in case of lubricated specimens are slightly higher. Similar conclusions were drawn also for the tensile strength of Dionysos marble (as obtained from diametral compression tests) as well as for its modulus of elasticity [13].

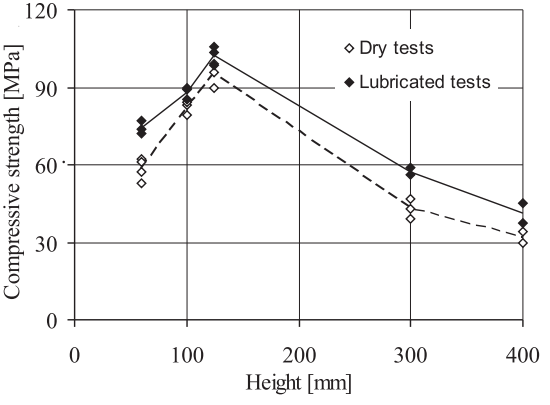

FIG. 2. The size effect for Dionysos marble.

3. Numerical modelling

3.1. Bending of restored marble architraves using cylindrical titanium bars

In actual conditions the architraves of a monument are loaded by an almost uniformly distributed load over their total length, since they carry their own weight and the weight of the superimposed structural elements. However, the realization of a bending test under homogeneous load in the laboratory is an extremely difficult experimental task and therefore, multi-point bending tests are carried out instead. In an effort to check the degree of approximation of the real conditions by the laboratory multi-point bending tests, a numerical analysis was carried out recently [14] using the Finite Element Method and the commercially available software ANSYS 9.0. As a first step and for CPU-time economy, intact marble architraves were considered in that study. Four loading types were simulated:

- Uniformly distributed load along the total length of the architrave (Fig. 3a),
- Uniformly distributed load along the span (Fig. 3b),
- Eight-point bending along the span (Fig. 3c), and
- Eight-point bending along the total length of the member (Fig. 3d).

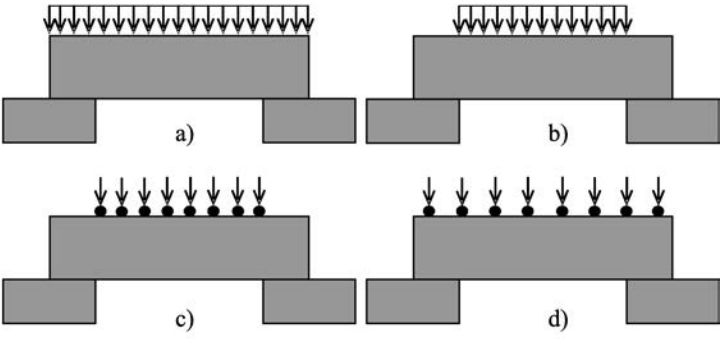

Fig. 3. The four loading cases studied numerically.

Among the most important conclusions of that study was the fact that the points most prone to failure were those in the vicinity of the corners of the supporting abacuses rather than those at the mid-span of the beam. The above conclusion is strongly supported by a thorough in-situ investigation of the architraves of the Parthenon Temple, which have never been removed from their original place from the antiquity until the present days: more than half of the fractures and the cracks observed (excluding those caused by interventions) have their origin very close to the edges of the abacuses [15].

It was also concluded that the strain is not linearly distributed along the height of the architraves but it exhibits a sigmoid variation, in accordance with earlier experimental results [16] and theoretical predictions [17]. The neutral axis of the bent architrave appeared to be displaced downwards. Finally it was indicated that the most intensive stress field developed at the central cross-section of the architrave was the one corresponding to the uniformly distributed load along the span (case b) rather than the one developed in the case of the eight-point bending. It was thus pointed out that the simulation of bending under uniform load with multi-point bending tests leads to underestimation of the stress field developed, which may be catastrophic if the design of the restoration is based on the results of the tests. Therefore an appropriate increase of the safety factors used by the design engineers appears to be absolutely necessary.

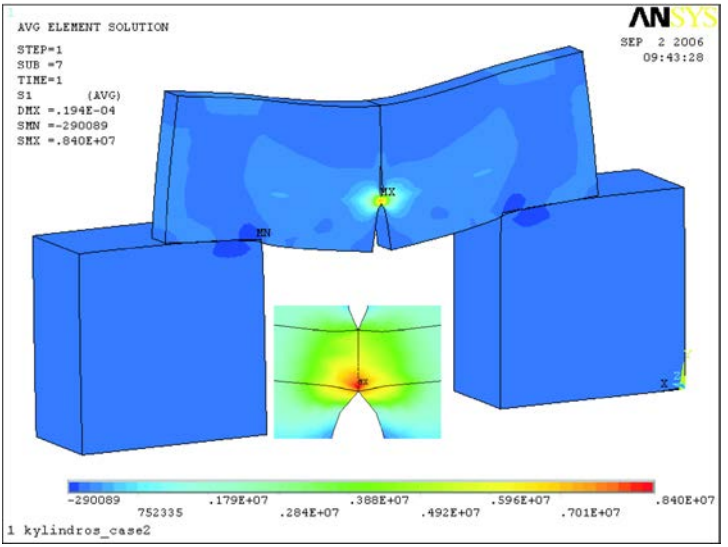

FIG. 4. The distribution of the 1st (maximum) principal stress in the restored architrave. The embedded figure shows a detail of the central section around the titanium bar.

As a second step, the problem of joining together the fragmented marble architraves using titanium bars was also explored numerically in the previous study, taking into account the conclusions drawn from the analysis concerning the intact architraves. The architrave was assumed to consist of two equal parts joined together by a single cylindrical titanium bar fully bonded with the marble. In other words, in this simplified analysis the influence of the threads of the titanium bars was ignored. The geometry of the model matched exactly that of the most damaged architrave of the north colonnade of the Parthenon Temple, namely the fifth external one, in a scale of 1:3. The architrave was subjected to

bending and the load was assumed to be uniformly distributed along the span of the architrave (case b), since it corresponds to the worst case concerning the magnitude of the stress field developed.

An overall view of the distribution of the first (maximum) principal stress in the case of the restored architrave is shown in Fig. 4. As it was expected, the situation is completely different compared to that of the intact member. The points most prone to fail were the ones in the immediate vicinity of the reinforcing bar rather than at the abacuses' corners. In addition it was indicated that in the vicinity of the bar, both beyond and below it, the contact of the two constituent marble parts of the architrave tends to be lost (Fig. 4, embedded figure).

3.2. Bending of restored marble architraves using bolted (threaded) titanium bars; The numerical model

Up to now, the bar-marble interface was not studied extensively since attention was paid to the qualitative and comparative description of the stress and strain fields all over the restored architrave. Therefore the reinforcing bar was considered to be cylindrical in perfect contact with the marble. However in praxis, the bars used are bolted in order to optimize the load transfer mechanism avoiding the pull-out failure. It appears therefore absolutely necessary to study thoroughly the interaction between marble and the reinforcing bar as well as the stress and strain concentrations, inevitably generated at the corners of the threads of the bolted titanium bars. In this direction the same problem was modelled by considering the exact geometrical characteristics of the titanium bars, used in the restoration of the Parthenon Temple.

The architrave was considered again to be centrally fractured and restored with a single titanium bar, which now is assumed to be bolted all over its length, as it is shown schematically in Fig. 5. The geometry of the beam matched again exactly that of the fifth external architrave of the north colonnade of the Parthenon Temple in the scale of 1:3 (length $L = 1.43$ m, thickness $w = 0.18$ m and height $h = 0.45$ m). However, for reduction of the "running time" and taking advantage of various symmetry planes, only one quarter of the configuration was modelled. The diameter of the reinforcing bar was calculated according to the approach introduced by Ioannidou and Paschalides [2] and Mentzini [3] and it was placed at a distance $h_t = 0.305$ m from the upper side of the architrave. The anchoring length at each one of the two equal parts of the architrave was $L = 0.4$ m and the total thread number corresponding to the anchoring length was 200. The thin layer of cement used in practice to increase the adhesion was ignored again. The geometrical characteristics of the titanium bar are presented in Table 2.

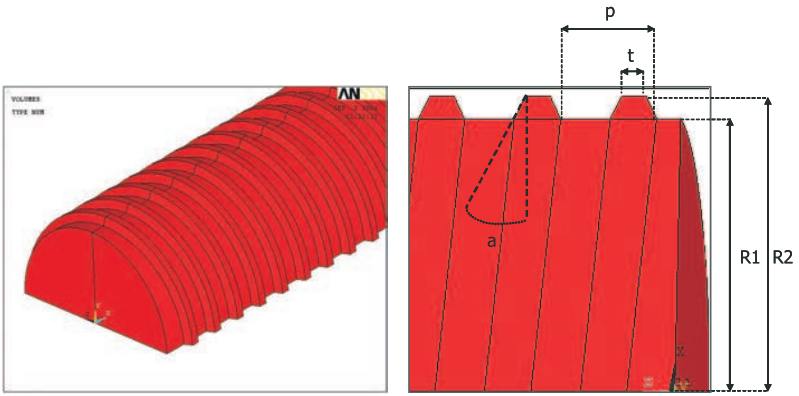

FIG. 5. Schematic representation of the geometrical characteristics of the bolted bar.

Table 2. Geometrical characteristics of the bolted titanium bar.

R1	R2	p	t	a
5.85 mm	6.35 mm	2 mm	0.5 mm	25^0

Assuming that the bedding planes of marble are parallel to the longitudinal axis of the architrave and the bending loads act normally to these planes, the transversely isotropic nature of Dionysos marble could be ignored. Its slight non-linearity and its bimodularity were ignored, also. According to these assumptions, the values of the mechanical properties of Dionysos marble used were those of the strong anisotropy direction of Table 1. The density of Dionysos marble was set equal to $\rho_m = 2.78$ g/cm^3 and the coefficient of static friction between the marble architrave and the marble abacuses was set equal to $\mu = 0.7$. The mechanical properties of the titanium bar were: Young's modulus $E_t = 105$ GPa, Poisson's ratio $v_t = 0.32$, density $\rho_t = 4.51$ g/cm^3. The coefficient of static friction between marble and titanium was assumed equal to 0.4.

The numerical model was discretized by creating a uniform and fine mesh in the vicinity of the titanium reinforcement, since this part of the model was, for the specific problem, the region of highest interest. In order to increase the flexibility of the model and to reduce the CPU running time , a marble "*cylinder*" was constructed around the titanium bar with radius R1+R2, where R1 and R2 are the minimum and maximum radii of the bolted bar, respectively. The regular mesh on the cylinder and the bolted bar was attained by using the Mapped Meshing Technique (Fig. 6b). According to this technique, a volume must have the shape of a brick or a wedge or a prism or even a tetrahedron, and must have equal numbers of element divisions specified on opposite sides. The two volumes (cylinder and bar) were constructed in an appropriate manner,

but without changing their primary geometrical characteristics, in order to take the shape imposed by the mapped mesh. For the remaining part of the model, a coarser mesh was created without employing the mapped meshing technique, but using suitable divisions and spacing ratios on the unmeshed lines (Fig. 6a). The element used for the meshing was the SOLID186, a higher order 3-D structural solid element defined by 20 nodes having three degrees of freedom per node: translations in the nodal x, y, and z directions (Fig. 7). It has quadratic displacement behaviour and is well suited for modelling irregular meshes. The final model consisted of 96784 such elements (Fig. 6a).

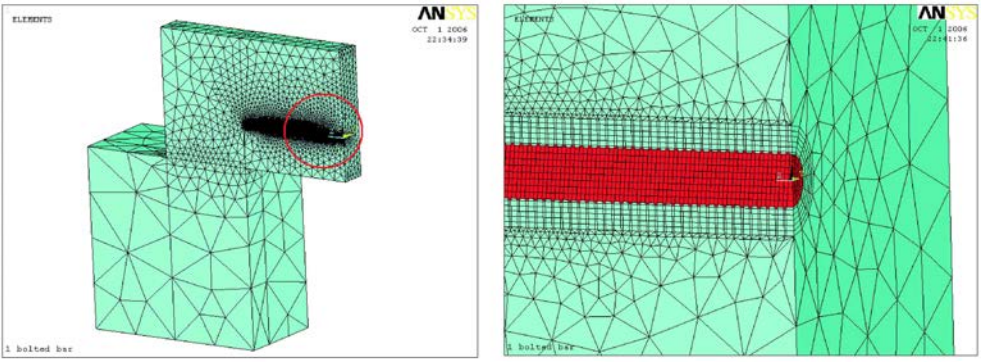

FIG. 6. An overall view of the mesh of the model (a), and a detailed view of the mesh in the vicinity of the titanium reinforcement (b).

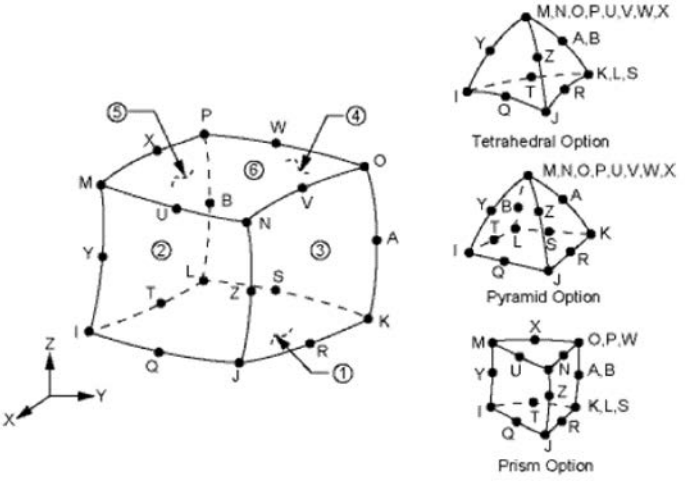

FIG. 7. The element SOLID186 used for the meshing of the model.

The next step of the numerical analysis was identification of the contact options of the problem according to which two surfaces, a "contact" one and a "target" one are to be defined. For modeling rigid-flexible contact, the rigid surface must be represented by the "target" surface. For the specific problem, three couples of 2D contact elements were created (Fig. 8). The first couple represented the contact between the architrave and the supporting abacus, which is a rigid-rigid contact since the contact surfaces are made of the same material (marble). In this context, the contact surface of the architrave was considered as the "target" and that of the abacus as the "contact". The second couple represented the contact between the architrave and the titanium bar, since for the specific problem the titanium bar was not considered to be fully bonded with the marble as in the previous model. Due to the fact that titanium is a rigid material, its contact surface was considered as the "target" and the respective one of the architrave as the "contact". Concerning the third couple, a new rigidly clamped area was created in the position of the central cross-section area of the architrave, in order to be in simple contact with the respective architrave's area. This new area was defined as the "target" surface and that of the architrave as the "contact" one. The elements used for the analysis were "TARGE170" and "CONTA174".

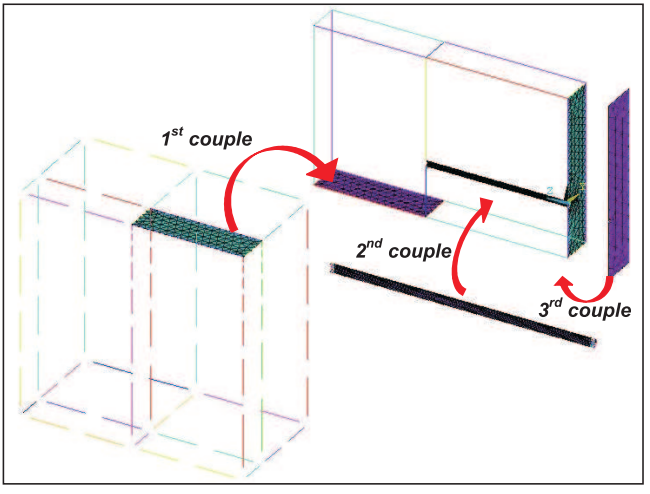

FIG. 8. Identification of the contact elements created for the model.

The boundary conditions were imposed in such a way that both the static determinacy of the problem as well as its symmetry were ensured since, as it has been already mentioned, only a quarter of the configuration was modelled (advantage was taken of the vertical plane of symmetry). In this context, the lower bases of the supporting abacuses were considered as rigidly clamped, while

the central cross-section area of the titanium bar was allowed to be free only along the vertical direction. On the other hand, the central cross-section area of the architrave was restricted only to the right horizontal direction by creating the rigidly clamped target surface described previously (third couple of contact elements).

The load was assumed to be uniformly distributed along the span of the architrave. Its magnitude was equal to 65 kN, i.e. the maximum load expected for the particular architrave, after the completion of the restoration of the Parthenon Temple.

4. Results and discussion

A detailed view of the distribution of the first (maximum principal stress) in the restored architrave and the reinforcing bar in the immediate vicinity of the central cross-section is shown in Fig. 9. From a qualitative point of view, the conclusions drawn are of similar nature compared to those in the case of a restored member with one cylindrical (unbolted) titanium bar: the major part of the architrave is relieved and only at the central cross-section, around the titanium bar, the stresses aproach the fracture stress of marble under direct tension (∼6–8 MPa) and reach the values of the order of about 8 MPa, remaining however far from the respective limit of titanium (∼300 MPa). Comparing the two models, i.e. the bolted and unbolted reinforcing bars (Figs. 9 and 4, respectively), it is noted that the use of bolted bars leads to much higher stresses than those generated by the cylindrical titanium bars.

The distribution of the other two principal stresses is plotted in Figs. 10 and 11. The change of sign of these stresses as one moves towards the interior of the architrave is noteworthy. In addition, similarity of the distribution of the 3rd principal stress with the cone-type fracture surface commonly observed during pure pull-out tests is striking.

In Fig. 12, the variation of the von Mises equivalent stress in the (ductile) titanium bar is plotted. As it should be expected, the maximum value is observed in the immediate vicinity of the central section and it approaches the value of about 20 MPa. As one moves towards the interior of the architrave, the equivalent stress in the titanium bar decreases rapidly and after the 20-th thread (out of 200), its value is only one tenth of the respective maximum one. The above conclusions become more clear in Fig. 13 in which the maximum value of the equivalent stress appearing at the peaks and the roots of the threads of a bolted bar are plotted versus the order of the thread (the thread at the central cross-section is considered as the first one). It is seen from this figure that the stress field is higher at the roots of the thread rather than at the respective peak. However, the most striking conclusion is that the stress on both the peak and

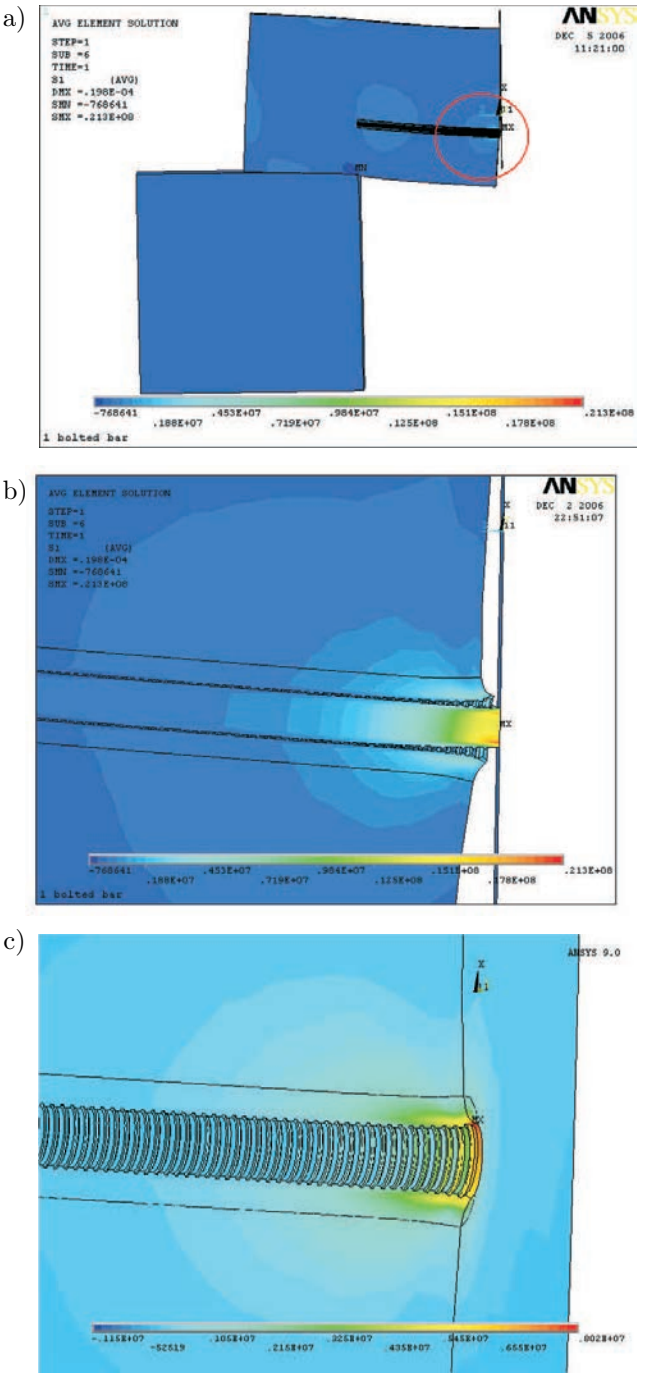

FIG. 9. The distribution of the 1st (maximum) principal stress in the restored architrave (a) and a detailed view of the central section of the titanium bar (b) and of the marble (c).

a) b)

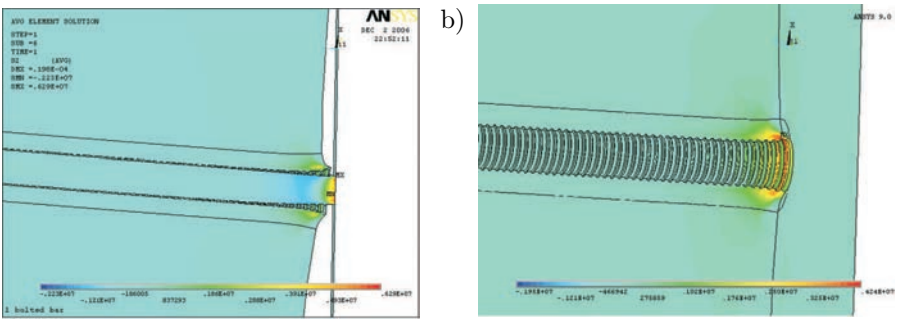

FIG. 10. A detailed view of the distribution of the 2-nd principal stress around the central cross-section area of the titanium bar (a) and of the marble (b).

a) b)

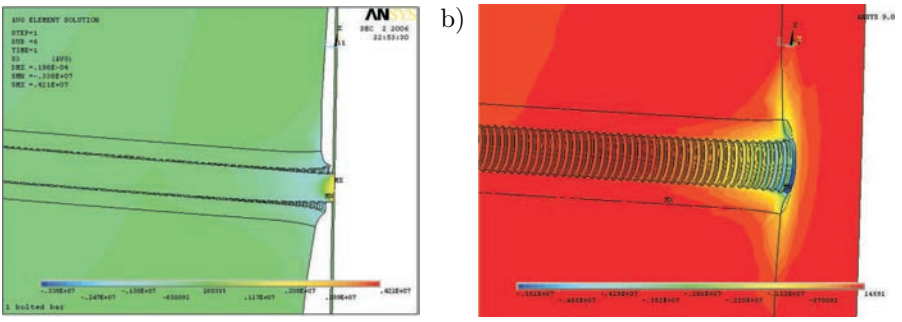

FIG. 11. A detailed view of the distribution of the 3-nd principal stress around the central cross-section area of the titanium bar (a) and of the marble (b).

the root of the threads is almost zero after the 50-th thread. From this point on, it increases very slightly as one approaches the end of the bar, but the maximum value reached does not exceed in any case the value of 1.5 MPa. Based on these observations, one should reconsider the empirical formulae yielding the anchoring length of the reinforcing bars, which is not in accordance with the minimum intervention principle.

In Fig. 14 the distribution of the maximum shear stress (Fig. 14a) and that of the maximum principal stress (Fig. 14b) are plotted in juxtaposition, around the area of the reinforcing bar. The non-monotonous variation of both stresses along the radial and the axial directions is clear from these figures, explaining the cone type fracture of marble during the pull-out tests [18].

In order to study the differences between the two models (bolted bar and cylindrical bar), a series of critical diagrams were plotted. As the first step, variation of the normal axial strain along the central vertical line of the cross-

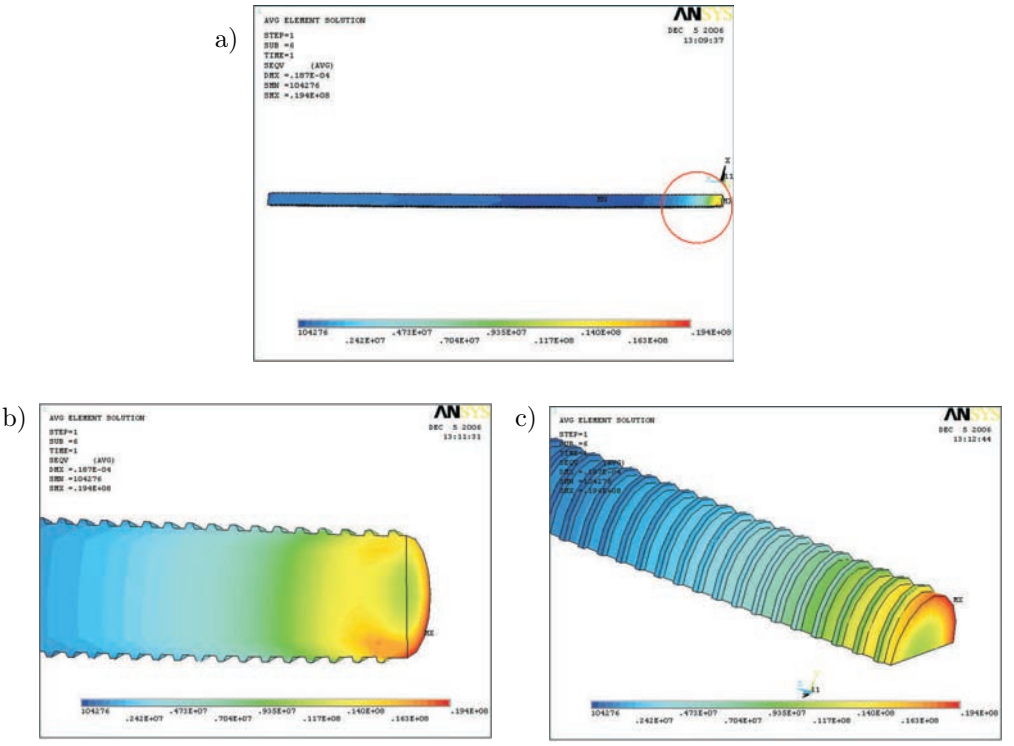

FIG. 12. The distribution of the equivalent stress in the reinforcing bar (a) and two detailed views in the vicinity of the central cross-section (b, c).

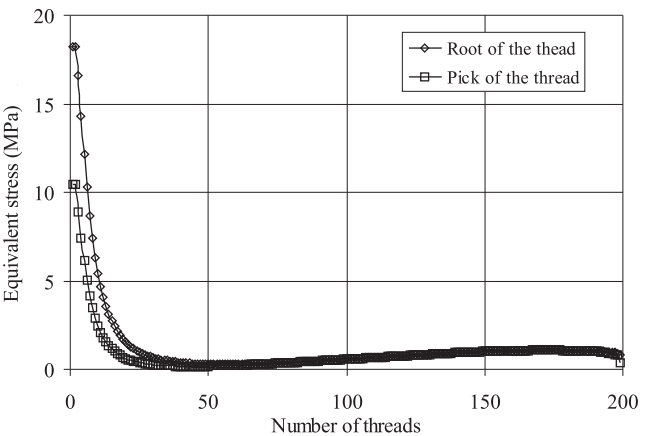

FIG. 13. The maximum equivalent stress at the peaks and the roots of the threads versus the order of the threads of the titanium bar.

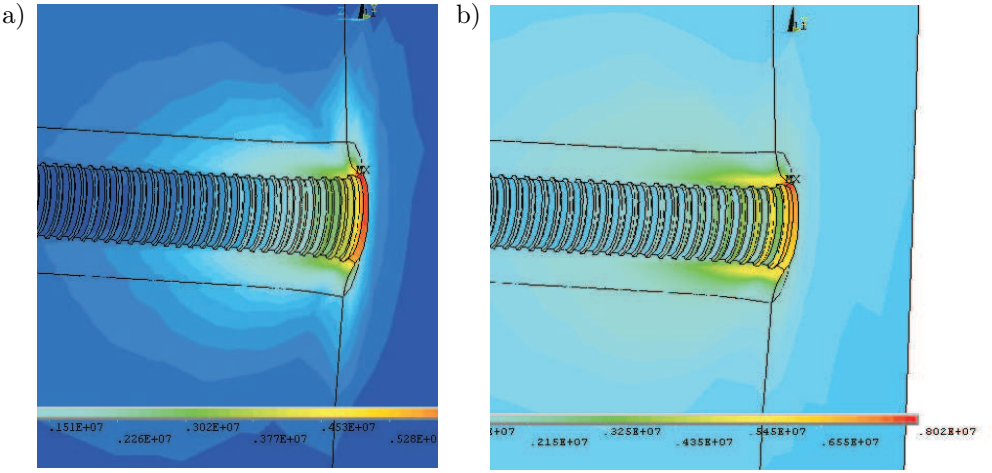

FIG. 14. The distribution of the maximum shear stress (a) and the maximum principal stress (b) in the marble in the central cross-section.

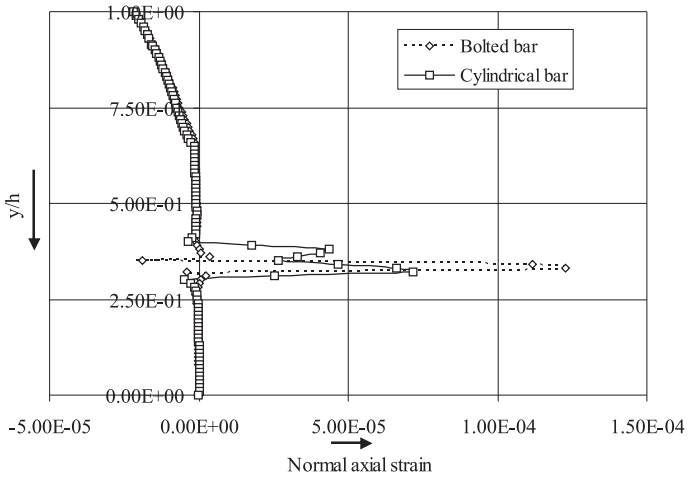

FIG. 15. The variation of the normal axial strain along the height of the architrave.

section of the architrave is plotted in Fig. 15. The vertical axis is reduced over the height of the beam, h, and is directed downwards. Point (0.00, 1.00) corresponds at the upper base of the architrave while point (0.00, 0.00) at the lower one. It is seen that in major part of the section, the values are of the same sign and order of magnitude for both models. For the upper one third of the height of the architrave, negative strain values are observed (corresponding to the compression exerted mutually from each part of the member on the other), which become zero

at the regions just above and below the titanium bars, since in these regions contact of the two parts of the architrave is lost, as it was already concluded from Fig. 9. In the immediate vicinity of the reinforcing bar, the strain reaches high tensile values of magnitude about 120 μstrain in case when the bar is bolted. This value is almost double the respective maximum one developed in the case of the model with an unbolted bar ($\sim$70 μstrain). In any case, since the maximum fracture strain of Dionysos marble is about 200 μstrain [19], it is concluded that even in the region of the titanium bar the member is safe, at least for the specific load used in this analysis.

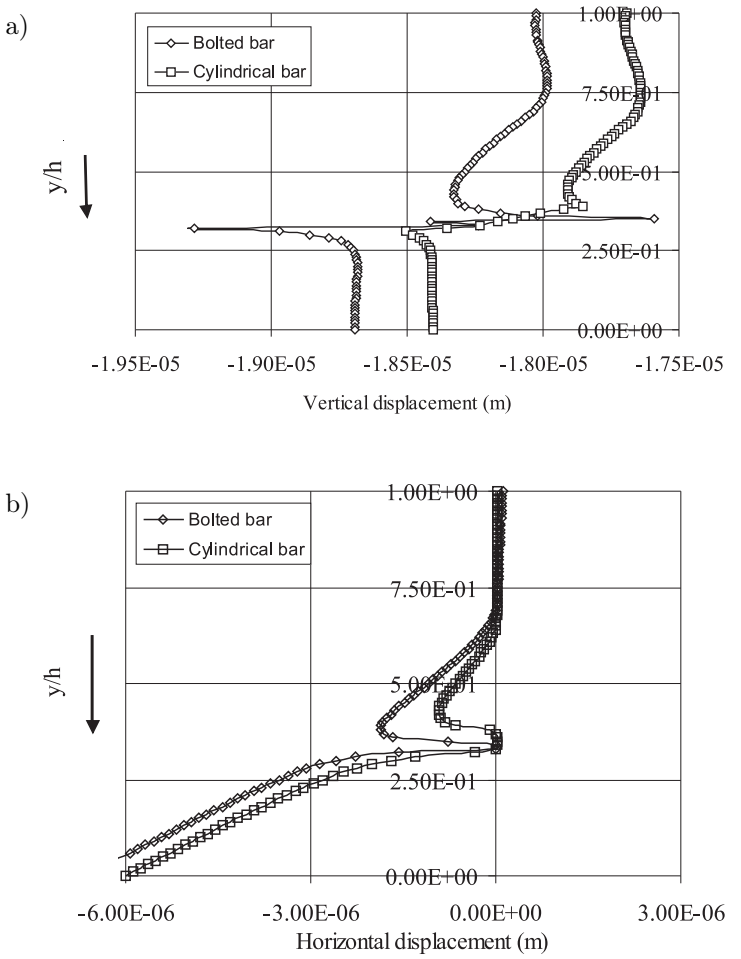

FIG. 16. The variation of the vertical (a) and the horizontal (b) displacements along the height of the architrave at its central cross-section.

Figure 16 describes variation of the components of the displacement vector along the same as previously line. As it is seen in Fig. 16a, where variation of the vertical displacement is plotted, behaviour of the two models is qualitatively similar. Indeed, in both cases, an almost constant (non-zero) vertical displacement is observed all along the height of the member, although it appears to increase slightly in the portion below the reinforcing bar. However, from a quantitative point of view the model with bolted bar exhibits deflections higher at any point of the architrave's height. In addition, the discontinuity observed close to the titanium bar is dramatically higher for this model: from -1.76×10^{-5} m the displacement reaches a value of -1.93×10^{-5}, namely it exhibits an abrupt change of almost 10%.

Similar conclusions are drawn for the variation of the horizontal displacement (Fig. 16b). The horizontal displacement is zero along the portions of the parts of architrave for which the contact is not lost (as it is expected, also, for symmetry reasons) and reaches considerably higher values, of the order of 6 μm, in the portions of the section where the contact of the two constituent parts is lost (both below and above the reinforcing titanium bar). Again the absolute values are higher in the case of the architrave restored using a bolted bar. Although such a displacement appears to be negligibly small, it must be considered seriously by experts working for the restoration projects, since it is the origin of a series of problems due to the penetration of moisture, bacteria etc in the body of the structural member.

Variation of the normal components of the stress field along the central horizontal line at the height of the axis of the reinforcing bar is plotted in Fig. 17(a,b). In this figure the horizontal axis is reduced over the half-length of the architrave and therefore point (0.00, 0.00) corresponds to the leftmost point of the member (resting on the capitals), while point (0.00, 1.00) corresponds to the mid-span of the architrave. It is observed that for the bolted bar, the axial stress (Fig. 17a) starts to increase abruptly as one approaches the central section and reaches a value of about 14 MPa, almost double as compared to the respective stress of the unbolted bar ($\sim$7 MPa). As one moves away from the central section, the axial stresses tend to decrease rapidly for both models and some perturbations are observed only in the region of the end of the titanium bar. The conclusions for the transverse normal stresses are of different nature. Compressive stresses appear at the region of the architrave resting on the abacuses which become tensile as one moves towards the central section (about 3.2 MPa for the unbolted bar and about 2.1 MPa for the bolted one). However, it should be mentioned that the use of the bolted bar creates high compressive values very close to the central section, just before the appearance of the tensile stresses at that section.

Finally, some interesting conclusions are drawn by plotting variation of the axial strain along the bottom central line of the member (Fig. 18). Initially the

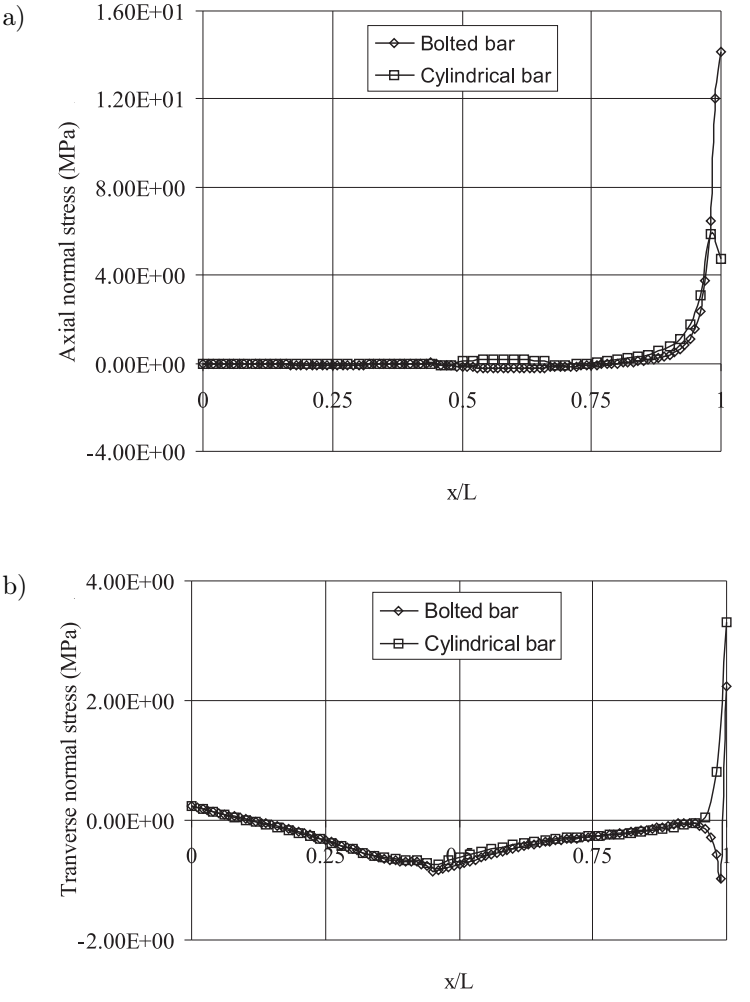

FIG. 17. The variation of the normal axial (a) and the normal transverse (b) stresses along the axial line passing from the centre of the reinforcing bar.

axial strain is almost zero for both models since part of the architrave, initially resting on the abacuses, tends to lift up losing the contact with the abacus in case when the load is applied only along the span of the member [4, 5]. However, as ones moves towards the corners of the supporting abacuses, the axial strain takes negative (compressive) values of the order of about -35 μstrain. From that point on, the strain starts to increase in an almost parabolic form until it becomes zero at the mid-span of the beam, where the contact between the two constituent parts is lost. Similarity of the variation of the strain along the bottom central line for the two models indicates that the stress and strain fields

at the bottom base of the member are almost independent of the geometrical details of the titanium bar used.

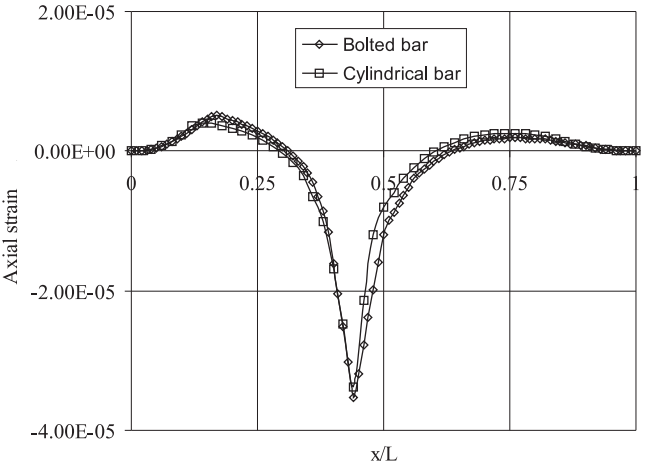

Fig. 18. The axial strain along the bottom central axial line.

5. Conclusions

The mechanical behaviour of fractured marble architraves restored with either cylindrical or bolted titanium bars was studied with the aid of the Finite Element Method. The findings of the analysis can be summarized as follows.

The simulation of bending under uniform load with multi-point laboratory bending tests leads to underestimate the stress field actually developed. In the vicinity of the reinforcing bar the contact between the two constituent marble parts of the architrave is lost.

The axial strain along the height of the architraves is not linear but of sigmoid variation. Taking into account, also, that the neutral axis of the bent architrave is displaced downwards (obviously due to the fact that the length – to – height ratio of typical architraves is lower than 4) it is indicated that higher order bending theories should be employed, compared to the simplified technical Bernoulli-Euler bending theory. Preliminary results using a modified Timoshenko bending theory indicate that the number of reinforcing bars should be slightly increased.

The existence of singularities at the corners and the roots of the threads yields more severe stress and strain fields in comparison to the restoration with unbolted bars. The equivalent stress in the titanium bar is more severe at the roots of the threads rather than at their respective peaks.

However, what is perhaps more important from a practical point of view, is the fact that the intensity of the stress field along the reinforcing bar decreases rapidly and is almost zero after the 50-th (out of 200) thread, indicating that the formula for the anchoring length of the reinforcing bars should be reconsidered in the direction of minimizing the intervention on the authentic stones.

Acknowledgements

The authors are indebted to the "*K. Liontos and Associates, Ansys Channel Partners of Greece*" company and especially to Mr George Ferentinos, for a continuous support during the preparation of the numerical models. Also, the assistance of Mr Panagiotis Chatzistergos is gratefully acknowledged. The present study is a part of the PhD Thesis of the second author (E. Ganniari-Papageorgiou).

References

1. C. Zambas, M. Ioannidou and A. Papanikolaou, *The use of titanium reinforcements for the restoration of marble architectural members of Acropolis Monuments*, Proc. IIC Congress on Case Studies in the Conservation of Stone and Wall Paintings, The International Institute for Conservation of Historic and Artistic Works, 138–143, Bologna 1986.

2. M. Ioannidou, and V. Paschalides, *Joining together beams of the Propyleae of Acropolis using titanium*, Proc. of the 5th Int. Symp. for the Restoration of the Acropolis Monuments, F. Mallouchou-Tufano [Ed.], Committee for the Preservation of the Acropolis Monuments, Athens, pp. 291–300, 2002.

3. M. Mentzini, *Joining together architraves and drums of the Parthenon: A new approach*, Proc. of the 5th Int. Symp. for the Restoration of the Acropolis Monuments, F. Mallouchou-Tufano [Ed.], Committee for the Preservation of the Acropolis Monuments, Athens, 233–242, 2002.

4. S. K. Kourkoulis, E. Ganniari-Papageorgiou and M. Mentzini, *Experimental and numerical evaluation of a new method for joining together fragmented structural members*, Heritage, Weathering and Conservation (HWC-2006) Conference, Madrid, Spain, June 2006, [in:] *Heritage, Weathering and Conservation*, R. Fort *et al.* [Eds.], Balkema, The Netherlands, 657–665, 2006.

5. S. K. Kourkoulis, E. Ganniari-Papageorgiou and M. Mentzini, *Joining Fragmented Marble Architraves Using Titanium Bars: A Numerical Analysis*, Special Symposium on Fracture and Failure of Natural Building Stones, 16th European Conference on Fracture (ECF 16), Alexandroupoli, Hellas, July 2006, [in:] *Fracture and Failure of Natural Building Stones – Applications in the Restoration of Ancient Monuments*, S. K. Kourkoulis [Ed.], Springer, Berlin, 269–287, 2006.

6. C. Zambas, *Mechanical Properties of Pentelik Marbles*, Committee for the Restoration of Parthenon Publications, Athens, Greece 2004.

7. I. Vardoulakis, G. E. Exadaktylos, S. K. Kourkoulis and C. Papadopoulos, *Characterization of Mechanical Properties and Damage of Natural Building Stones in Historical Monuments'*, C., Proc. 4th International Symposium on the Conservation of Monu-

ments in the Mediterranean, Rhodes, Greece, 6–11 May, 1997, A. Moropoulou, *et al.* [Eds.], Technical Chamber of Greece, **2**, 193–206, 1997.

8. V. Perdikatsis, K. Kritsotakis, Th. Markopoulos and K. Laskaridis, *Discrimitation of Greek marbles by trace-, isotope-, and mineralogical* analysis, Special Symposium on Fracture and Failure of Natural Building Stones, 16th European Conference on Fracture (ECF 16), Alexandroupoli, Hellas, July 2006, [in:] *Fracture and Failure of Natural Building Stones – Applications in the Restoration of Ancient Monuments*, S. K. Kourkoulis [Ed.], Springer, Berlin, 497–515, 2006.
9. A. G. Tassogiannopoulos, *A contribution to the study of the properties of structural natural stones of Greece*, Ph.D. Dissertation, National Technical University of Athens, Greece 1986.
10. P. S. Theocaris and E. Coroneos, *Experimental study of the stability of Parthenon*, Publications of the Academy of Athens **44**, 1–80, 1979.
11. I. Vardoulakis and S. K. Kourkoulis, *Mechanical properties of Dionysos marble*, Final report of the Environment Project EV5V-CT93-0300: Monuments under seismic action, National Technical University of Athens, Greece 1997.
12. G.E. Exadaktylos, I. Vardoulakis and S. K. Kourkoulis, *Influence of nonlinearity and double elasticity on flexure of rock beams – I. Technical theory*, International Journal of Solids and Structures, **38**, 4091–4117, 2001.
13. K. N. Kaklis, and I. Vardoulakis, *An experimental investigation of the size effect in indirect tensile test on Dionysos marble*, [in:] Proc. 7th Nat. Congress on Mechanics, A. Kounadis, C. Providakis and G. Exadaktylos [Eds.], Technical University of Crete, **II**, 151–157, 2004.
14. S. K. Kourkoulis, E. Ganniari-Papageorgiou and M. Mentzini, *Dionysos marble beams under bending: A contribution towards understanding the fracture of the Parthenon architraves*, Engineering Geology, to appear, 2007.
15. M. Mentzini, *Methodology of structural interventions on the Acropolis Monuments*, The Acropolis restoration news – Journal of the Committee for the Preservation of the Acropolis Monuments, **6**, 15–18, 2006.
16. G. E. Exadaktylos, I. Vardoulakis and S. K. Kourkoulis, *Influence of nonlinearity and double elasticity on flexure of rock beams – II. Characterization of Dionysos marble*, International Journal of Solids and Structures, **38**, 4119–4145, 2001.
17. L. Dufort, S. Drapier, M. Grediac, *Closed-Form Solution for the Cross-Section Warping in Short Beams Under Three-Point Bending*, Composite Structures, **52**, 233–246, 2001.
18. S. K. Kourkoulis, S.-A. Papanicolpulos, A. Marinelli, I. Vayas, *Restaurierung antiker Tempel: Experimentelle Untersuchungen zum Ausziehverhalten von Verankerungen im Marmor*, Bautechnik, **85**, 2, 2008.
19. S. K. Kourkoulis, G. E. Exadaktylos and I. Vardoulakis, *U-notched Dionysos Pentelicon marble in three-point bending: The effect of nonlinearity, anisotropy and microstructure*, International Journal of Fracture, **98**, 369–392, 1999.

Received February 09, 2007; revised version November 24, 2007.